REDUCING THE UNCERTAINTY OF THERMAL MODEL CALIBRATION USING ON-MACHINE PROBING AND DATA FUSION

AKSHAY ANAND POTDAR

A thesis submitted to the University of Huddersfield in partial fulfilment of the requirements for the degree of Doctor of Philosophy

Date of Submission: 13/12/16

Abstract

Various sources of error hinder the possibility of achieving tight accuracy requirements for high-value manufacturing processes. These are often classified as: pseudo-static geometric errors; non-rigid body errors; thermal errors; and dynamic errors. It is comparatively complicated to obtain an accurate error map for the thermal errors because they are influenced by various factors with different materials, time constants, asymmetric heating sources and machining process, environmental effects, etc. Their transient nature and complex interaction mean that they are relatively difficult to compensate using pre-calibration methods.

For error correction, the magnitude and sign of the error must first be measured or estimated. Pre-calibrated thermal compensation has been shown to be an effective means of improving accuracy. However, the time required to acquire the calibration data is prohibitive, reducing the uptake of this technology in industrial applications. Furthermore, changing conditions of the machine or factory environment are not adequately accommodated by pre-calibrated compensation, leading to degradation in performance. The supplementary use of on-machine probing, which is often installed for process control, can help to achieve better results.

During the probing operation, the probe is carried by the machine tool axes. Therefore, the measurement data that it takes inevitably includes both the probing errors and those originating from the inaccuracies of a machine tool as well as any deviation in the part or artefact being measured. Each of these error sources must be understood and evaluated to be able to establish a measurement with a stated uncertainty. This is a vital preliminary step to ensure that the calibration parameters of the thermal model are not contaminated by other effects.

This thesis investigates the various sources of measurement uncertainties for probing on a CNC machine tool and quantify their effects in the particular case where the on-machine probing is used to calibrate the thermal error model.

Thermal errors constitute the largest uncertainty source for on-machine probing. The maximum observed thermal displacement error was approximately 220 μm for both X and

Z-axis heating test at 100 % speed. To reduce the influence of this uncertainty source, sensor data fusion model using artificial neural network and principal component analysis was developed. The output of this model showed better than 90 % correlation to the measured thermal displacement. This data fusion model was developed for the temperature and FBG sensors.

To facilitate the integration of the sensor and to ease the communication with machine tool controller, a modular machine tool structural monitoring system using LabVIEW environment was developed.

Finally, to improve the performance of the data fusion model in order to reduce the thermal uncertainty, a novel photo-microsensor based sensing head for displacement measurement is presented and analysed in detail. This prototype sensor has measurement range of 20 μm and resolution of 21 nm.

Acknowledgement

Working as a Ph.D. student at the Centre for Precision Technologies – ECMPG group was a huge as well as challenging experience to me. However, it would not have been possible without the support and encouragement of various people in my life who either directly or indirectly contributed towards my effort in accomplishing this achievement.

Firstly, I would like to express my deepest gratitude to my supervisor Dr Andrew Longstaff for introducing me to the world of research. It's only because of his tremendous support and guidance that I was able to submit my thesis in a respectable manner. I would like to thank him for providing me with so many wonderful opportunities. His advice both on research as well as my career have been valuable. If it wasn't for him, I could have never reached the heights or explored the depths.

I would also like to thank my co-supervisor Dr Simon Fletcher, without whose continuous supervision, I would not be able to perform such complex experiments. Throughout the course of Ph.D., I interacted with him on a regular basis, which has helped me learn many valuable things and grow in the right direction.

Secondly, my sincere thanks to my family – My parents – Mrs Anuradha & Justice (Retd.) Anand Vasantrao Potdar and brother – Shri Rohan Potdar. I am privileged to have a family who has shown an enormous amount of faith & patience in me. No words are enough to express my thankfulness towards them.

I would also like to thank Dr Naeem Mian, Andrew Bell (Applications Engineer), Ali Abdulshahed, my friends and colleagues. It is a pleasure to acknowledge the helpful suggestions and timely support provided throughout the course.

Last but not the least; I would love to take the opportunity of thanking my funding body EPSRC, who supported my work for 3 years of Ph.D. Without their support, this thesis would not have materialised.

Contents

List of abbreviations

ANFIS	Adaptive Neuro-Fuzzy Inference System
ANN	Artificial Neural Network
ANSI	American National Standards Institute
ASME	American Society of Mechanical Engineers
BMS	Bi-Material Strip
CMM	Co-ordinate Measuring Machine
CNC	Computer Numerically Controlled
CTE	Co-efficient of Thermal Expansion
DAQ	Data Acquisition System
DDE	Dynamic Data Exchange
DOF	Degree Of Freedom
FBG	Fibre Brag Grating
GUM	Guide to the expression of Uncertainty in Measurement
ISO	International Standard Organization
MCM	Monte Carlo Method
MCS	Monte Carlo Simulation
OMP	On Machine Probing
OMM	On Machine Measurement
SD	Standard Deviation
TCP	Tool Centre Point
USB	Universal Serial Bus
UV	Ultra Violet

List of figures

List of tables

List of publications

Journal papers

1. Potdar, A. A., Fletcher, S., & Longstaff, A. P. (2016). Performance characterisation of a new photo-microsensor based sensing head for displacement measurement. *Sensors and Actuators A: Physical*, *238*, 60-70.

2. Abdulshahed, A.M., Longstaff, A. P., Fletcher, S., & Potdar, A. A. (2016). Thermal error modelling of a gantry-type 5-axis machine tool using a Grey Neural Network Model. Journal of Manufacturing Systems, 41, 130-142.

Conference Papers

1. Potdar, Akshay, Longstaff, Andrew P., Fletcher, Simon and Mian, Naeem S. (2015) Application of multi sensor data fusion based on Principal Component Analysis and Artificial Neural Network for machine tool thermal monitoring. In: Laser Metrology and Machine Performance XI, LAMDAMAP 2015. EUSPEN, Huddersfield, UK, pp. 228-237. ISBN 978-0-9566790-5-5

2. Potdar, A., Longstaff, A., Fletcher, S., & Abudulshahed, A. (2013). Development of modular machine tool structural monitoring system. *Advanced Manufacturing Engineering and Technologies NEWTECH 2013 Stockholm, Sweden 27-30 October 2013*, 263.

Chapter 1 –Introduction

Metrology is the science of measurement [1] and its corresponding accuracy, precision and uncertainty [2]. To measure is to ascertain a numerical value to quantity, magnitude or dimension in terms of physical unit. Measurements are usually performed for verification purpose. It enables us to know the accuracy of the measurement and to ensure common standards are used.

1.1 Dimensional Metrology and quality control

In the world of manufacturing, dimensional metrology is synonymous with dimensional measurement [3]. Metrology in manufacturing begins from the setting of tools; it continues through in-process measurement, product verification and through life monitoring [4]. Dimensional metrology is a central part of any manufacturing system because it is essential for making parts correctly [5]. It means it can be guaranteed that the manufactured parts fit together and perform as they were intended to.

One of the key processes in industrial quality control is a dimensional measurement of the manufactured parts and in most modern industries measurement process can cost up to 10-15 % of the production cost [6]. Good measurements can however significantly increase the effectiveness and quality of the product.

Dimensional quality control makes sure that the dimensional properties of the produced part comply with the assigned tolerances. Tolerances allow defining how much property can deviate from its nominal value. This is necessary, as it is impossible to manufacture a part with exact nominal specifications. The narrower the value of tolerance limits, the more expensive the manufactured part [7].

The measurement instruments and knowledge of measuring uncertainties for product verification is an indispensable part of a quality management to guarantee that the products are within specified tolerances. If the product is not within tolerance, it requires either rework or is scraped. If the product is within tolerance but rejected by the customer due to non-compliance with their tolerance specifications, it results in an even greater economic loss. Hence, there is a clear relationship between economics and measurement errors.

1.2 Machine tools in manufacturing

Manufacturing has evolved dramatically from the days of artisans producing quality products and skilled machine operator altering the cutting parameters based on his experience and as a direct response to the machine behaviour [8]. Production in high value manufacturing (HVM) is increasingly becoming reliant on computer numerically controlled (CNC) machine tools, due to the several advantages offered by them over manually operated machines. CNC machines provide an improvement in consistency, flexibility, productivity and quality with shorter and predictable time scales. They also reduce manufacturing costs by keeping the production of scrap and rework of out of tolerance components low.

The primary goal of the CNC machines is to automate the process to achieve higher accuracy to meet the greater quality requirements. Machining accuracy, one of the key performance variables for manufacturing process, is chiefly governed by the relative position between cutting tool and ideal workpiece [9]. Workpiece accuracy can be defined as the degree to which the finished part conforms to dimensional and geometrical specifications [10].

1.2.1 Machine tool error sources

Machining errors occur due to the mismatch between theoretical and actual machine tool trajectory, which is a result of the influence of various errors on the machine tool motion. Inaccuracies in the machine tool are caused by the rigid body geometric errors due to machine's structural components, thermal errors due the thermal distortions, loading effect and errors due to other sources like cutting forces, servo errors, etc. [11, 12].

Rigid body geometric errors are normally caused by manufacturing imperfections, mechanical misalignments, static deflection of the structural elements, etc. Two main components of these errors are systematic and random errors. They are further categorized into translational (linear positioning, horizontal and vertical straightness), angular (roll, pitch and yaw) and squareness errors. 3-axis machine normally has 21 geometric error components [11].

Extensive research has been carried out on geometric error compensation methods as they make up one of the major source of inaccuracy in the machine tools [10, 13, 14].

Improvements in the volumetric accuracy of up to 97% were achieved for 3-axis machine tool in the research carried out by Longstaff et al [15].

Non-rigid errors are caused by the lack of rigidity in the structural components of the machine tool. They are also called "load induced" errors. Inertia, workpiece, machine tool and cutting tool mass, fixture stiffness and cutting loads, etc. are some of the common factors that give rise to these errors. Effect of these errors are small when compared to uncompensated geometric errors but can become significant in the case of larger machines [10].

Thermal errors can contribute more than 50% of the total machine error [16-18] and are caused by the thermo-elastic deformation in the machine. Non-linear thermal expansion of the structural elements caused by the thermal gradient produces an intricate interaction between tool and workpiece [19].

Thermal errors are into the internal and external heat sources. Internal heat sources are often the major contributors, which are typically motors, belts drives, spindle bearings, gear boxes, hydraulic systems, etc. [20]. Typical examples of external heat sources include heat generated by the machining process, machine electric components, cabling and cabinets, other machines, workshop heating, etc., [21].

Other sources of machine tool error include servo errors, fixture errors, tool wear, etc. These errors depending on the process are comparatively not as significant as geometric, non-rigid and thermal errors. They are mainly caused by the use of incorrect feed rates, improper setup procedures, workload and life of the machine tool. This type of errors can be restricted or prevented by careful selection of feed rates, using proper setup procedures and regular inspection of the tool [10].

1.2.2 Error mitigation

There are stringent requirements on the dimensional accuracy to be achieved in precision machining applications. "How to improve the accuracy of the machine tool has become a hot issue for many scholars" [22]. Two basic approaches to improving the machine tool accuracy are error avoidance and error compensation [10].

Error avoidance involves reduction or elimination of machine tool errors by careful design and manufacturing efforts. Whereas in **error compensation**, machine errors are mapped and then effects of these errors are compensated by electronic adjustment to the axis trajectory.

It is more desirable to use error avoidance comprising the refinement of a machine tool or its environment to control the error sources. This is a generally accepted idea. However, in several cases this is not practically feasible, there are physical limitations of machine tool accuracy that cannot be overcome solely by production and design techniques and due to the additional cost involved in the refinement of the machine tool structure. This makes error compensation techniques more attractive than error avoidance [23].

To understand the possible causes and magnitudes of the machine tool errors, machine tool calibration is necessary. Periodic calibration can provide advanced warning signs of when machine tool is going to require attention for repair. Calibration helps to characterise the machine performance, gives raw data which can be used for error compensation and provides a means to identify accuracy problems [20]. Regular CNC machine tool calibration provides the information to maintain the asset within its tolerance, delivering higher throughput, allowing parts to be manufactured with higher accuracy and reducing the cost occurring from field services and production cycle interruptions for critical maintenance activities.

Machine tool calibration using purpose-made equipment often requires high levels of skill, it can be resource intensive in addition to sometimes being time consuming, and cost involved in assigning resource as well as time can at times exceed the benefits gained by the reduced scrap and rework. There may be non- standard methods available for calibration but due to the lack of knowledge and insufficient expertise, companies may not be able to utilize them. Additional cost may incur in hiring the consultancy to provide the required solution [21].

In the case of pre-calibrated systems, the error is measured before the machining process and the data is utilised to compensate the tool path during subsequent operational cycles. This method is dictated by the assumption that both machining and measurement process are repeatable in nature [11]. Good machine tool design and build generally means that high quality machine tools will, have repeatable rigid body geometric errors, meaning that, error mapping is relatively easy to achieve. However, thermal errors are comparatively

complicated to accurately map, because they are dependent on various factors such as machining process, environmental effects, etc. Whereas for active error compensation, an on-line semi-closed loop system, the error is monitored during the actual process and the same is used for on-line error compensation. Thus, active error compensation is a potentially more desirable solution in an industrial application. The downside to such a strategy is the additional cost requirement and physical constraints that such a system would require [24].

An attractive solution is to fuse on-line measurement to supplement a pre-calibration schema. The offline measurement can reduce the number of online sensors required while the online system can supplement deficiencies due to time-variant factors.

Thus, there is a need for an on-line measurement system for error monitoring so the machining process can be altered during the same operation. On-machine probing is a readily available technology that can help achieve this.

1.3 On-machine probing

Owing to the increasing popularity of CNC machine tools, it has become essential to further automate and accelerate the speed of the quality control of final machined parts in order to meet the industry demands forever-growing accuracy without adversely influencing production times. This was made possible using measuring devices mounted on the machine that can be automatically selected in place of the cutting tool. These "on-machine" probes can aid in setting the location of the un-machined workpiece and its direct measurement on machine tool itself. Additional equipment is also installed on some machines to establish the length and diameter of the cutting tool. Such a devices are known as on-machine tool setting probes.

In conventional manufacturing processes, part inspection is carried out on standalone measurement systems such as coordinate measuring machines (CMM), which are normally located at a different location than machine tool in the separate quality control area, room or building. It is also known as "**post-process measurement**" or "**out-of-cycle measurement**" [25, 26]. Figure 1 illustrates the post processing measurement inspection technique.

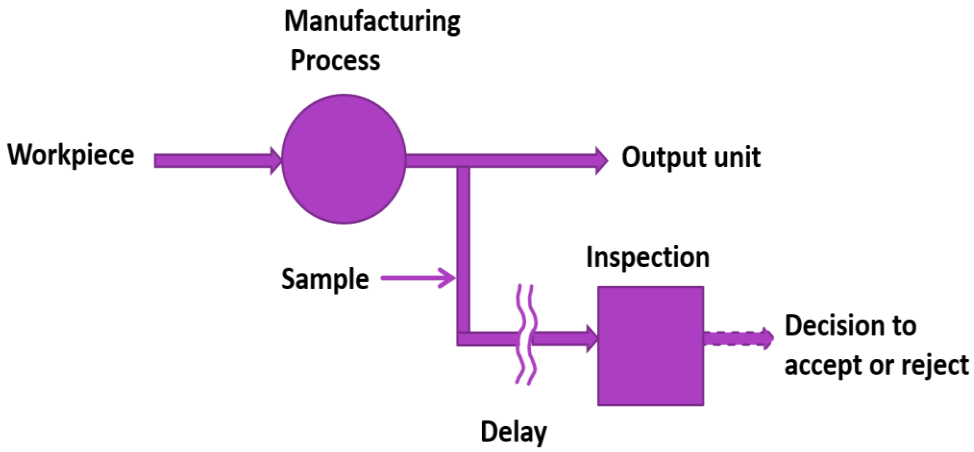

Figure 1 Post-process measurement

This increases the overall manufacturing cost and time to obtain the final product and can potentially create bottleneck phenomenon by product stagnation due the time lag between manufacturing and inspection process in case of the flexible manufacturing system. A part that fails post process inspection by CMM results in rework or increases scrap cost. Additionally, it can be hard to transfer, fixture and measure the complex, large sized parts [26].

In "**In-cycle measurement**" also known as "**on-machine measurement**", machining must be stopped while the measurement takes place during the process cycle. Figure 2 shows the in-cycle measurement method. With this measurement method, the workpiece can be assessed between cuts or after completion, prior to removal from setup [24, 26, 27].

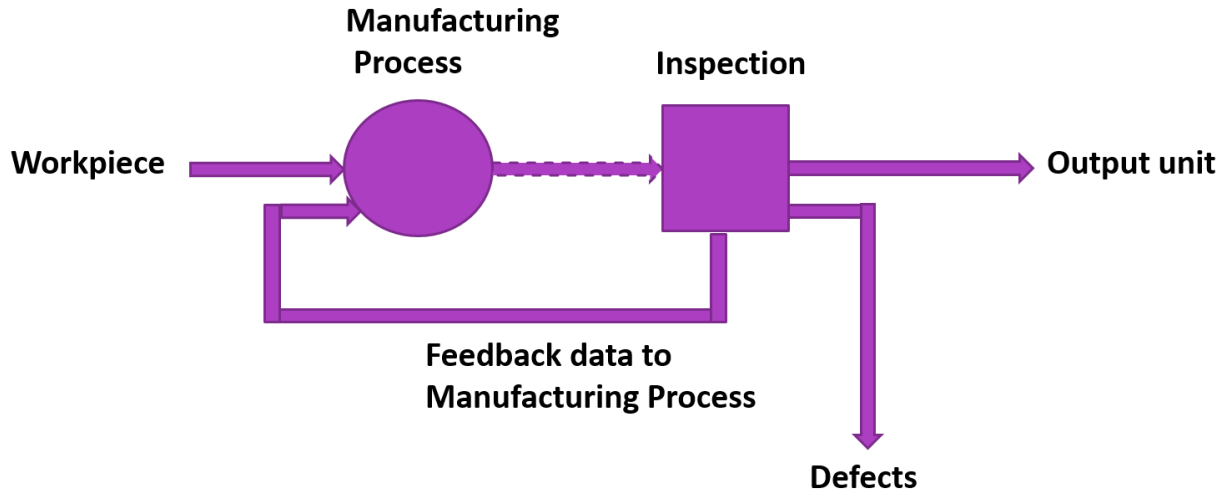

Figure 2 In-cycle measurement

An on-machine probe is a relatively inexpensive and easy to use accessory that can be directly and automatically mounted on the spindle of CNC milling machine or in the lathe turret. Thus, this kind of arrangement provides functionality similar to a CMM measurement [28]. Figure 3 demonstrates the schematic of a probe mounted 3-axis CNC machine for on-machine measurement.

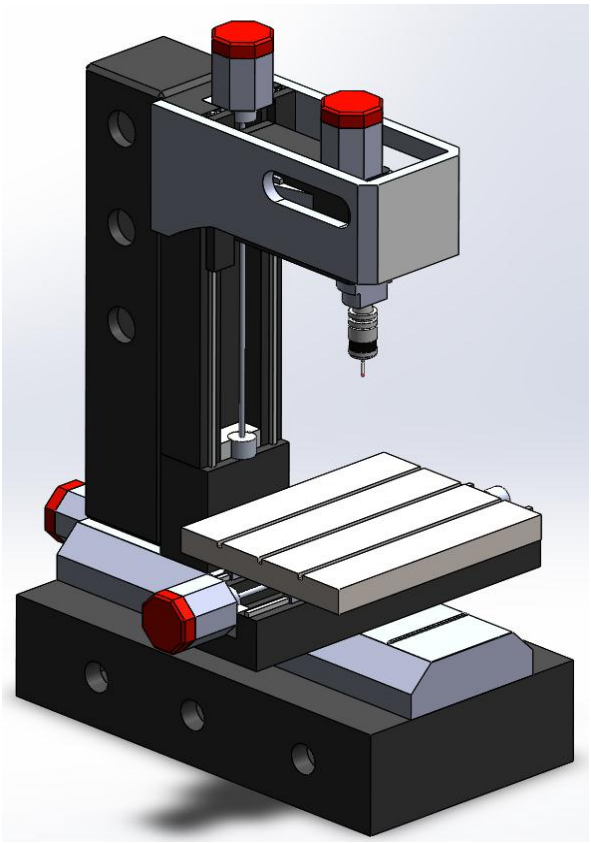

Figure 3 Schematic of a probe mounted 3-axis CNC machine

However compared to CMM, on-machine measurements (OMM) are exposed to a number of additional issues such as thermal dilatations, clamping forces, dirty environments, limited accuracy of production machines and higher trigging forces of machine tool probes [29]. Probe measurement results are also affected by environmental influences. The most important influences are deviations from the reference temperature of 20°C causing thermal expansion and shrinkage of the work-piece and the measuring system. Thermal gradients inside the work-piece and measuring system including probing create more trouble, because they lead to deformations like bending [30]. Factors that influence the measuring

performance are stylus length, direction and speed of approach, indexing angles, pre travel variations, etc. [31].

The main limiting factor in using the probe as a reliable, traceable part of the quality audit for a produced part is that the same axes that create the part also drive the measurement device. This means that some of the errors in machining will not be picked up by the measuring procedure; it is not an independent check [32]. Probes measure parts moving along the erroneous machine tool axes, thus on machine measurement data inevitably include the probing errors as well as errors originated from the inaccuracies of a machine tool [33]. These probing errors are required to be identified and eliminated from the measured data to obtain true machining error.

ISO 230-10:2011 [34] provides a standard for determining the measuring performance of probing systems for machine tools. These methods are based on the measurement of different types of appropriate standard artefacts that include reference spheres, gauge rings and corners. This system allows checking the measurement performance of the entire system and thus does not permit isolating the probe errors from machine tool errors. Use of a master artefact is an indirect method for determining the accuracy of machine tool probe. They are used because of their simplicity but it requires the use of high precision machine tools [29], to gain any information regarding the accuracy of the probe itself. Most of the CNC machines used in industrial settings fail to satisfy this condition [35].

Indirect methods described were used for CMM probing with dedicated measurement setup, which is heavy and complex and thus unsuitable for shop floor usage. Testing of machine probe on the machine itself requires portable setup. This kind of setup eliminates time and trouble required to dismantle probe and its setup [35]. Nevertheless, probe calibrated in this manner does not provide enough information about the entire volume of the machine as it offers only localised effect.

1.3.1 Probe types for on-machine measurement

There are several types of probes available for various measurement tasks on the shop floor as well as in metrology environment. They can be primarily classified into two groups**:** **contact probes** and **non-contact probes**. Contact probes are also referred as tactile probes and since non-contact probes chiefly use optical techniques for point detection; they

are normally called as optical probes. Non-contact probe also uses inductive and capacitive systems for surface detection purpose [30].

Non-contact probes do not require material contact with the surface being measured in order to function [11]. Hence, they are faster in operation compared to contact probes. Furthermore, they will not affect the surface being probed. Contact probes as the name suggest requires a material contact with the surface being measured in order to function [11]. They mostly have the advantage of being more accurate and reliable.

The most widely used probe for on-machine measurement is a touch-trigger probe. When the probe approaches the surface of a workpiece, the probe tip touches the surface, causing deflection of the stylus. The probe sensor senses this deflection and that triggers the machine to read out the position of the machine tool axes. The position of the point on the surface can be determined by accounting for the diameter of the probing tip. Commercially available touch-trigger probes mostly use electrical switch (Kinematic resistive) or strain gaug**e** mechanisms for sensing purpose. Figure 4 shows the schematic of both (a) switching and (b) strain gauge probe.

The **switching probe** consists of a set of spheres and rods. The stylus is located such that all degrees of freedom are constrained by six points of contact between spheres and rods in a kinematic location. Figure 4 (a) illustrates the kinematic mechanism of the switching probe. In Figure 4, F_c is a contact force, F_s is a spring foce, L is the length of the stylus and R stands for the pivot distance. Spring holds the stylus carrier against the kinematic contacts. An electrical circuit is formed by six contacts and the electrical resistance is continuously monitored. When the stylus of the probe makes contacts with the measurement surface, the resulting force acts against the retaining spring and subsequently changing the position of the one or two pairs of the contacts, causing the change in electrical resistance of the circuit. This change in the resistance is sensed by the probe electronics. Due to this kinematic arrangement pre-travel variation is significant for switching probe [36].

In the case of **strain gauge probe**, three strain gauges are installed above the kinematic mechanism on a thin web of the probe structure so that they can sense the strain. The kinematic mechanism provides the mechanical repeatability to the stylus. Strain gauges are mounted in such a way that they can sense a triggering force in any direction when the

stylus makes contact with the surface. For thermal drift compensation of the three measuring gauges, the fourth strain gauge is used [36].

The strain gauges are very sensitive and can trigger at forces, which do not unseat the kinematics. At these forces, the kinematic mechanism is effectively solid.
A key advantage of strain-gauge sensing is the ability to combine the forces in each direction and trigger at a constant force, whichever direction the contact occurs. This significantly reduces the pre-travel variation effects of the switching probes, as the trigger circuit does not constitute a kinematic structure [37].

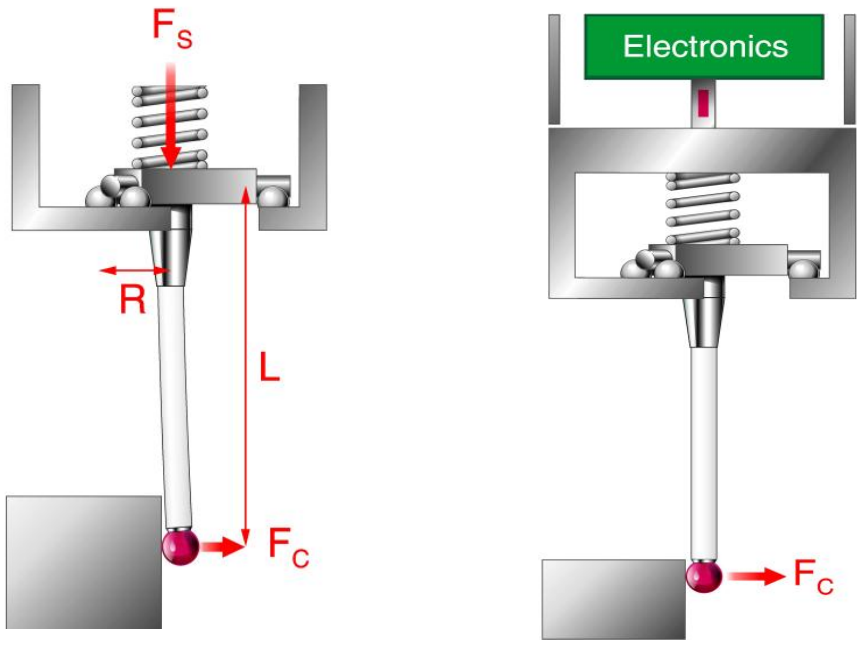

a. b.

Figure 4 Schematic of a touch-trigger probes, a) switching probe b) strain gauge probe, adapted from [37].

As discussed earlier, touch trigger probes, switching (kinematic resistive) and strain gauge sensors, are commonly used sensors for on-machine measurement on CNC machine tools. The strain gauge sensors have better performance characteristics in terms of sub-micron repeatability, longer operational life with low and uniform pre-travel variation. Despite the above mentioned qualities, kinematic probes are the most popularly employed for CNC machine tool. This is due to their simple, cost-effective, very compact and rugged

construction. Hence, even though stain gauge sensor probe would offer lower measurement uncertainty, switching probe was selected in this study so that this research would be applicable to wider applications. Thus, by performing worst-case analysis we are ensuring that all the uncertainty contributors are identified and evaluated

Proportional probes not only detects the deflection of the probe but also measures the amount of deflection proportional to a displacement of the stylus tip. These probes used in measuring mode are usually more accurate than touch-trigger probes. Probes used in scanning modes can be less accurate due to accelerations and stick-slip but are capable of measuring a large number of points in short time [38].

The technology in the field of on-machine probing is evolving continuously. Some of the noticeable new technologies are on-machine temperature probe [39], integrated blower jets for cleaning a measuring point and collision protection for touch probe's housing [40]. However, a detailed discussion of these technologies is beyond the scope of this document.

1.4 Uncertainty of measurements

When a measurement of any kind is performed, there is an uncertainty that measured value will never be an exact representation of the true value. In a measurement process, there are variety of factors that influence the measurement result and the related uncertainty. Measurement uncertainty is a parameter associated with the measurement result that characterises the dispersion of the values that could reasonably be attributed to the measurand [41].

In the manufacturing sector, uncertainties are evaluated to determine if the required tolerances are met or not. Component specifications are often defined in upper and lower tolerance limits. Conformance or non-conformance is very straightforward in the simple case of when measurement uncertainties are not considered. When the measurements lie within the tolerance limits, there is a conformance and when they lie outside the defined limits, there is a non-conformance.

Nonetheless, the uncertainty of measurement needs to be taken into consideration in a practical scenario. This results in a zone of uncertainty instead of the sharp boundary between conformance and non-conformance. This concept is demonstrated in Figure 5. The conformance zone is illustrated by green region and non-conformance zone is shown by

orange area. The remainder is a zone of uncertainty [42]. The case of false acceptance and false rejection can be envisaged from Figure 5. If the measurement value is in tolerance but uncertainty of measurement can make it out-of-tolerance, resulting in a case of false rejection. Conversely, false acceptance situation can arise if measurement result is out-of-tolerance but the uncertainty of measurement brings it in tolerance. Therefore, measurement values that fall within conformance zone, with given confidence level, are certain to be in a tolerance zone.

The dispersion of this uncertainty zone is dependent on the magnitude of the measurement uncertainty. As a result, it is not possible to accept the component without specification of measurement uncertainty. The increase in uncertainty zone results in a reduction of conformance zone. High value and high quality manufacturing industries have tight tolerances. Reducing the measurement uncertainty will help in reduction of false rejection and scrap work. Therefore, it is necessary to evaluate the measurement uncertainty when using the probing system for on-machine measurement.

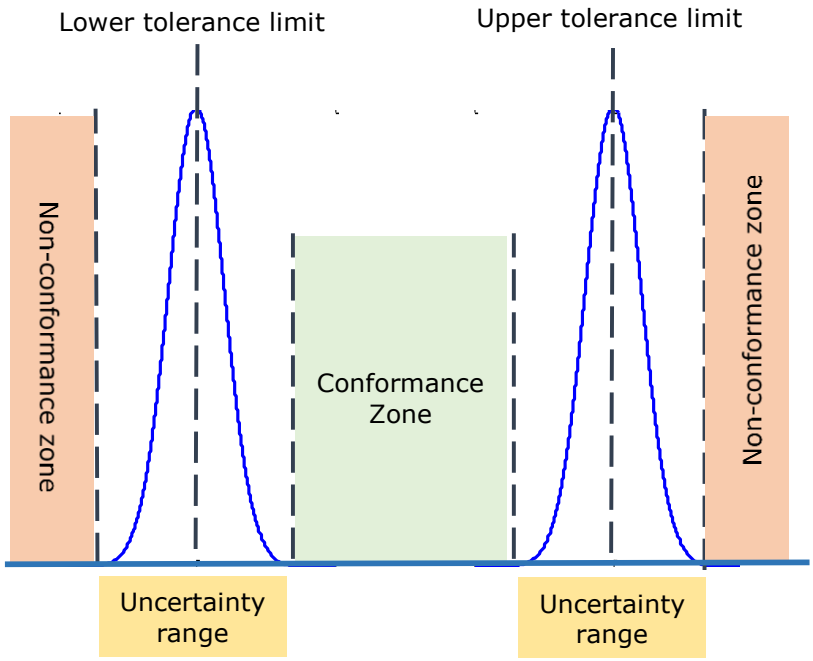

Figure 5 Role of measurement uncertainty in component conformance or non-conformance

The uncertainty evaluation of the on-machine probing system is a complex task due the intricate interaction of the many uncertainty contributors mentioned in section 1.3. They

can be roughly classified into the hardware, probing system, environment and workpiece factors. These contributors of uncertainty are discussed in detail in chapter 2.

The measurement uncertainty is normally determined by "Guide to the expression of uncertainty in measurement", known as ISO-GUM [43]. A popular alternative to conventional GUM for uncertainty determination is a computer simulation. GUM supplement 1 describes the propagation of probability distribution through a mathematical model of measurement as a basic for determining measurement uncertainty and its implementation using a Monte Carlo Method (MCM) [44].

1.5 Motivation

Since, the probing operation measures a workpiece/part along the erroneous machine tool axes, the measured data it takes inevitably include the errors originated from the structural and operational characteristics of a touch probe including errors inherited from a machine tool. In addition, thermal and mechanical properties of a part being measured influence the measurement uncertainty. Environmental factors also play a key role during on-machine measurement.

Thus, it is necessary to investigate the various sources of uncertainties of measurement when using on-machine probing for machine tool thermal error model calibration.

Motivation for this work is a low cost solution for displacement measurement, to be fused with temperature data to reduce uncertainty of on-machine probing.

1.6 Scope

1. In this research work, on-machine probe means switching touch trigger probe. Other types of probes have not been investigated in this project unless specifically mentioned.

2. For the purpose of modelling of an uncertainty of measurement using MCM, only those contributors of OMP uncertainty are considered which affect the thermal error model.

1.7 Aim and Objectives

1.7.1 Aims

The aims of this research work are:

1. To investigate and evaluate the uncertainties of on-machine probing for machine tool thermal error model calibration.

2. To reduce the uncertainty using sensor data fusion.

3. To develop a novel displacement measurement sensor.

1.7.2 Objectives

To meet the aims of this research, following specific objectives have been considered:

1. Identify the sources of uncertainty for on-machine probing and for traditional methods of calibrating machine tool thermal error models.

2. Develop, execute and evaluate a test regime to examine the effect of uncertainty sources for on-machine probing.

3. Design and develop a novel displacement measurement sensor.

4. Design and implement software capable of data acquisition and sensor fusion, and integrate a novel displacement sensor.

5. Investigate the use of sensor data fusion techniques to improve the uncertainty of measurement due to the thermal errors when probing.

Chapter 2- Review of previous research

In order to evaluate measurement uncertainty due to on-machine probing (OMP), it is necessary to identify and quantify all the uncertainty contributors. Due to the complex nature of the interaction between various contributors, it is difficult to make a strict classification.

In terms of hardware requirement, by merely replacing cutting tool to measuring probe it is possible to perform part/artefact inspection on the machine tool itself. Albeit machine tools are designed to operate in a harsh environments and CMMs are typically housed in a controlled conditions, it is possible to argue that during the measurement cycle when cutting operation is not taking place, machine tool will experience similar sources of error as CMM; differing in magnitude and dynamics of those errors [45].

Various authors have made attempt to classify the sources of uncertainty in CMM measurement. Wilhem et al [46], organised the sources of uncertainty into five groups: hardware, workpiece, sampling strategy, algorithms and extrinsic factors. Weckenmann and Knauer [47], subdivided the factors that influence the uncertainty of measurements into four categories: equipment, environment, workpiece and operator. Classification made by Kruth et al [48], consisted of workpiece, hardware, sampling and evaluation strategy. Salsbury [49], used a categorization scheme of machine components, probe components, part components and repeatability components.

Nonetheless, rather than a classification scheme, it is important to determine all the sources of uncertainty and to incorporate them in the uncertainty assessment of the measurement. Each principle error source should be further considered at a granular level. The errors are divided into four logical categories based on their source of occurrence: machine tool, probe system, environment, workpiece/ artefact factors, thus providing modular architecture to facilitate the determination of uncertainty. This would create a framework that would allow analysis of the different machine configurations in different environmental conditions under different machining processes.

The four categories are:

Machine tool: This category contains errors originating from machine tool components, caused by mechanical misalignment, manufacturing imperfections [13], thermos-elastic

deformation [18] in the machine structure etc. Based on above mentioned sources, factors that are considered are geometric errors, machine tool repeatability and thermal errors.

Probe system: Probe system will usually have a notable influence on measurement uncertainty. The influence of probing error will depend on type of probe that is used. The factors included in this category are repeatability of probing system (including probing-tool changing and relocation repeatability), various probing parameters (switching speed, force and stylus length etc.) [30] and sampling strategy (number and location of probing points) [48].

Environment: Environmental conditions will have important influence on measurement uncertainty. Temperature here is of extreme importance. Other environmental factor like vibrations can also influence the measurement uncertainty [45].

Workpiece/artefact factors: The workpiece itself has an important influence on measurement uncertainty. These uncertainties relate to properties of the workpiece and measurement interaction with workpiece. Common sources of uncertainty are thermal distortion of workpiece due to the heat loss-taking place during probing when performed intermittently or immediately after machining [50], effect of clamping force [51] and presence of surface contamination [30].

Figure 6 illustrates the categories of factors influencing the uncertainty in OMP performance and further levels of complexity are detailed in Table 1. The factors mentioned in Table 1 are discussed in-depth in the subsequent sections of this chapter. It can be pointed out that not all factors are of equal importance in every application and it is possible that in most circumstances a few of these error sources will outweigh the others. Effects of thermal errors are normally significant, contributing more than 50% of total machine error [18]. Also, the uncompensated rigid body errors of the machine tool are important.

Based on the effectiveness of uncertainty factors in thermal error model correction, they are further short listed and utilized in probing system uncertainty model.

2.1 Sources of uncertainty in On-Machine Probing

During the probing operation, the machine tool axes carry the probe. Therefore, the measurement data that it takes inevitably includes the probing errors and those originating from the inaccuracies of a machine tool as well as any deviation in the part or artefact being measured. Each of these error sources must be understood and evaluated to be able to establish a measurement with a stated uncertainty. This section describes the sources of uncertainty in OMP in detail.

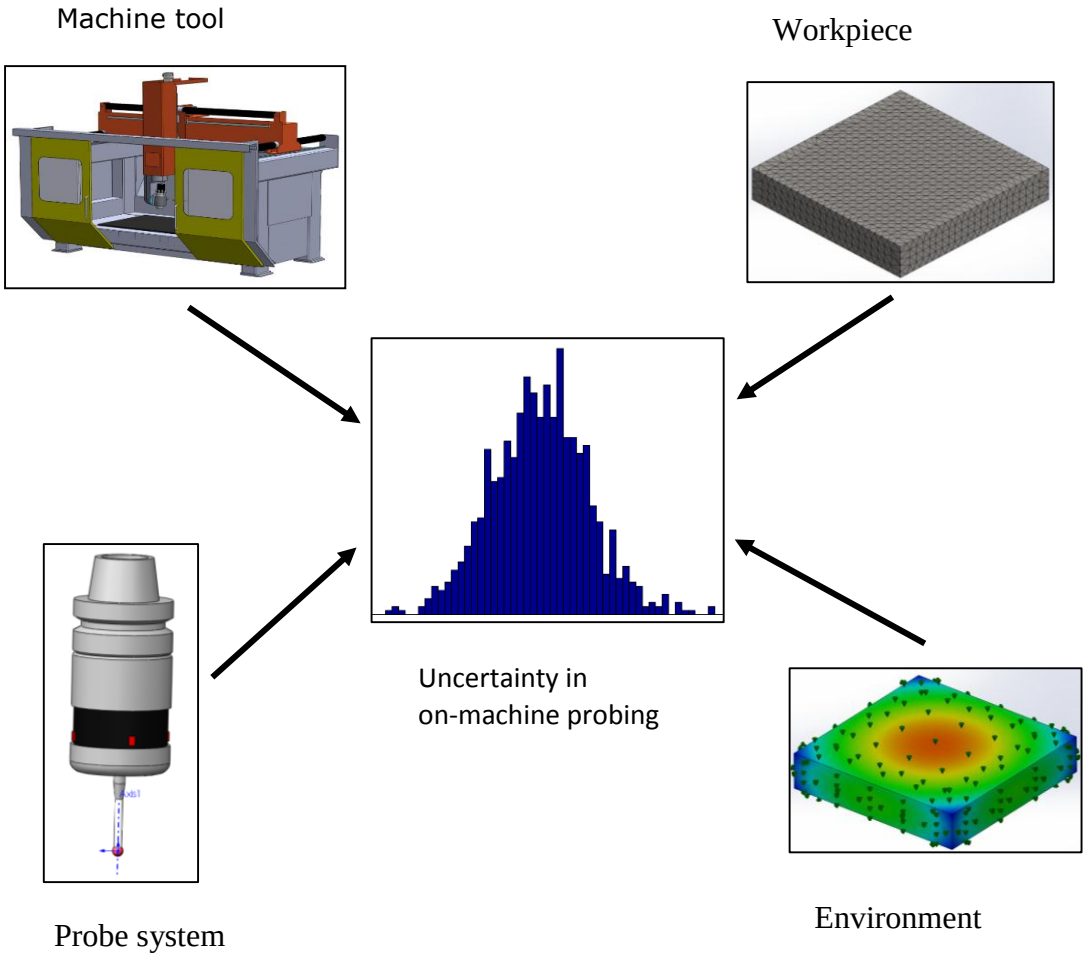

Figure 6 Categories of factors influencing the performance of the on-machine probing

Category	Factors
Machine tool	Geometric errors
	Machine tool repeatability
	Thermal errors
Probe system	Probe qualification
	Repeatability of probing system, including Probing-tool changing and relocation repeatability
	Time delay and time delay variation
	Pre-travel variation
	Over travel distance
	Switching speed and force
	Stylus length
	Number and location of probing points
Environment	Temperature
	Vibration
Workpiece/Artefact factors	Workpiece/artefact thermal distortion
	Surface contamination
	Fixture distortion

Table 1 Factors influencing the measurement performance of the on-machine probing system

2.1.1 Machine tool

Errors originating from machine tool that influences the OMP operation are further categorised into geometric errors, thermal errors and machine tool repeatability.

2.1.1.1 Geometric errors and machine tool repeatability

Uncompensated machine tool rigid body geometric errors are one of the important sources of error. For each linear axis, six functions of axis position are required: position error along the axis, straightness in the two orthogonal directions and three angular errors namely roll, pitch and yaw as well as out of squareness value for each axis pair. Thus giving a total of 21 error components for a three axis Cartesian machine tool [8]. The introduction of the rotary axis would require a similar set of six functions and additional two squareness parameters.

While all the parameters mentioned above can be measured, the calibration process is time consuming depending on the size of the machine tool, in the order of a week or more and requires skilled personnel [52].

2.1.1.2 Thermal errors

Thermal errors can contribute more than 50% of the total machine error [16-18]. They are caused by the thermo-elastic deformation in the machine structure and results in geometric inaccuracies of the work-piece. Non-linear thermal expansion of the structural elements caused by the thermal gradient produces an intricate interaction between tool and workpiece. Different heat sources combined with a different mechanism of heat transfer causes the temperature distribution of a machine tool to change in time. As a result, the relative position and orientation of a tool with respect to the workpiece table changes in time and with axis position, since the materials commonly used (for e.g. steel, aluminium, etc.) expand and /or bend with temperature (gradient) rise. These thermally induced errors can deteriorate the positioning accuracy of machine tools leading to the geometrical deviations of manufactured workpiece. Thermal deformation of the machine tool and consequent changes in accuracy arising as a result of this constitute a major problem [19].

Thermal errors are usually categorised as deriving from internal and external heat sources. Internal heat sources are often the major contributors, which are typically motors, belts drives, spindle bearings, gear boxes, hydraulic systems, etc. [20]. Examples of external heat sources include heat generated by the machining process, machine electric components, cabling and cabinets, other machines, workshop heating, etc., [21]. Also, daily day and night temperature fluctuations create a variable response of the machine structure, temperature variations particularly affecting multi-shift production [12]. Environmental influences cause slow variations of machine tool temperature but affect the whole volumetric performance. Internal influences lead to a local deformation of the machine tool structure, which changes the volumetric performance partially. Displacements caused by internal heat sources are less predictable and can change faster than those caused by the environment [18].

Thermal errors are the major source of error among the various sources of error in machine tool accuracy. Reducing these errors is the key to improve the CNC machine accuracy [19]. Review of thermal error modelling techniques is performed in section 2.4.

2.1.2 Probing system errors

Apart from machine tool errors, probing systems can have a significant effect on the uncertainty of on-machine probing as the probe is an integral part of the measurements system. The main influences on the performance of the probing system are repeatability of probing system [35], including Probing-tool changing and relocation repeatability [34], probe qualification, time delay and time delay variation, switching speed and force, pre-travel variation, stylus length and number of probing points [30].

2.1.3 Environment errors

Every measurement is influenced by the environmental temperature change and vibration [52]. In case of on-machine probing, machine is in static condition at the time of probe measurement. Thus, influence of machine vibration can be neglected [45].

2.1.4 Workpiece/artefact errors

These errors originate from properties of the workpiece material and measurement interaction with the workpiece.

2.1.4.1 Fixture-workpiece distortion

Fixture distortion, in this case, means distortion of the workpiece induced by the clamping forces. This distortion results in the workpiece dimensional error. For every combination of machine, cutting tool and workpiece material, selection of suitable clamping force is essential. The clamping mechanism should hold the workpiece in its position while machining is taking place without causing permanent distortion to it [53].

The errors originating from clamping force essentially comes from three aspects. Firstly, the insufficient clamping force can cause the workpiece to slip and vibrate during machining, resulting in error, and can potentially damage workpiece and cutting tool. Secondly, improper clamping procedures and uneven clamping forces can shift the workpiece from its ideal position, consequently introducing the further error. Thirdly, the clamping force can elastically deform the workpiece. Thus, after the machining when the force is released, due to the spring back deformation phenomenon, the part can get measured inaccurately.

Whereas, under the clamped condition part might be measured with required accuracy [51, 54].

2.1.4.2 Workpiece/artefact thermal distortion during machining

The mechanical and thermal loads affect a workpiece geometric shape and properties during metal cutting operation [55]. During the machining operation, high temperatures are generated, depending on the cutting parameters and material, at the interface between cutting tool and the workpiece due to the plastic deformation and friction. This heat generation influences the material's properties and cutting force [56]. The temperature can reach up to 1000 ^{o}C in the cutting zone, while tool-chip interface experiences the maximum temperature [57].

Most of the heat flows with chip while 10-25 % of the heat generated is conducted into the workpiece [58]. The process induced heat produces high temperature in the workpiece (>100 ^{O}C) with inhomogeneous temperature distribution. In addition, the heat induced into the workpiece is different for roughing and finishing operations. The heat induced during the finishing process is three times the roughing process. Due to the high thermal gradients, movement of heat sources and poor accessibility of the workpiece, it is difficult to measure the temperatures during the machining process [50].

During the on-machine probing measurement, cutting tool is replaced by the probe [26]. Thus, no more heat is induced in the workpiece. In fact, while probing is taking place, workpiece is loosing the heat to the surrounding due to the temperature difference and causing the distortion of the workpiece. Affected by the number of probing points and strategy used, this can introduce an uncertainty in OMP. The more the number points and complex the strategy, it is going to take longer time to complete the probing routine, resulting in more distortion of the workpiece and vice versa.

2.1.4.3 Surface contamination

The contamination of the surface due to the swarf (thin metal chips produced during machining) and coolant can have an influence on the measurement of OMP [34]. The presence of contamination can be falsely regarded as a workpiece or artefact itself, resulting in a distorted readings. Hence, the surface to be measured should be clean to avoid any

deviation in the OMP results. During the machining coolant is often used, it helps to clean the surface of any swarf and dust particles but traces of coolant remain on the surface [30]. One way to make sure reliable surface detection for on-machine measurement is to clean the surface manually. However, this is a time consuming, cumbersome and non-automated process.

2.2 Displacement sensor

Displacement is one of the fundamental variables which are required to be measured, indicated, transmitted or controlled in many industries or scientific fields for various applications. Displacement sensors can, therefore, be used to detect a range of measurands such as deformation, distortion, thermal expansion, vibration, strain, mechanical shock and much more [59-61]. Several physical properties are utilized in different types of displacement transducers [62, 63]. Some of the commonly commercially available sensors are based upon capacitance [64], induction, eddy current [65], linear variable differential transformers (LVDT) [66], optical interferometry [67], optical linear encoders [68], laser triangulation [69], confocal principle [70], etc. Often the measuring range, resolution, bandwidth, etc. can vary significantly even for sensors utilising the same physical properties either due to the sensor design or the signal conditioning. It is, therefore, difficult to give precise general descriptions of their capabilities as a generalisation. However, some example values can be provided based on a review of specification sheets and values in the review article by Fleming [71].

2.2.1 Review of commonly used technologies

Capacitive sensors have a typical measurement range of 10 µm to 10 mm with a resolution in the order of 1 nm. Eddy current sensors typically have a linear range of 100 µm to 80 mm and resolution in the order of 10 nm. Interferometers (excluding those designed for short range surface measurement) can operate over several metres and typically have a resolution of 1 nm. LVDT's usually operate over 0.5 mm to 500 mm with a resolution of 5 nm [71]. Optical sensors based on the laser triangulation principle generally have a measuring range of few millimetres and a resolution of 0.005 % of Full Scale Output (FSO) [72]. Laser confocal sensors have a typical measurement range of 0.3 mm to 30 mm with a resolution of 0.004% of FSO [73].

Capacitive sensors are relatively simple in construction and provide the highest resolution over short ranges. However, they are sensitive to the surface irregularities, variations in humidity and temperature. Also, their performance is affected by the contamination of interfacial fluid (air in most cases) which is important in industrial environments where clean measuring surfaces and environments cannot be guaranteed [74]. Eddy current sensors are insensitive to dirt, dust, oil and moisture/coolant and can be used with all electrically conductive materials [75] but are more sensitive to temperature than capacitive sensors [76]. Inductive sensors have also been developed, but nanometric resolution remains difficult to reach because of magnetic disturbances and variability in the subsurface material causing electrical run-out. LVDT sensors are among the most popular in industrial applications. They are simple and hence robust, have a high intrinsic linearity and can be magnetically shielded. However, their maximum resolution is limited by the physical construction of the transducer which is generally suited to ranges greater than 1 mm [71].

Compared to other sensor technologies, laser interferometers and optical linear encoders provide a good solution in terms of nanometre resolution over longer distances such as a few metres of range. Nevertheless their price, complexity of installation, alignment and relatively large space requirement for operation can be prohibitive in many applications [77]. The triangulation based optical displacement sensor operation is dependent upon the surface texture (energy reflectance characteristics of surfaces being examined) of the target [78] and the sensor head is relatively large compared to other systems due to the integrated electronics and optical detector. They have also been found to have significant issues of self-heating, requiring periods of tens of minutes to achieve thermal equilibrium. The laser confocal sensor requires a clean environment in the optical path for accurate operation.

Sensors are also fundamental in closed loop control systems. The capability to develop integrated and compact apparatus is still a key point for most measurement and control systems [79]. It is, therefore, imperative that they are robust to self-induced or unwanted exogenous influences.

Optical sensors are particularly useful in a number of applications since they are often relatively immune to various perturbations like stray electromagnetic effect, capacitive effect, etc., which are observed in many non-optical sensors [73, 80]. However, such systems can be affected by thermal distortion (misalignment of optical receivers) [61] or contamination by ambient light [81]. They must, therefore, be fully evaluated before being

applied to measurement or control problems. Fibre Bragg Grating (FBG) displacement sensors are receiving more attention owing to all the inherent advantages of optical fibre [82] and due to the advantages such as wavelength encoded information, they offer immunity against power source fluctuations as well as insusceptible to noise caused by variations in light levels [83]. However, the cost of interrogation systems for FBG sensors is very high. In addition, temperature compensation is required for pure displacement measurement applications, increasing the complexity of the system [84].

2.2.2 Research into low cost solution

A significant amount of research has been carried out to develop sensors or measurement systems combining the advantages of simplicity, high resolution and low price. Low-level technological barriers can be rapidly addressed by making adapted use of mass-produced components for consumer electronics. Due to the various advantages discussed above, low cost optical sensors have been investigated for use for displacement measurement. For example, Delmas [85] proposed a system where the displacement of a moving stem is measured by an optoelectronic displacement measuring sensor consisting of a light source (Light Emitting Diode) and light sensitive sensor (Photodiode). A similar optoelectronic displacement sensor has been designed for the absolute measurement of displacement in the micrometre range [86].

A significant amount of research has been carried out to develop sensors or measurement systems combining the advantages of simplicity, high resolution and low price. Low-level technological barriers can be rapidly addressed by making adapted use of mass-produced components for consumer electronics. Due to the various advantages discussed above, low cost optical sensors have been investigated for use for displacement measurement. For example, Delmas [85] proposed a system where the displacement of a moving stem is measured by an optoelectronic displacement measuring sensor consisting of a light source (Light Emitting Diode) and light sensitive sensor (Photodiode). A similar optoelectronic displacement sensor has been designed for the absolute measurement of displacement in the micrometre range [86].

Shan et al. [87] evaluated the performance of a low cost reflective IR (focussed and non-focussed) sensor for measurement of a ± 200 μm range and found that its performance (focussed) was comparable with the commercially available inductive sensor in terms of linear distortion, range and bandwidth. The unfiltered resolution of the IR sensor was within

sub-microlevel range but the specific value was not quoted. The observed maximum sensitivity was 0.010 V/μm and 0.002 V/μm for non-focussed and focussed IR sensors respectively. This type of sensor requires sufficiently large reflective target size (at least twice the lens surface area for focussed sensor and six times for non-focussed). The performance of the reflective sensor based on the intensity of the back scattered IR light is dependent on the reflectance of the surrounding object and can produce imprecise results [88] and requires more complex techniques such as phase shift measurement and triangulation for range measurement. Lin et al. [81] used a single transmissive IR photo-interrupter (with collimated lenses in front of source and collector) with knife edge to develop a displacement sensor with a range greater than 100 μm and the experimentally obtained maximum sensitivity was 0.2 V/μm. To lower the effect of the thermal expansion of the steel knife-edge, another block of aluminium coated silica was prepared, but the experimental results of use of this new block were not mentioned.

The effects of ambient light variation have not been considered in the evaluation of Shan et al [87], or Lin et al [81], where the entire setup was covered in opaque box with external lights turned off. In an industrial environment, variation in ambient light conditions is inevitable unless uninterrupted guarding is present, so it is necessary to study its impact on the output of the sensor. Neither paper reported the effects of environmental temperature fluctuations or the long-term stability of the sensor.

2.3 Machine tool structural monitoring system and sensor data fusion

The primary goal of the machine tool is to automate the cutting process to achieve higher accuracy to meet the greater quality requirements. Several factors play a crucial role such as machining conditions, cutting tool, type of workpiece etc. Various sources of error like shifting mass, component weight, temperature etc., hinder the possibility of achieving strict accuracy demands for the manufacturing process. Errors arise during building of the machine or occur over the time [10, 89]. Error reduction requires greater understanding of the machine tool capabilities and error sources. This results in the need for a machine tool structural monitoring system. Studies have been carried out on monitoring techniques that are based on the application of single or multiple sensors [90, 91]. Application of different sensors provides the ability to detect a wide range of system parameters like temperature, displacement, strain etc.

Sensor fusion provides the complete outlook of the process, thus, state of the machine [91] delivering more reliable and accurate information. For example, by observing the change in the strain of the structure with respect to variation in temperature provides the response of the system, which would be difficult to obtain by simply monitoring either strain or temperature; change in strain can derive from several causes while explicit prediction of distribution from temperature is a major challenge. Synergetic combination of data available from multiple sensors is called sensor fusion [92]. Varieties of techniques are used for sensor fusion such as Kalman filter, algebraic functions, weighted average, Bayesian estimation etc. [92, 93]. For high performance operational systems neural network [94, 95] and fuzzy logic [96, 97] techniques are applied for fusion purposes.

Developing data acquisition software (DAQ) for machine tool monitoring sensor fusion is a major challenge. At the moment, any commercial sensor in the market has either some application provided by manufacturer or open source software for capturing and/or analysing data. There is no general DAQ software available for this purpose. Software provided by manufacturers has restricted usage for research application. They often lack the flexibility and extensibility required for research.

Fusion of sensor data is an indirect method. It involves feeding of numerous sensor signals into the fusion model. Fusion model is fundamentally a function developed to extract corroborative and relevant information on the state of the manufacturing operation. In machining, application of sensor fusion is inspired from the perspective where sensors can be used that can operate reliably in an industrial environment. Each can sensor can sense a different variable with different correlation efficiency and their effective and cooperative fusion is expected to produce better estimation result [95].

2.4 Review of analytical methods for thermal error modelling

With increased global competition, the manufacturing sector is vigorously working on enhancing the efficiency of manufacturing processes in terms of quality and cost. Consistent product quality is important for both machine tool manufacturers and end users. To improve this quality, the stability and accuracy of the machine tools needs to be enhanced. Machining accuracy is chiefly governed by the relative position between cutting tool and nominal workpiece and this directly affects the dimensional accuracy of machined parts [18]. The main causes of errors in manufactured workpiece are low static stiffens of

the machine structure, low dynamic performance of the feed drives, tool wear and thermal deformation of the tool, machine and workpiece [17, 98].

Thermal errors can contribute more than 50 % of the total machine errors [16] and with effective compensation of other error sources, this percentage can be much higher. Thermally induced deformations in machine tools leads to varying displacements between tool and workpiece [89]. A non-uniform temperature distribution increases the complexity of thermal errors in CNC machine tool; this distribution becomes non-linear and non-stationary and varies with time. The mutual coupling of the strength of the heat sources and different heat transfer and expansion coefficients of various components of a machine tool structure create complex thermal characteristics [99]. Thermal deformations are determined by not only the instantaneous thermal environment, but also the previous thermal status of the machine tool. This thermal memorizing phenomenon leads to a hysteresis effect [12] can reduce the robustness of the static modelling approach, and thus compensation of the error [100].

According to available literature, various methods have been employed for characterising the thermal performance of the machine, e.g., finite element analysis (FEA) [101], multiple regression analysis (MRA) [102], fuzzy expert system [103], artificial neural networks (ANNs), adaptive neuro-fuzzy inference system (ANFIS) [104] etc.

The use of **FEA technique** for thermal characterisation of the machine tool is well-established. In FEA method, machine structure is divided into smaller elements and each element is subjected to heat flow. Standard heat flow equations (convection, conduction and radiation) are used to estimate the thermal behaviour. Each element is exhibits thermal effect on its neighbours, leading to overall estimate of the structure [20].

FEA has been efficiently used for thermal error estimation and reduction from 70 μm to 10 μm for a production machine and FEA results were closely correlated (65% to 90%) to the experimental results for various tests [101]. In another study, thermal error compensation accuracy of 80% was achieved using FEA [105].

However, building a numerical model can be a great challenge due to the problems of establishing the boundary conditions, structural complexity of the machine geometry, and accurately obtaining the characteristics of heat transfer. This requires testing of the machine tool for successful application of the technique. Thus, developing these models can be time

consuming, expensive and in some cases practically unfeasible for real-world machines [82].

The **MRA technique** is a statistical modelling method to establish a relation between input variable (temperature, mechanical strain etc.) and resultant output variable (thermal displacement of the machine tool). Multiple Linear regression (MLR) is the simplest technique, least-square and least absolute deviation approach is used by Miao et. al. [102], to develop a thermal error models. The least-square (LS-MLR) technique is more mature in terms of theory and is commonly used in practical applications. The least absolute deviation (LA-MLR) method is comparatively less susceptible to outliers, thus, is a more robust technique. But, LA-MLR is an computationally intensive process. However, performance of LS-MLR was found to be more superior to LA-MLR for well-managed data in the case of large quantity of data [102].

Although, MRA can provide reasonable results for a particular test regime, thermal errors are stochastic in nature and can change with variation in machining process, and environmental conditions, thus, resulting in an erroneous model output.

Fuzzy inference systems (FIS) can be used in a situation where there is sufficient knowledge available about the system and that knowledge is intended to be added into the model. These systems are called 'white box', since the model designer can explicitly determine how the model achieved its goal. The membership functions are usually manually tuned by trial and error approach [103] based on the experience of experts. Fuzzy models are easy to understand, since, they are based on natural language. Also, they have good extrapolation capability.

Nonetheless, there are no standard methods to transform expert knowledge into fuzzy models. Compared to neural networks they have poor generalization capability. In addition, FIS are prone to a loss of accuracy due to engineering judgements, since, they are based on expert knowledge [106].

ANNs have the ability to learn from the available data rather than assumptions based on expert knowledge. Models can be developed with minimal system information. They are called 'black box', since, there is no information available regarding the method by which the goal is achieved. ANNs have better generalisation capability than FIS [106].

A number of methods have been derived from the working principals of ANNs and used for machine tool thermal error modelling. Feed forward neural networks (FNN). Integrated recurrent neural network (IRNN), hybrid networks, back propagation network (BPN) and cerebellar model articulation controller networks (CMAC) etc. Chen [107] implemented FNN to measure and compensate thermally induced errors of the spindle and leadscrew. The experimental results showed more than 85% thermal errors can be reduced after compensation. Yang et. al. [108] developed an IRNN to track non-linear time varying machine tool error under varying thermal conditions. IRNN could predict 80% maximum thermal error with maximum residual error less than 15 μm due to spindle rotation. Yang et. al. [109] proposed a CMAC neural network for spindle drift error. This model showed insensitivity to sensor placement and robustness to sensor failure compared to MRA.

The research based on NNs has revealed good prediction accuracy and creation of robust models for the validation exercises reported. It can also be determined that NN models can be created by finding temperature key points without knowledge of the actual structure. Thus, ANN was selected for thermal error modelling in this study [20].

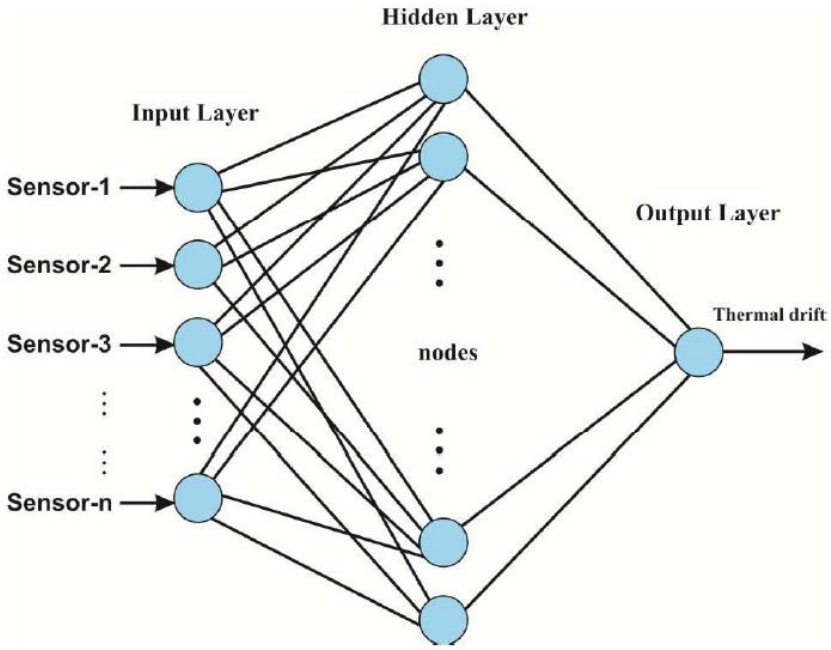

Figure 7. Basic ANN architecture [110]

Nevertheless, for reliable prediction model, sensor must be robust and should be placed strategically. Also, there is no deterministic approach available to find NN parameters

(number of hidden layers, number of nodes in hidden layers etc.). Since, it's a 'black box' approach, obtained optimal solution can exhibit unrealistic characteristics that might not extrapolate in other situations [110].

Figure 7 demonstrates the basic architecture of the ANN. The detail design steps for ANN are shown in Figure 9. In Figure 9, R stands for correlation coefficient between measured output and predicted output.

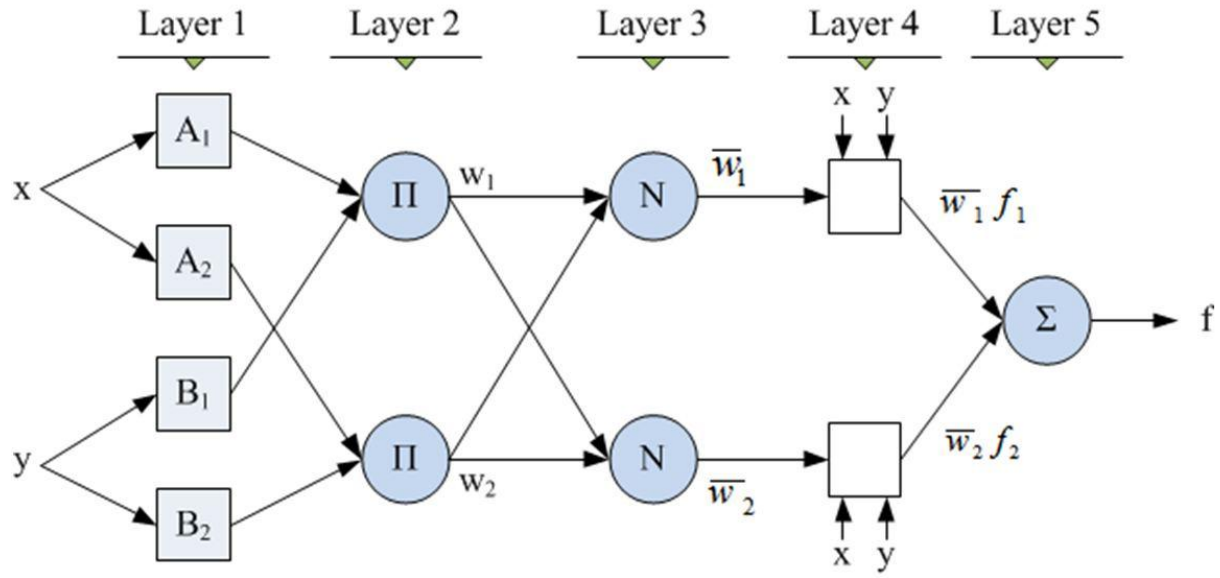

Figure 8. Basic ANFIS architecture [111]

The **ANFIS** is an Adaptive Neuro-Fuzzy Inference System that utilises fuzzy system and neural network in the same system. The ANN is used to optimise the fuzzy parameters, thus, allowing the model to learn from training set of data. The model designer can evaluate the solution mapped out by the FIS, consequently, permitting a realistic representation of the system [111]. The nodes and hidden layers are determined precisely FIS in the ANFIS network, therefore, eliminating the well-known difficulty in the modelling of ANN of defining hidden layers and improving forecasting capability. However, number of fuzzy rules increases exponentially when number of input variables rises, thus, creating a computational burden [112].

Figure 8 shows the basic ANFIS architecture. The detail design steps for ANFIS are shown in Figure 10.

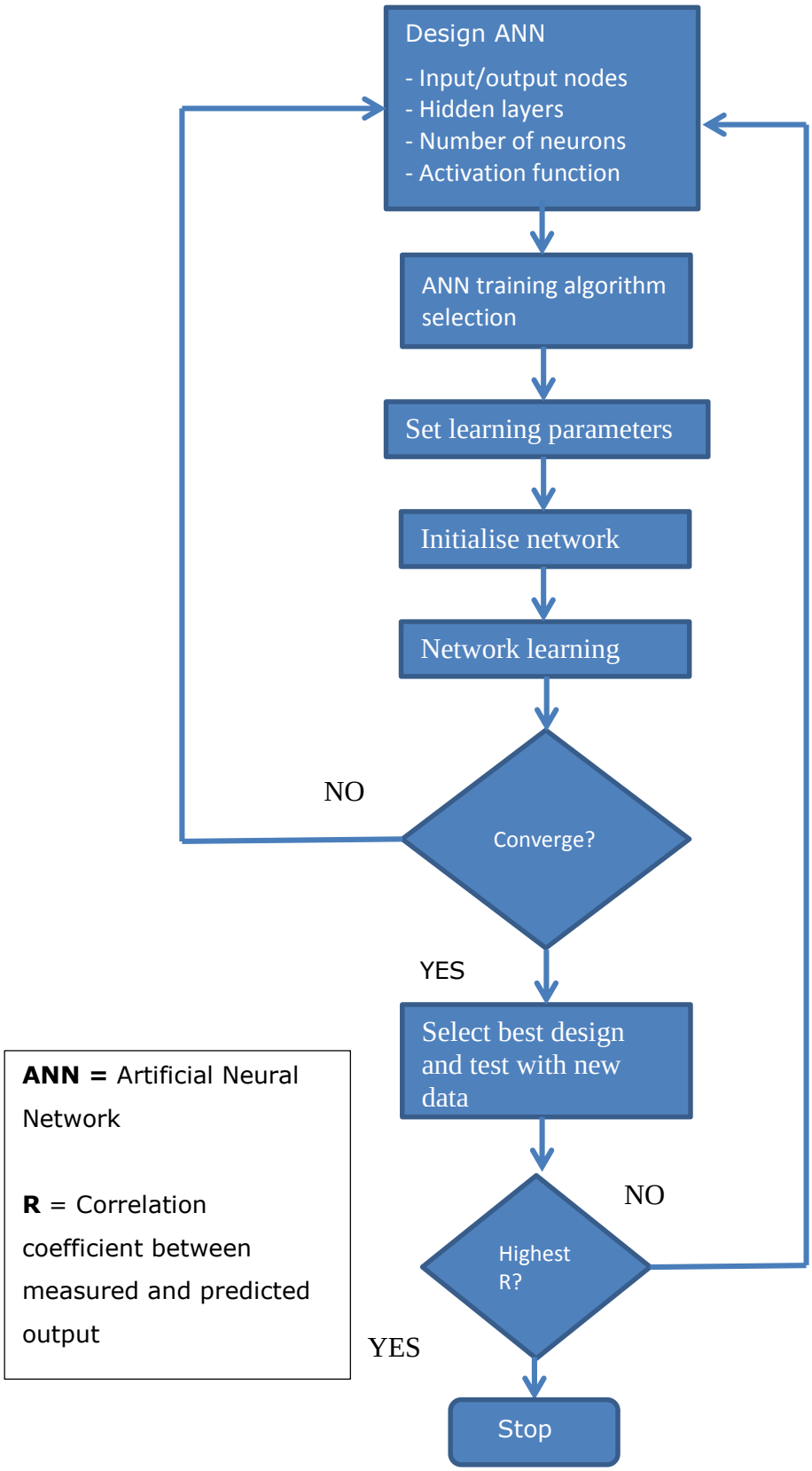

Figure 9. Design steps for ideal ANN model

Thus, based on the literature study, ANN and ANFIS techniques were deemed suitable for the thermal error analysis and reduction.

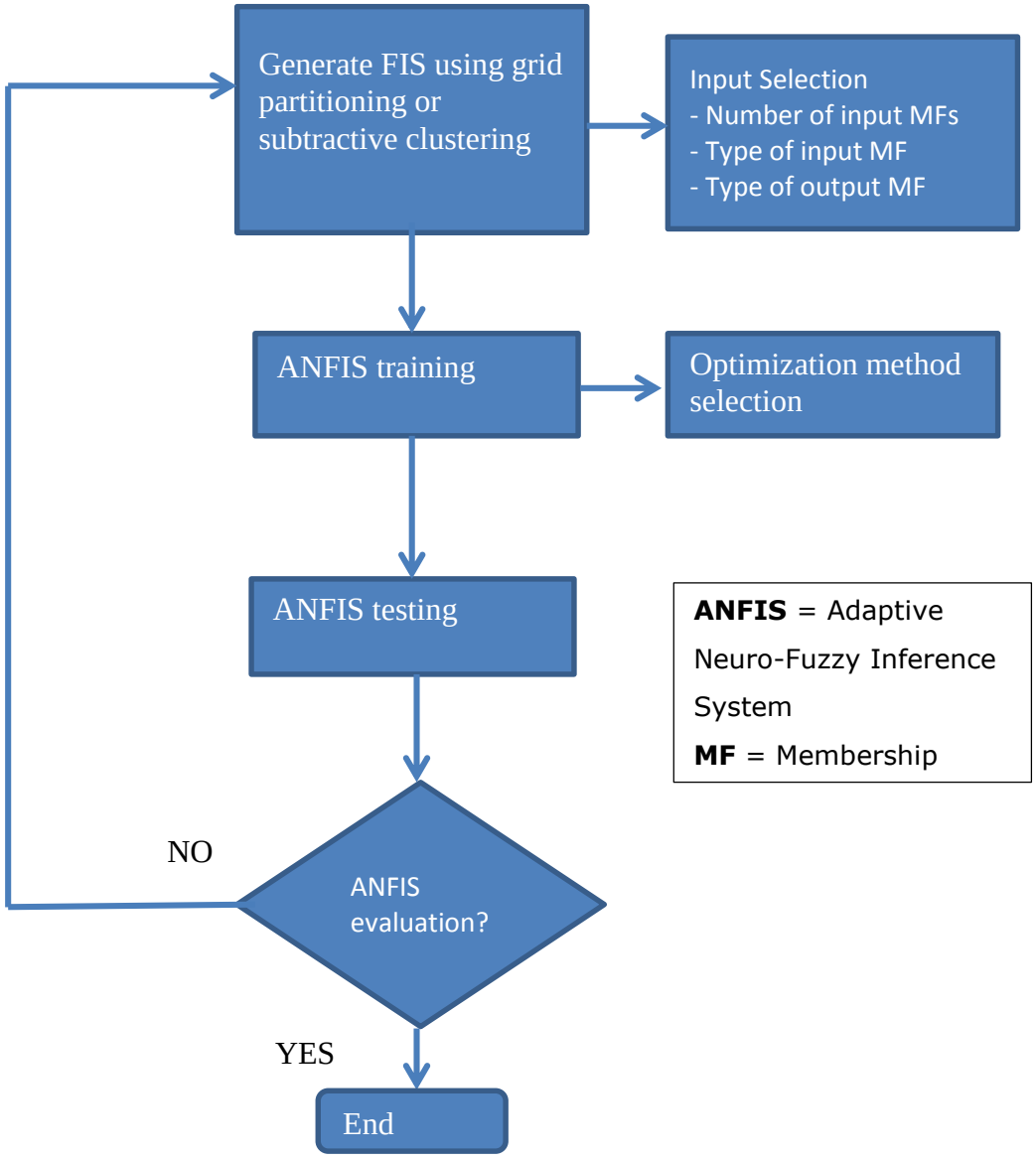

Figure 10. Design steps for ideal ANFIS model

2.5 Methodology

To achieve the aims and objectives set in the thesis, a methodology based on literature study and experimental design is developed.

Various sources of uncertainty for on-machine probing are investigated in section 2.1 and are broadly classified into four categories: machine tool, probe system, environment and workpiece/artefact factors. To evaluate each of the uncertainty categories, they are further sub-divided at a granular level.

In **Chapter 3**, a series of experiments and simulations are designed to estimate the magnitude of uncertainty contributors. To study the **errors originating from the machine tool**, geometric and thermal errors, a 3-axis c-type machine, with axis travel of X= 500 mm, Y=400 mm, and Z=300mm, is selected to carry out the experiments. This machine was chosen because it represents a large proportion of the manufacturing machine tool base. It was also readily available for experimentation.

Since probe is carried by the machine tool for the OMP application, data obtained from the probing operation is contaminated by the errors originating from machine tool axes. Thus, it is necessary to evaluate the machine tool errors.

To evaluate geometric error, experiments based on international standards such as the ISO230 series, were designed and executed at a nominally constant temperature. Thermal errors are investigated by inducing heat by oscillating the machine axes at various feed rates to simulate machining. Temperature is measured by thermal sensors and the resultant distortion is measured by a standard OEM probe routine.

To understand the influence of the **probe system errors**, tests are designed to analyse probe repeatability, and probe-tool changing and relocation repeatability. Tests are performed on several machines by probing the centre of the top surface of a workpiece 10 times. For probe tool relocation repeatability, the same test is conducted but this time the probe is removed from the turret and replaced again. By testing on separate machines, the influence of the probe alone can be deduced.

The errors of a calibrated probe can be compensated if they have a specific known value. These include: stylus length, speed and particular probing direction, other factors such as pre-travel variation, time delay and time delay variation.

The effect of **environmental** temperature changes on OMP is evaluated by keeping the machine stationary and probing the test spheres at regular intervals. During on-machine probing, if the probing speed is consistent then the influence of machine vibration can be neglected.

For errors originating from **workpiece factors**, finite element analysis (FEA) simulations using SolidWorks are designed to study distortion caused by clamping force and thermal loading while machining. According to available literature, FEA is a well-established technique, and its application to machine design and analysis is well-accepted. Therefore, further validation with experiments is not considered. Experiment is designed to understand the influence of workpiece surface contamination on OMP using coolant of different viscosity by varying its concentration.

Thermal distortion is a problem on machine tools because large parts of the structure are not covered by the feedback loop. To overcome this, many researchers use temperature measurement and estimate the resultant distortion for machine members outside this loop. However, this approach results in inaccuracies because of thermal hysteresis, assumptions regarding thermal coefficients etc. Another solution is directly monitoring the distortion. However, this approach is difficult or expensive.

Synergetic combination of data available from multiple sensors is called sensor fusion. Sensor fusion culminates in a more holistic view of the process and in turn the state of the machine. Different signals have different correlation efficiency and their effective and cooperative fusion is expected to produce better estimation result. By observing the change in the strain of the structure with respect to variation in temperature provides the response of the system, which would be difficult to obtain by simply monitoring either strain or temperature; change in strain can derive from several causes while explicit prediction of distribution from temperature is a major challenge. In the current work, data is acquired from two sources: temperature sensors for temperature measurement and Fibre Bragg Grating (FBG) sensors or the newly developed sensor for strain measurement.

In **Chapter 4**, a novel displacement sensor is developed for sensor data fusion to reduce uncertainty of on-machine probing. Various tests are performed to characterise this sensor. First, the characteristic curve is calibrated to obtain sensitivity, linear range and non-linearity. The repeatability of the sensor is found out by experiments and analysis based on ISO 5725. The resolution of the sensor head is determined by applying a sinusoidal signal with varying amplitude to PZT and measuring the corresponding response of the sensor. Immunity of the sensor against power supply variation is checked by varying the power supply voltage and against ambient light variation by generating strobe light effect using white LED source. To study sensor drift, an experiment is conducted in a temperature-controlled room for 9 hours and thermal response of the sensor is checked by varying the temperature of the room.

In **Chapter 5,** a modular machine tool structural monitoring system is designed and implemented based on LabVIEW. It is developed to facilitate sensor data fusion by acquiring the data from various sensors, as described in Chapter 3, and fuse it using various techniques selected from the literature review. This program is also capable of performing bi-directional communication with the machine controller (Siemens 840Dsl), thus, allowing transfer of error compensation values to the machine controller.

In **Chapter 6**, a multi sensor data fusion model is developed using principal component analysis (PCA) and artificial neural networks (ANN), to reduce the thermal errors. Fibre Bragg Grating (FBG) and temperature sensors were used to train the sensor fusion model. Experiments are performed on the ram of a 5-axis gantry machine. This machine was chosen because its thermal errors are sufficiently large to present the system with a significant challenge.

Chapter 3- Sources of on-machine probing uncertainty

3.1 Sources of uncertainty in On-Machine Probing

During the probing operation, the machine tool axes carry the probe. Therefore, the measurement data that it takes inevitably includes the probing errors and those originating from the inaccuracies of a machine tool as well as any deviation in the part or artefact being measured. Each of these error sources must be understood and evaluated to be able to establish a measurement with a stated uncertainty. This section describes the sources of uncertainty in OMP in detail.

3.1.1 Machine tool

Errors originating from machine tool that influences the OMP operation are further categorised into geometric errors, thermal errors and machine tool repeatability.

3.1.1.1 Geometric errors and machine tool repeatability

In order to understand the geometric errors of the machine tool the parametric errors of the x-axis of the 3-axis machine tool were measured using laser interferometer (Renishaw make). The result of the positional deviation in x-direction is shown in Figure 11.

The measurement of position error showed a considerable error of 14 µm over a 450 mm travel of X-axis. It is likely that the positional deviation can be reduced by recalibrating the machine tool. However, it not possible to eliminate the error. The machine was installed in an industrial environment and the part of the positional deviation can be attributed to the surrounding and machine tool temperature changes.

As it can be observed from Figure 11, the error is not constant along the entire x-axis. Similarly, other parametric errors along the Y and Z-axis will change throughout the travel. Thus, value of all the components of geometric errors will in general vary in the entire volume of the machine. Same can be said about the machine tool axis repeatability, it will vary over the working volume of the machine.

At each location in the working volume of the machine, there will be a distribution of the measured values. Thus, every time the point is measured using the probe in the working space, some value will be drawn from that distribution. This value needs to combined with other uncertainty contributors to give the overall point uncertainty. This point uncertainty has to propagate further through the measurement uncertainty to get the overall uncertainty.

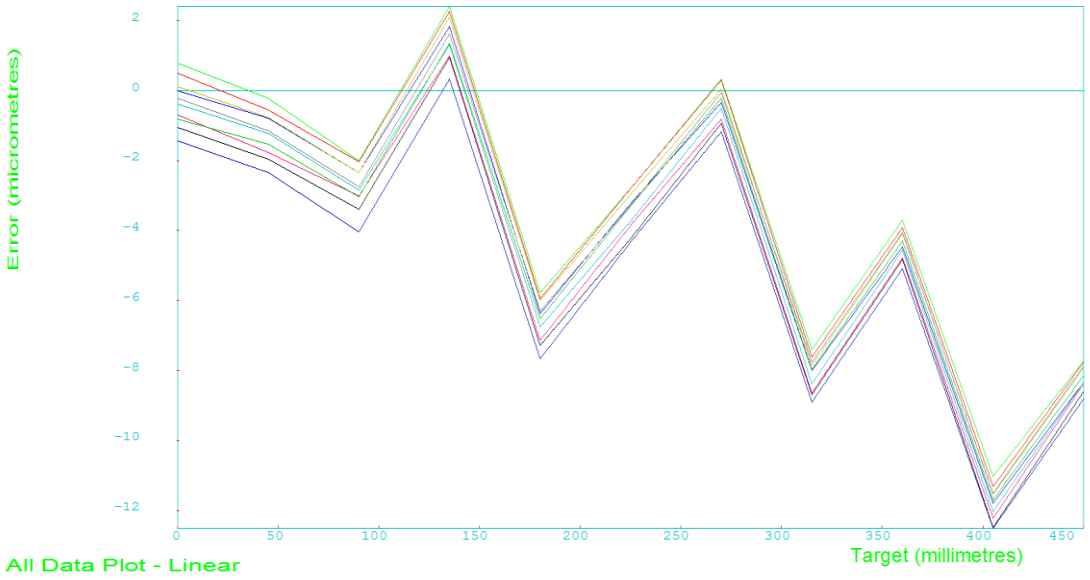

Figure 11 Measurement of position error Exx

3.1.1.2 Thermal errors

Based on literature review, thermal errors play significant role in the accuracy of machine tool. Therefore, They must be reduce. To better understand the thermal errors series of experiments were conducted in a 3-axis machine tool. The schematic of the test setup is shown Figure 12.

Initially thermography was used to obtain the thermal signature estimation of the machine structural elements. The Location of temperature sensors was decided after examining the heat distribution measured using the thermal imaging camera (FLIR ThermaCAM S65) [111], engineering judgement and based on the previously conducted tests.

Total 43 temperature sensors (digital DS18B20 sensors) were used to monitor the thermal distribution of the entire machine structure. Thirteen sensors were attached on spindle carrier, fifteen on the column, two on spindle and seven on three Cartesian axis (axis motor, ballscrew nut and bearing cap). To measure the ambient temperature, six more temperature sensors were placed around the machine.

The above mentioned sensor locations were selected in order to gain the information about thermal status of the machine when any individual axis or combination of axes heating test is performed with or without spindle in operation, and ambient temperature data in varying environmental conditions.

In this section, our objective is to simply evaluate the thermal error rather than to determine the relation between thermal error and corresponding sensitive temperature sensors. Furthermore, various sensor optimization techniques can be utilised, e.g. clustering, FEA, correlation coefficients etc., to reduce the number of temperature sensors for thermal error analysis to reduce the overall system cost and improve the robustness of thermal error modelling. We have used correlation coefficient technique with principle component analysis (PCA) to reduce the number of temperature sensors. This is discussed in detail in chapter 6.

In addition, the test setup consists of four measurement spheres mounted on the table-top in a specific arrangement to measure the thermal error to cover the working volume of the machine that is used in most of the cases on this type of production machine and to isolate X, Y and Z components efficiently.

The touch trigger kinematic probe RMP60 was used for the measurement purpose. Table 2 provides the description of all the sensors and their location.

The tests were carried out for X and Z-axis at 50 and 100 % of their speed at various heating and cooling cycles. Similarly, spindle-heating tests with different speeds and cycles were performed.

Test result for Z-axis heating test is shown Figure 13 and test conditions are given in Table 3 Test condition for Z- axis heating test at 100%Table 3. From Figure 13, it can be observed that the maximum error of 220 µm for sphere 2 in z-direction and similar magnitude of the

error can be seen for sphere 3 and 4. The thermal displacement error is 90 µm for sphere 1. Thus, magnitude of the thermal error in Z-direction is position dependent

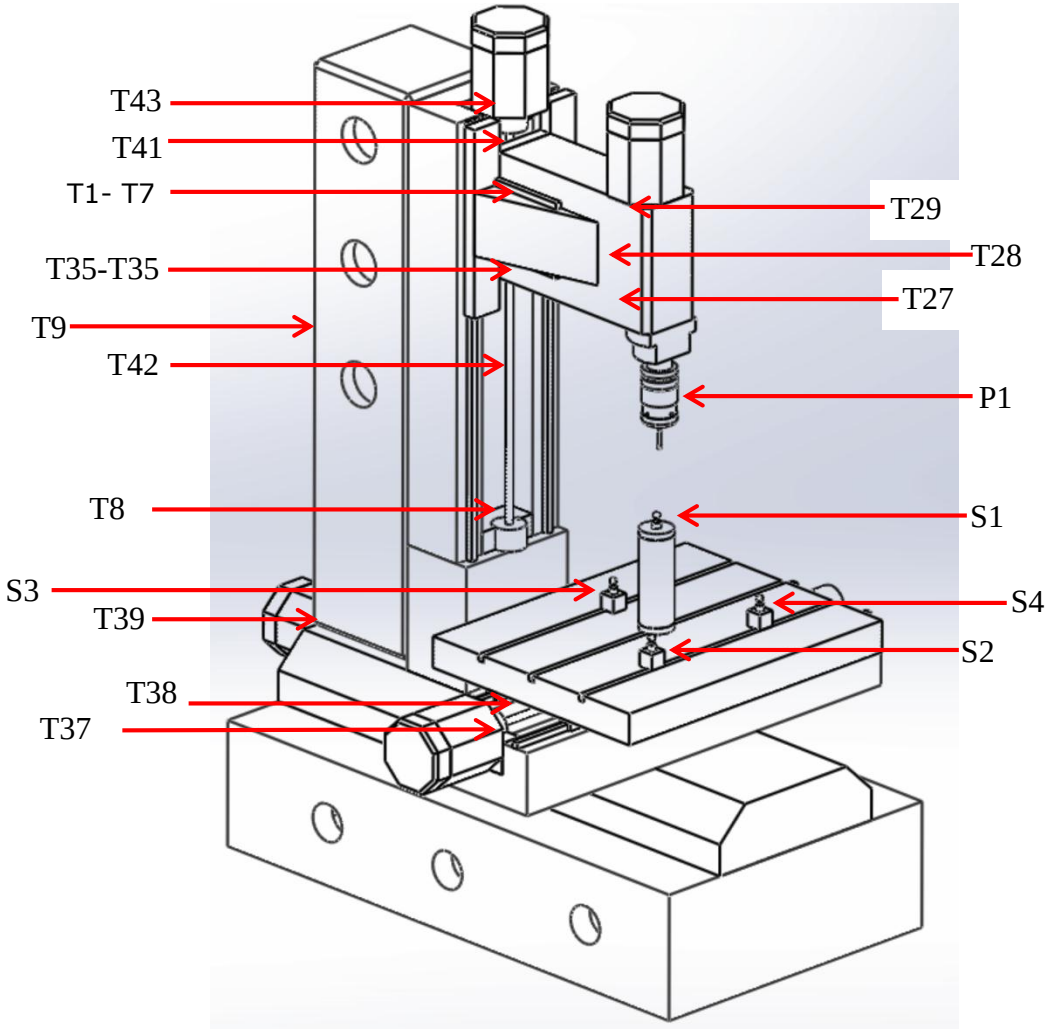

Figure 12 Schematic of the thermal error test setup

Sensors	Location	Function
T1-T7	Carrier temperature sensor strip (bottom)	Carrier surface temperature measurement
T8	Z-axis bearing bottom	Ambient temperature measurement (Z-axis)
T9	Column – Electric panel	Ambient temperature measurement (column/ electric panel)
T10	Column Bolt Bottom	Column surface temperature measurement
T11	Column Bolt Top	Column surface temperature measurement

T12	Column front internal	Column surface temperature measurement
T13	Column front internal	Ambient temperature measurement
T14-T15	Column rear internal	Column surface temperature measurement
T16	Column rear external	Ambient temperature measurement (column)
T17-T21	Column front external	Column surface temperature measurement
T22-T26	Column rear external	Column surface temperature measurement
T27	Spindle front bottom	Spindle temperature measurement
T28	Spindle ambient	Ambient temperature measurement (spindle)
T29	Spindle motor	Spindle temperature measurement
T30-T35	Carrier temperature sensor strip (top)	Carrier surface temperature measurement
T36	Carrier left side	Carrier ambient temperature
T37	X-axis bearing cap	X-axis temperature measurement
T38	X Ballnut	
T39	Y Axis Motor	Y-axis temperature measurement
T40	Y Ballnut	
T41	Z Axis Bearing Cap	Z-axis temperature measurement
T42	Z Ballnut	
T43	Z Motor	
P1	On-machine probe	Thermal deformation measurement in X,Y and Z direction
S1-S4	Top of machine tool table	Measurement spheres

Table 2 Sensor description

Test Conditions				
Cycle	Traverse Speed (%)	Duration(min)	Probes interval(min)	No. of probes
Initial condition	0	30	10	3+1
Heating	100	120	10	12
Cooling	0	60	variable	10+6
Description	1. Initially machine is at rest for 30 mins with probing every 10 mins. 2. During the **Heating cycles** machine performs bidirectional runs along **Z-axis** at **100% (35000mm/min)** speed for 2 hours. Probing is			

	performed every 10 mins 3. Heating cycle is followed by **the cooling cycle** of **1** hour. Probing interval is variable.
Cooling Probing routine	1. 1st 10 continuous probe cycles without any time interval. 2. After 10 continuous cycles, probing after every 5 mins for 6 cycles. 3. Thus total probing cycles during cooling is 10+6=16
Probe Routine	1. Reference probing speed = 800mm/min 2. Measurement probing speed = 30mm/min 3. Total probing cycles = 31

Table 3 Test condition for Z- axis heating test at 100%

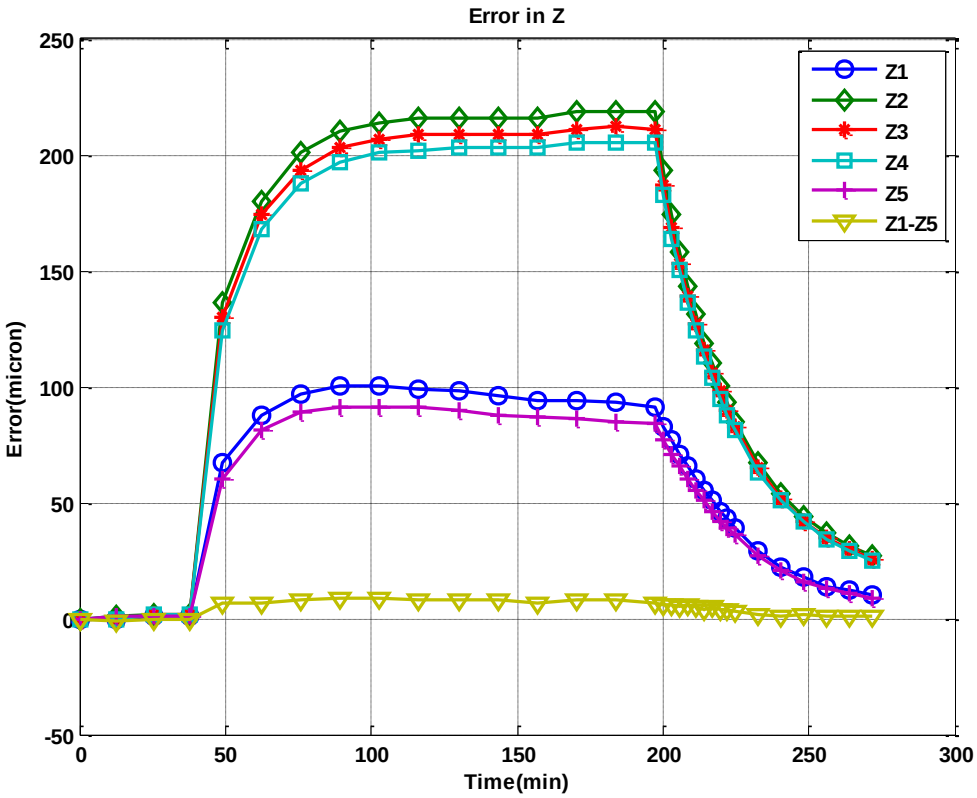

Figure 13 Z-axis heating test at 100 % speed, thermal displacement error in Z-direction

Spheres 2, 3 and 4 are the same height. Whereas, sphere 1 is at higher level than rest of them. Smaller magnitude of the thermal displacement in Z-direction of sphere 1 can be possibly explained the bending phenomenon of Z-axis due to the heat induced into it. Thus, as Z-axis travel in the positive direction error reduces.

When the same test was performed at the 50 % speed, magnitude of the thermal error is reduced for all the spheres. In case of sphere 1 it was found to be 70 µm and for spheres 2, 3 and 4 it was approximately 130 µm.

Similar results were obtained while carrying out the test using X-axis heating. Nonetheless, magnitude of the thermal displacement error is significant as compared to geometric errors. Hence, thermal errors can be considered as the largest contributor of the uncertainty for on-machine probing.

3.1.2 Probing system errors

In this section, errors originating from probing system are studied. The main influences on the performance of the probing system are Repeatability of probing system, including Probing-tool changing and relocation repeatability, probe qualification, time delay and time delay variation, switching speed and force, pre-travel variation, stylus length and number of probing points.

To understand the influence of the probe repeatability test was performed on a 3-axis machine tool using a kinematic touch trigger probe RMP60. The setup is shown in a Figure 15. The centre of the top surface of the workpiece was probed in Z direction 10 times with delay of 1 sec in between. Then the standard deviation of all 10 readings were calculated. It was 0.3 µm.

To understand the effect of the probe-tool changing and relocation repeatability same set up as shown in Figure 12 was used and again 10 readings were measured at top centre of sphere 1. However, this time probe was removed from the spindle turret and replaced again. The repeatability in X and Z was 0.1 µm. and in Y was 0.05 µm.

All other factors can have a significant effect in the case of uncalibrated probe is used for measurement. But, when the probe is calibrated for a particular stylus length, speed and particular probing direction, other factors such as pre-travel variation, time delay and time delay variation can have a specific known value. Thus, they can be compensated.

Number of probing points and their location can introduce a measurement uncertainty, when probing is performed right after the machining due to distortion of the workpiece. This

is discussed in detail in section 2.1.4.2. It is possible to avoid this situation if enough cool down is provided to the workpiece but this can be time consuming and expert knowledge is required to calculate the cool down period for the workpiece.

3.1.3 Environment errors

To understand the influence of environmental temperature on as an uncertainty contributor test was performed using the setup shown in Figure 12. This test was performed right after one of the axis heating tests. For this test machine was in a stationary condition and probing was taking place every 10 mins. Tests results for X-axis thermal displacement error with temperature data is shown Figure 14.

It can be observed from Figure 14 that initially when the temperature is dropping after the heating test thermal error is also reducing for approximately 500 mins. After that when temperature settles down, error is within +/- 1 µm. That means there is a direct correlation between environmental temperature variation and thermal error displacement. Thus, if there are greater variations in environmental temperature, corresponding variations in displacement error can be expected.

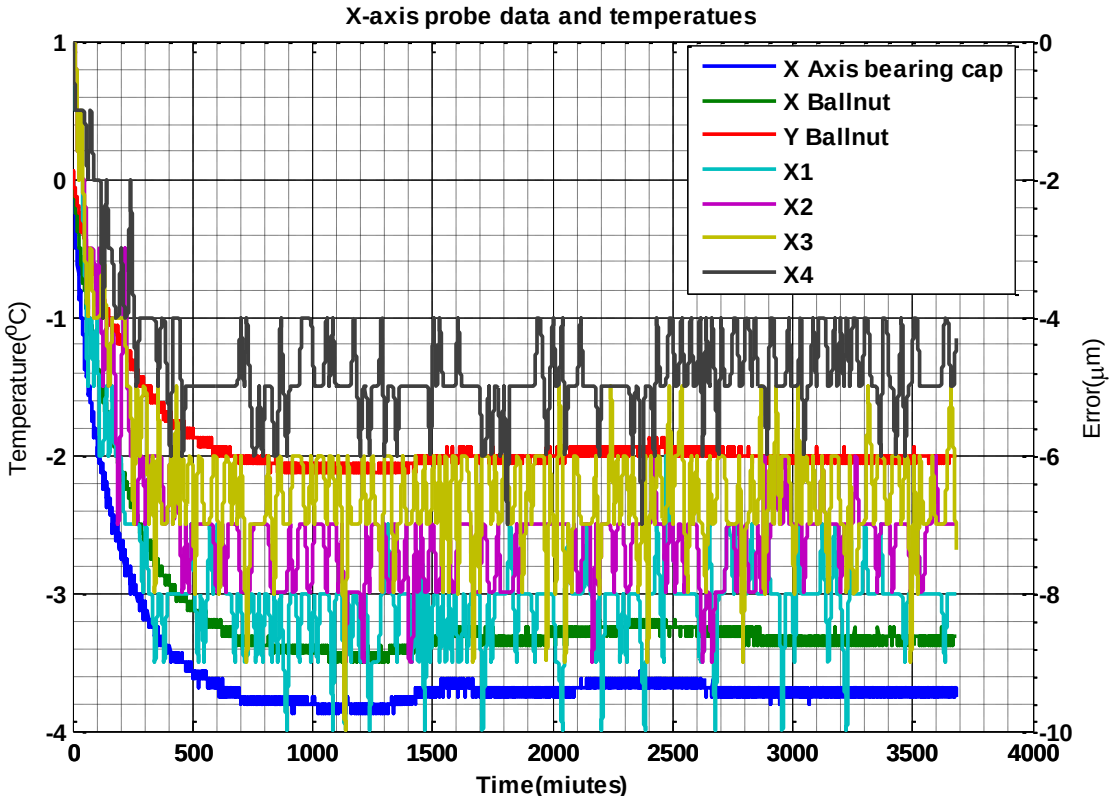

Figure 14 Environmental test, temperature and thermal displacement error

3.1.4 Workpiece/artefact errors

These errors originate from properties of the workpiece material and measurement interaction with the workpiece.

3.1.4.1 Fixture-workpiece distortion

To understand the impact of clamping force on workpiece deformation, a case study was undertaken. Figure 15 shows the clamping mechanism with workpiece before machining.

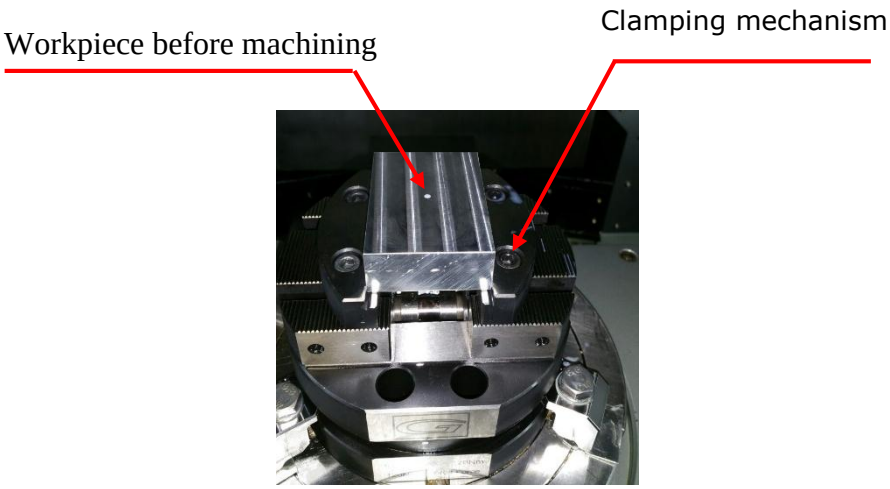

Figure 15 The clamping mechanism with workpiece before machining

In this study, simulation using finite element method (FEM) of different magnitudes of clamping forces on a workpiece with various materials was carried out. SolidWorks 2015 software was used for the purpose of FEM analysis.

There are several off-the-shelf commercial software packages available to perform finite element analysis (FEA), e.g. Abaqus, ANSYS, SolidWorks Simulation etc. Each software has certain advantages and disadvantages over the others in terms of their ability to handle complex geometries, nonlinear analysis capabilities, mesh robustness, boundary condition controls, user-friendly interface, cost of the package, and steepness of the learning curve involved.

In this study, simple geometry (solid block of dimension 200mm x 200mm x 50mm) is used to analyse the structural distortion of a workpiece due to the clamping forces and thermally induced geometric distortion due to the heat generated while machining. The effect of clamping force was investigated by a static linear study.

The influence of thermal distortion was examined by steady state and transient thermal study with nonlinear displacement analysis. A standard mesh was applied for both the cases. (Next section 3.1.4.2)

The criteria for FEA package selection was based on ability to solve simple geometry with linear and nonlinear analysis, automated mesh control, seamless integration of CAD design with FEA module, user-friendly interface, ready availability and easy learning curve.

SolidWorks is a readily CAD design software with integrated SolidWorks Simulation package with FEA capability. Abaqus and ANSYS are capable of solving complex geometries with nonlinear analysis. Since, only simple geometry with rudimentary FEA was required in the study, SoildWorks was seemed suitable for this study. However, investigation of complex geometries with in-depth nonlinear analysis is a subject of further work, where an alternative may be required.

The FEA is a computational mechanics technique to develop and simulate discretised mathematical model of a continuum system using a numerical method [20] and is extremely valuable tool used to calculate various aspects such as stresses, deformations etc., resulting from mechanical and thermal loads.

Numerous studies have demonstrated that FEA results qualitatively agree well with experimentally obtained values. Mian et al [101] in their study on thermal error prediction in a machine tool have validated FEA results are in close agreement with experimental results ranging from 65% to 90% for variety of test regimes reducing the error from 70 μm to 10 μm. In the study carried out by Creighton et al [105] on analysis of high speed micro-milling spindle, thermal errors were well predicted using FEA and led to compensation accuracy of 80% under a random speed test. Temperature distribution within the workpiece and thermo-mechanical behaviour of the structural part has been successfully investigated and predicted using FEA in various research activities [50, 55]. A good agreement between numerical and experimental data shows the validity of the FEA based simulation models in handling real-world problems.

The finite element analysis is a well-established technique, and its application to machine design and analysis is well-accepted. However, care must be taken with parameterisation, especially of boundary conditions. Nevertheless, the literature study provided enough confidence to trust FEA results for analysis of simple geometries without further experimental validation.

Figure 16 demonstrates the effect of clamping force on the workpiece deformation; it shows the schematic of a workpiece (8a) of dimension 200mm x 200mm x 50mm with its finite analysis model (8b). The finite analysis model was constructed using a standard solid mesh in Soildworks. The force was applied on the two sides of the workpiece (8c) for this study and fixed geometry was applied to the rear surface. Figure 16d illustrates the case of deformation caused by the application of equal amount of clamping forces on the two opposite surfaces of the workpiece and Figuree exhibits the case of application of uneven forces on the workpiece.

Workpiece Material	Force		
	0.1KN	1KN	10KN
	Resultant maximum displacement (μm)	Resultant maximum displacement (μm)	Resultant maximum displacement (μm)
1060 Aluminium Alloy	0.006	0.06	0.6
Plain carbon steel	0.004	0.039	0.39
Malleable cast iron	0.004	0.043	0.43
Stainless steel (ferritic)	0.004	0.041	0.41

Table 4 Simulation results of deformation caused by clamping forces

Simulation results for equal forces (Figure 16d) are given in Table 4. Four commonly used workpiece materials [113] were used in the simulation; 1060 aluminium alloy, plain carbon steel, malleable cast iron and stainless steel. The clamping force in normal conditions can vary from few Newtons to kilo- Newtons [53, 55, 114]. For this study, clamping force normal to the workpiece surface was applied at 0.1, 1 and 10KN magnitude. The force of 10KN was chosen to produce greatest possible deformation on the workpiece to reduce the effect of other factors on simulation result [53]. The maximum resultant displacement from the nominal position of the node for all the combinations of forces and materials is reported in Table 4. The resultant displacement is a combination of displacements in X, Y and Z

direction. The nodes at four corners of front surface experiences the maximum resultant displacement.

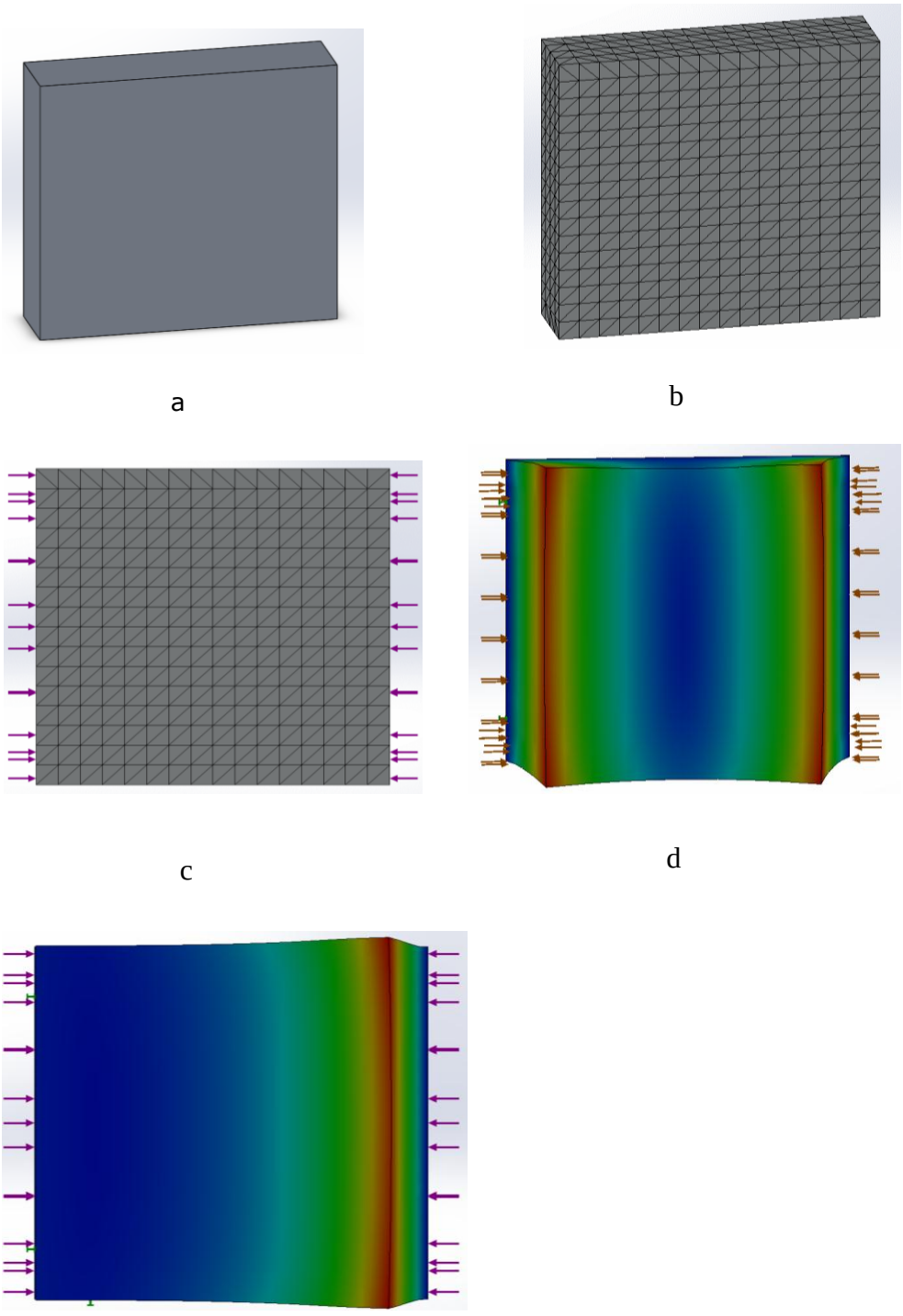

Figure 16 Deformation of workpiece due to the clamping force. a) Schematic of workpiece to be machined b) The finite element model c) Application of clamping force d) Simulation result of equal force e) Simulation result of uneven force

When uneven forces of 1KN and 10KN are applied to the opposite sides of the workpiece (Figure 16e) for 1060 aluminium alloy (simulation was carried out only on aluminium alloy since this is the softest material of all the 4 materials. Hence, maximum resultant displacement can be observed in this case), maximum resultant displacement of 1.2 µm in the direction of 10KN force and 0.04 µm in the direction of 1 KN was observed. This uneven deformation is clearly a result of uneven application of clamping force.

The simulation results for deformation caused by the equal clamping force is in the range of 0.004 µm to 0.6 µm depending on applied force and the material. This deformation on a whole is insignificant. In the case of uneven force, deformation up to 1 µm is observed for aluminium alloy. However, corresponding applied force is too large (10KN) and the opposite forces differ by the magnitude of 9KN, which is not a good practice. Thus, in general effect of clamping force can be ignored as a significant OMP uncertainty contributor.

3.1.4.2 Workpiece/artefact thermal distortion during machining

To study this case, we performed the finite element analysis on the workpiece block. We considered block of the same dimension as shown in Figure 16a. Material used for the analysis is aluminium alloy 1060.

Based on the literature study, during machining process, cutting region temperature can reach up to $1000^{O}C$ [57] and 10-25 % of the heat generated is conducted into the workpiece [58]. The workpiece heat input fluctuates massively and is dependent on the machining process, and the process parameters. The quantitative statement pertaining to a percentage share of heat distribution cannot be made, due to pronounced variations in workpiece geometry, material properties, and cutting conditions. The process-induced heat produces high temperatures (>$100^{o}C$) in the workpiece resulting into omnidirectional distortion, due to inhomogeneous temperature distribution [50]. Thus, according to available literature [50, 57, 58], the temperature of $150^{o}C$ is deemed representative of machining induced thermal loading of the block for this work.

In this study, simple geometry is used to perform rudimentary FEA; hence, the bulk temperature was considered instead of regional fluctuations in the workpiece temperature to estimate the thermal distortion. However, to further analyse distortion resulting from

inhomogeneous temperature field, local variation should be considered. This is an area for further research.

The FEA was performed using SolidWorks 2015. Three-step procedure was followed for this exercise. First the static thermal analysis was performed with the initial temperatures of 150 ^{O}C (just after the machining process as discussed earlier) applied to the entire workpiece. Then transient thermal analysis was performed for 300 sec with step size of 10 sec while ambient temperature of 20 ^{O}C and convection coefficient of 6 W/m^{2}k. The third step was to perform non-linear displacement study corresponding to each step of the transient thermal study and the resultant displacement was measured from its initial condition at different time stamps.

The resultant thermal error and change in temperature for 300 sec is shown in Figure 17. The Figure 18 shows the thermally distorted workpiece and node 9268 used for the measurement. The resultant thermal error of 12.65 µm can be observed with drop in temperature of 5.5 ^{O}C in 300 sec. These values are specific to the particular material and node of measurement. Thus, these parameters have to considered while on-machine measurement. Thus, depending on the time it takes for probing routine to complete, workpiece distortion is going to be different, resulting in the uncertainty of measurement.

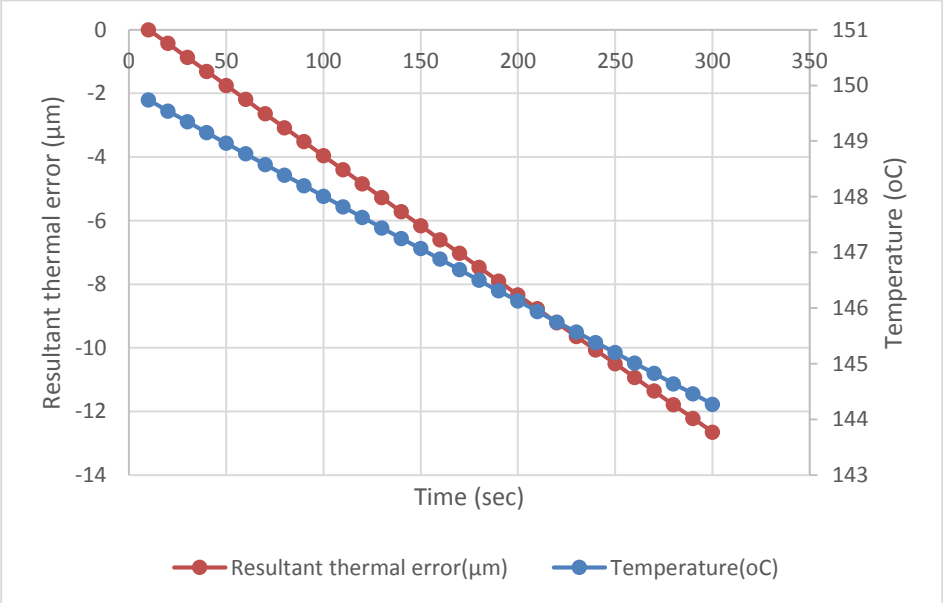

Figure 17 Change in temperature and resultant thermal error at node 9268 with respect to time

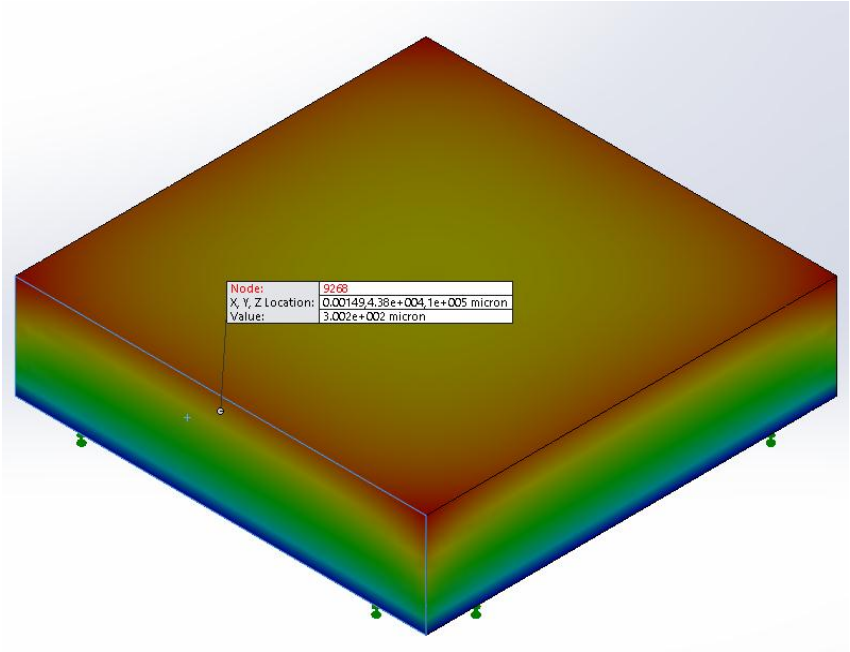

Figure 18 Thermally distorted workpiece with node 9268

3.1.4.3 Surface contamination

To analyse the influence of presence of coolant several tests were conducted. The setup for the tests is shown in Figure 15. The probe used for this study was Renishaw RMP60 with 100 mm stylus. The coolant used in this case was QUAKERCOOL 7101 LF. The tests were performed using various concentrations (2.2, 4.2 and 6.2 %) of the coolant. The machine tool manufacturer recommended concentration is 4.2 %.

For these tests, the coolant was placed on the top surface of a workpiece. The workpiece was probed in Z direction at the same location (the centre of the top surface)10 times and probing repeatability was found out as given in Table 5 using the standard deviation of the readings. The probing repeatability is 0.3 µm without coolant and 0.5 µm with coolant. Interestingly, no variation in repeatability can be observed in case of variation of concentration of coolant.

Thus, it can be commented that the presence of a thin film of the coolant on the surface of the workpiece has insignificant effect on the probing repeatability. However, further

investigation is required in case the coolant is not used during the machining, resulting in a surface contamination due to the swarf and dust.

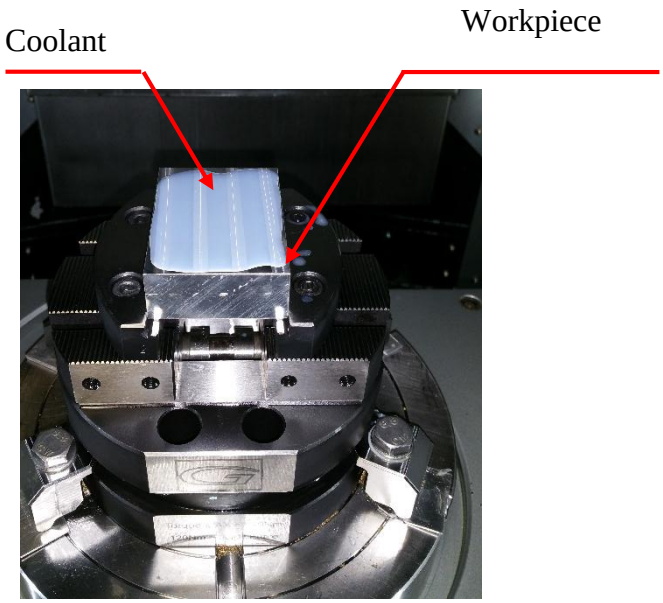

Figure 19 Test setup to measure influence of surface contamination

Coolant concentration	Probe repetitions	Repeatability (µm)
No coolant	10	0.3
Coolant (2.2%)	10	0.5
Coolant (4.2%)	10	0.5
Coolant (6.2%)	10	0.5

Table 5 Influence of a presence of a coolant on pobe repeatability

3.3 Summary

In this chapter, we investigated the various sources of uncertainty for on-machine probing. They are broadly categorised into machine tool, probing system, environment and workpiece/artefact factors.

In case of machine tool, errors due the geometric, thermal and machine tool repeatability, all contribute significantly towards the on-machine measurement uncertainty.

Environmental temperature directly influences the measurement error. Factors such as surface contamination due to thin film of coolant and workpiece distortion due to the clamping do not contribute significantly to the uncertainty. Distortion of workpiece during machining and probing routine due variation in thermal field needs to be considered.

Thermal errors are the largest contributing factors for on-machine measurement, reaching magnitude up to 220 μm. Hence, they need to be reduced significantly.

Chapter 4 – Novel displacement senor

This chapter is published in a journal article by Potdar et. al. [115].

This chapter presents a robust displacement sensor with nanometre-scale resolution over a micrometre range. It is composed of low cost commercially available slotted photo-microsensors (SPMs). The displacement sensor is designed with a particular arrangement of a compact array of SPMs with specially designed shutter assembly and signal processing to significantly reduce sensitivity to ambient light, input voltage variation, circuit electronics drift, etc. The sensor principle and the characterisation results are described in this chapter. The proposed prototype sensor has a linear measurement range of 20 μm and resolution of 21 nm. This kind of sensor has several potential applications, including mechanical structural deformation monitoring system.

4.1 Principle of measurement

The principle of measurement for the new displacement sensing head is based upon optoelectronic sensing of the position of the specially designed moving mechanical shutter. Figure 20a illustrates the principle of operation of the sensors. Each sensor is composed of an infrared emitter (light emitting diode) on one side and an infrared detector (phototransistor) on the other side facing each other, separated by a small gap in which the mechanical shutter is situated. The movement of the shutter is proportional to the displacement encountered by it, resulting in a change in the amount of obstruction to the optical path between the emitter and receiver. Since the output voltage from the receiver is a function of the intensity of light beam incident on it, the corresponding movement of the shutter will be detected. The sensing range depends upon the gap between emitter and receiver.

It was observed during the benchmark testing that the single sensor output voltage is sensitive to the supply voltage variations, ambient light and temperature changes; this is to be expected given that the sensors are typically used for binary presence detection in process control applications and such small drifts would not be an issue. To improve the stability of the sensor, the head design incorporates four SPMs, S1 to S4, acting together with a specially designed shutter (Figure 20b) to provide cancellation. The shutter is designed to cluster the sensors pairwise; it blocks the light to one sensor while

simultaneously allowing the light on the second sensor. Thus, sensor S1 and S2 form a pair; when S1 loses the light, S2 gains the light in same proportion. Similarly, S3 and S4 form another pair. This produces a differential voltage output for each pair, cancelling the effect of input voltage variation. Averaging the two differential outputs reduces the influence of ambient light variations and differential thermally induced expansion between the sensor circuit and shutter. This novel arrangement allows self-correction for the external perturbations as mentioned earlier. Equation 1 represents the displacement of the shutter with output voltages of all the sensors.

$$D = K \times \frac{\left[\frac{(V1-V2)}{2}+\frac{(V3-V4)}{2}\right]}{2} \quad (1)$$

Where, D is the displacement (μm), K is a calibration constant (μm/ mV), V1 to V4 are the output voltages of SPM1 to SPM4 (V).

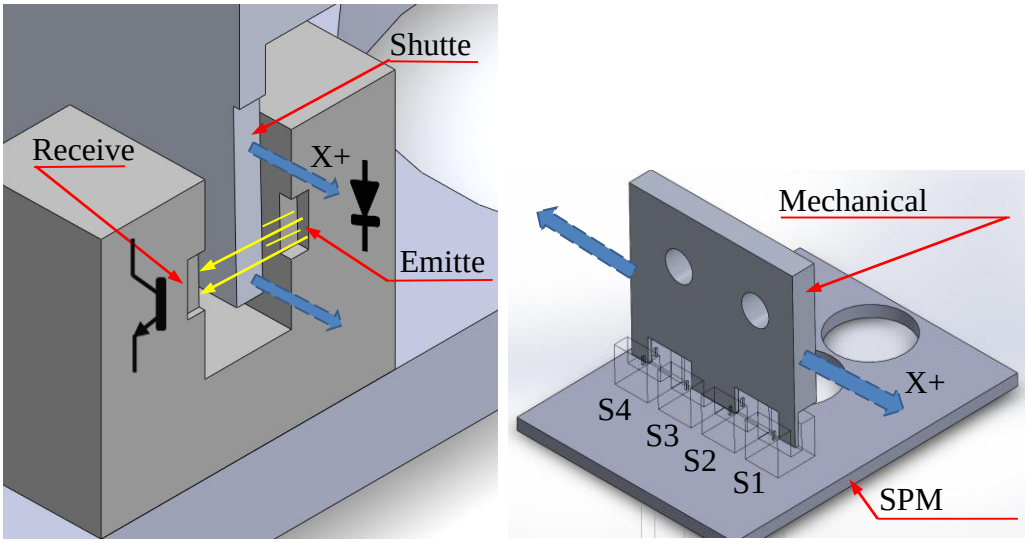

(a) (b)

Figure 20 (a) Cross section view of a single sensor and shutter and (b) schematic of the overall system

4.2 Prototype system

The design of the proposed prototype opto-electro-mechanical head assembly is shown in

Figure 21. The shutter is mounted on the shutter head and the SPM board, which will then be attached to an amplification device, while the SPM board is mounted on the reference

structure. There are vast array of different SPM sensors available in the market. The type used in the prototype device was selected on the basis of its low cost, compact size (3.4 mm x 3 mm X 3 mm) and small aperture width of 150 µm for high sensitivity. Additionally, the chosen unit has a gap between emitter and receiver of 1 mm, which is sufficiently small that it reduces the effect of incident ambient light variation with free movement of the shutter; this ensures optimum light transfer. The realisation and physical dimensions of the SPM board are represented in Figure 22

The biasing circuit used to establish proper operating conditions for the SPMs, is designed to be remote from the SPM board in order to avoid the effect of local self-heating from electrical components.

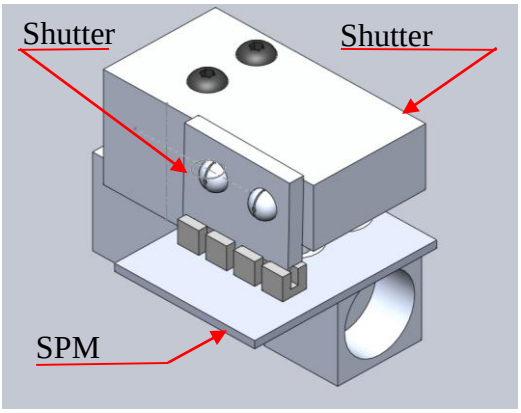

Figure 21 Sensing head

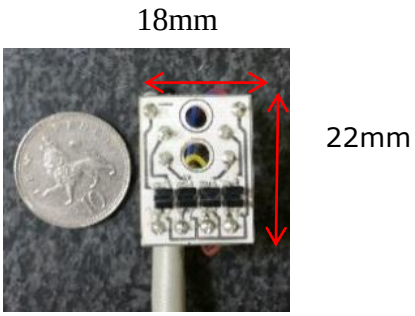

Figure 22 Prototype SPM board

Figure 23 shows a thermal image of the first design of the SPM board, highlighting the heat input from the biasing resistors where the SPMs and their corresponding biasing resistors were on the same board. It can be seen that temperature of the resistors is significantly

higher than the SPMs. In order to minimise the cost of the overall setup, standard resistors (330Ω, 1/2W) were used.

The mechanical shutter, shutter head and sensor base were manufactured using aluminium to reduce the thermally induced errors in the sensor. Although aluminium has a high coefficient of thermal expansion, using the same material throughout, coupled with the high thermal conductivity, means that the head assembly and self-correction mechanism of the setup will be more reliable than using more exotic materials, for the given cost.
A Farnell L30-2 stabilized power supply is used to provide power to the entire electric circuit. Raw output voltages generated by the sensing head proportional to the displacement are fed into the analogue to digital converter (ADC: NI-USB 6363, 16-bit resolution). This ADC output is then further given to the data logging computer. An in-house developed LabVIEW program [116] is used to convert the voltages into the equivalent displacement using equation 1.

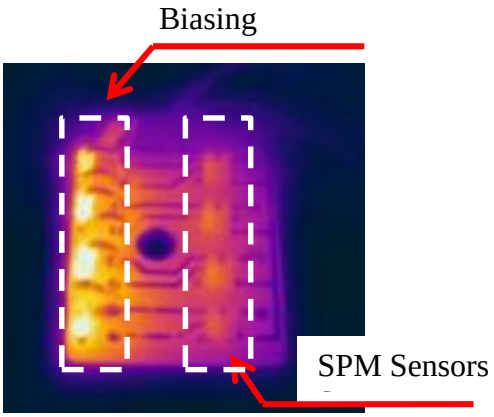

Figure 23 Thermal image of the biasing resistors

4.3 Sensor characterization

A schematic of the experimental setup used to perform a series of tests on the sensing head for characterisation is shown in the Figure 24. Figure 25 shows a photograph of the actual setup. The equipment was placed on the granite bed of a Coordinate Measuring Machine (CMM) (Zeiss Prismo Access 09/18/09) as a mechanically and thermally stable reference. In particular, the SPM board was located on the granite bed and the shutter head was mounted on the head of the CMM. The CMM was located in a temperature controlled room which was measured to be 21 oC± 1oC, during the entire duration of the tests, with the exception of tests requiring specific temperature variation for thermal characterisation. For

the purpose of this test, the CMM axes were used to produce the required displacement. This was convenient and provided good control for small movements.

Tests were performed by moving the CMM over the entire range of the sensor head in increments of 2 µm. A Renishaw XL-80 laser Interferometer system (accuracy: ±0.5 ppm, resolution: 1 nm and range 80 m) was used as the independent reference measurement of the displacement. Retro-reflector optics of the laser were attached to the bottom of the CMM head and the shutter of the sensor was fixed to the one end of the retro reflector (Figure 26). Thus, the shutter of the SPM head and the laser's optics experiences the same displacement. Test results are discussed in the subsequent sections.

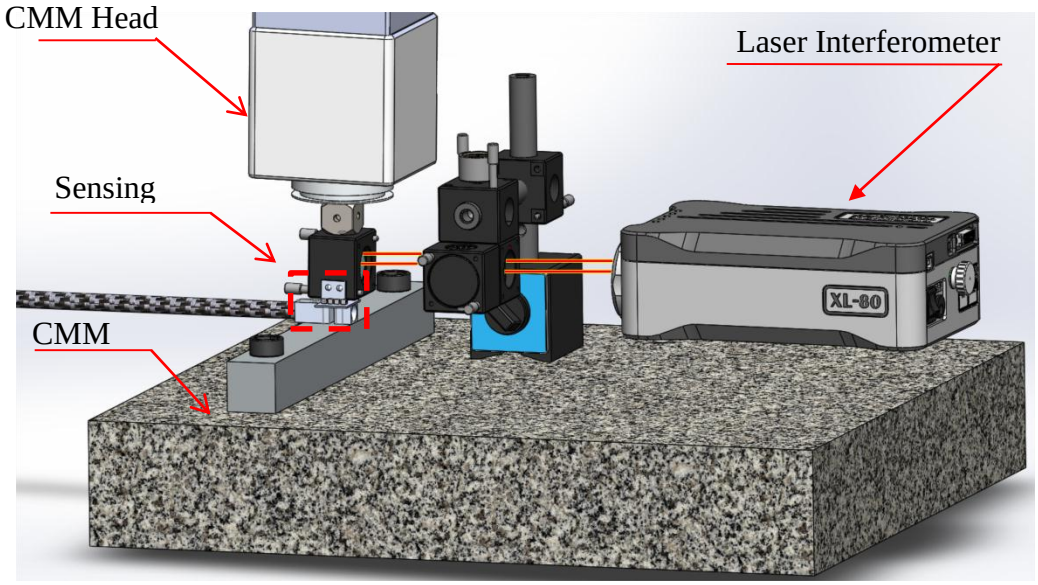

Figure 24 Schematic of sensor calibration setup

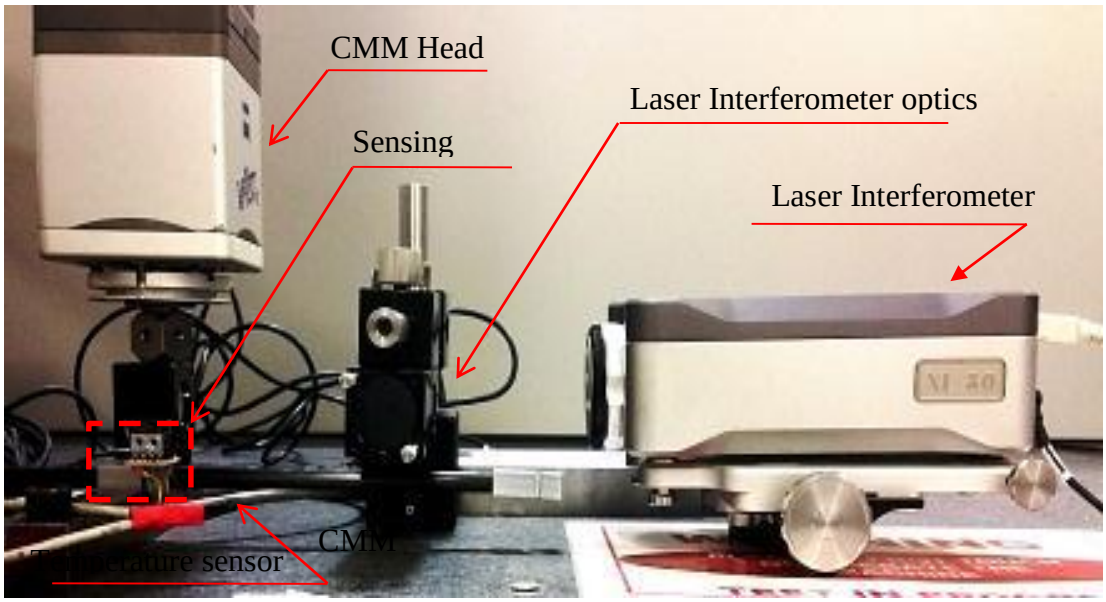

Figure 25 Sensor calibration setup

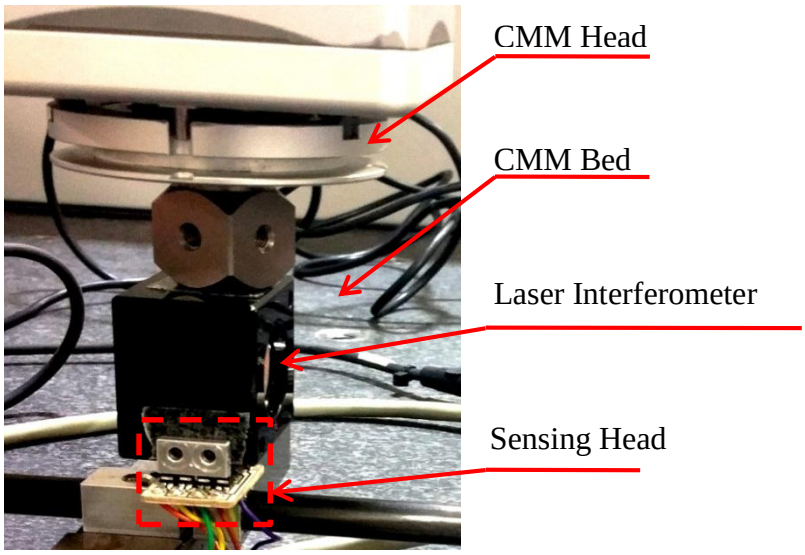

Figure 26 Close up of CMM and SPM sensor head setup

4.3.1 Characteristic curve

The experimentally obtained static characteristic curve of the sensor is shown in Figure 27, illustrating the variation in SPM head output voltages with change in shutter position measured by the XL-80 laser interferometer. It can be observed that the relationship

between measured voltage and displacement is non-linear in nature and the sensitivity (gradient) of the curve is not consistent over the entire input displacement range.
The characteristic curve was divided into three sections based upon the change in the slope by finding the first derivative; the two end sections (1 and 3) have non-linear response and a middle section (2) where the output is proportional to the input. The slope of section 2 was found to be 0.17 V/μm. This characteristic allows the sensor to be used reliably over the given input range with a well-determined output. Sections 1 and 3 could also be used with further refinement, but for the remainder of this work, only the linear portion is investigated.

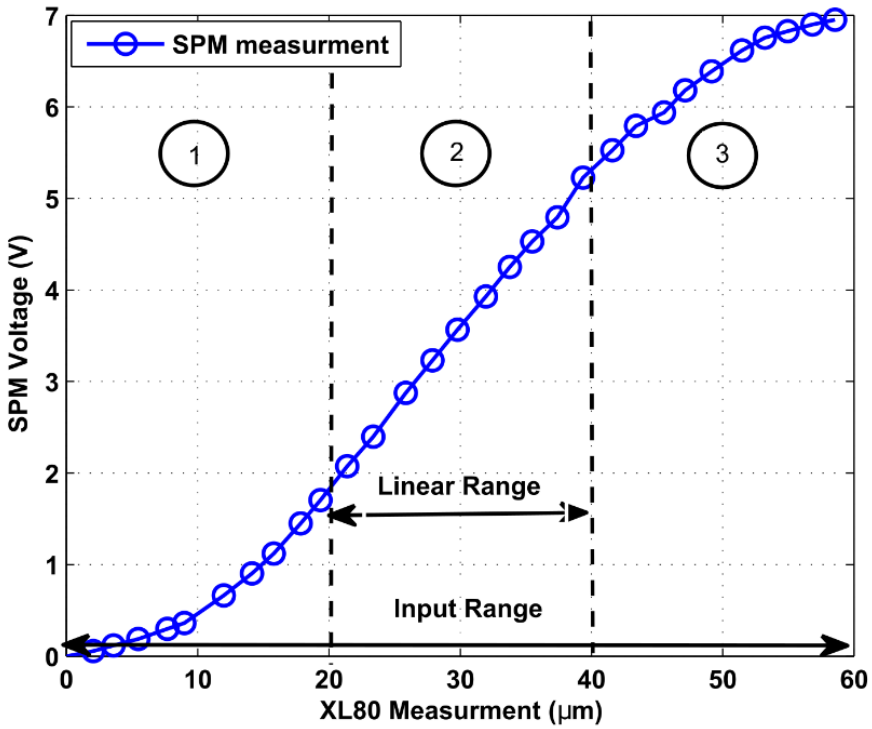

Figure 27 Characteristic curve of SPM head

4.3.2 Calibration of the characteristic curve and linear range of the sensor

Calibration of the curve is performed using the Least Square Regression (LSR) technique. The linearly fit curve is specified by equation 2.

$$V = sD + d_o \qquad (2)$$

Where V is the SPM output voltage (V), s is the sensitivity (V/μm), D is the displacement (μm) and d_o is an offset.

The mean value of the sensitivity obtained by LSR is 0.1648 V/μm with confidence interval of $\pm$ 0.0009 for 99% confidence level using student's t-distribution. For all further calculations, this value will be used over the full scale range (FSR) of 20 μm.

Since the linearization function described by equation 2 is an approximation of the actual curve, it does not describe the actual curve perfectly introducing the mapping linearity error. Figure 28 shows the mapping linearity error in terms of percentage of FSR after least square fitting was removed. It is calculated using equation 3 and 4.

$$e_m(v) = f_a(v) - f_{cal}(v) \quad (3)$$

Where, em(v) is a mapping error in volts, fa(v) is an actual output obtained by experiment and fcal(v) is the predicted value obtained by calibration curve. The value of me(v) is then converted into microns using the value of sensitivity achieved from equation 2.

$$mapping\ error\ (\%) = \pm \frac{max|e_m|}{FSR} \times 100 \quad (4)$$

Where, $max|e_m|$ is a maximum mapping error, which is within $\pm$ 0.2 μm. Thus, the linearity error due to the calibration curve approximation is found to be within ±1 % of FSR

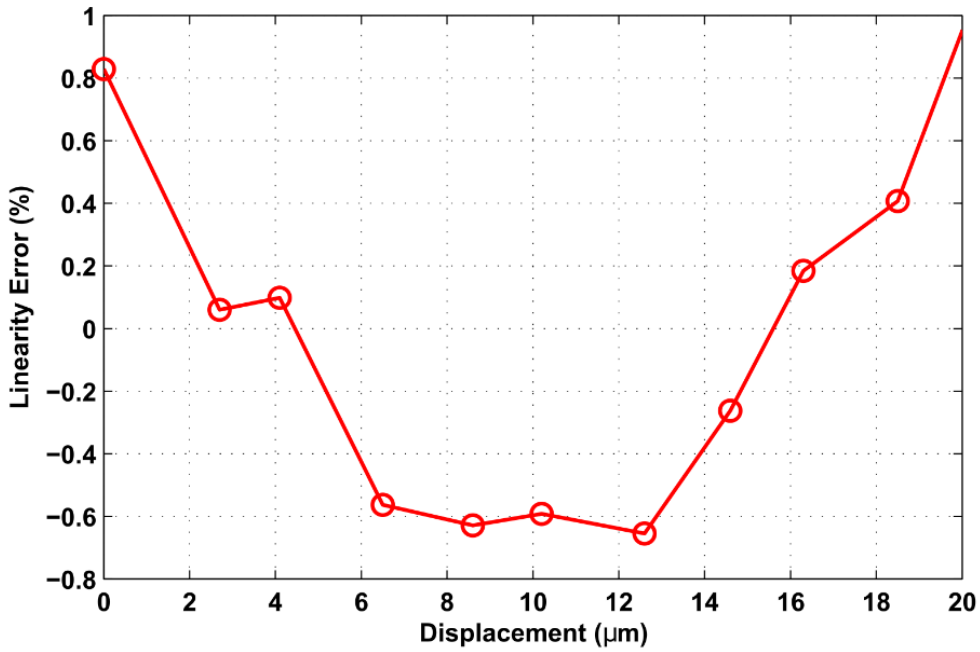

Figure 28 Mapping Error due to calibration curve approximation

4.3.3 Repeatability

In order to find the sensor repeatability, the same test was repeated five times over the entire linear range under the same operating conditions. The output value of the SPM head and corresponding XL-80 laser interferometer reading was recorded for targets every 2µm of CMM displacement in a bi-directional test. Figure 29 illustrates the deviation in SPM measurement readings from the laser for the five tests. The standard deviation (SD) at every target position was calculated and the maximum SD among all the positions in both the directions was considered as the repeatability of the sensor; the ISO 5725 defines the repeatability as the precision (one SD) under repeatability condition [117]. Table 6 shows the SD of all positions in the forward and reverse direction. Thus, the proposed sensor has a repeatability of 90 nm.

Displacement (µm)	0	2	4	6	8	10	12	14	16	18	20
Forward SD (nm)	0	47	60	33	28	31	41	35	50	42	60
Reverse SD (nm)	21	35	62	35	71	25	73	77	48	86	60

Table 6 The Standard deviation (SD) at each position

4.3.4 Resolution and noise

The resolution of sensors is often limited by the noise in the overall measurement system rather than the ADC resolution (which in this case is 1 nm using 16-bit ADC for 0.1648 V/µm of sensitivity). An uncertainty is introduced in the measured displacement value due to random noise. This uncertainty can produce an error in the sensor output if the measured readings are closer to each other than the value of the uncertainty. The resolution can be quantified then by a multiple of the standard deviation (σ) of the noise.

The noise level is calculated to be 6σ to achieve 99.7% confidence [71].
The sensor was quantified for static performance at ten places along its measurement range. The data was captured at 1 kHz and the corresponding standard deviations were calculated. The worst case, at one of the extremities, is presented in
Figure 30 This therefore shows a worst-case noise floor of $6\sigma = 21$ nm across the sensor's measurement range, when used statically.

To validate the resolution of the sensor in dynamic operation, a small PZT (Lead Zirconate Titanate) actuator P-810.10 from Physik Instrumente (PI) GmbH was utilized to generate very small movements. The PZT was directly attached to the rear end of the XL-80 retro reflector. The resolution of the sensor head was determined by applying a sinusoidal signal with varying amplitude from a function generator to PZT actuator. The amplitude of the signal was reduced in each cycle until the SPM head was unable to detect the sinusoidal wave. The PZT was excited by a sinusoidal signal of 1Hz frequency with amplitude of 0.6 V and corresponding readings were measured.

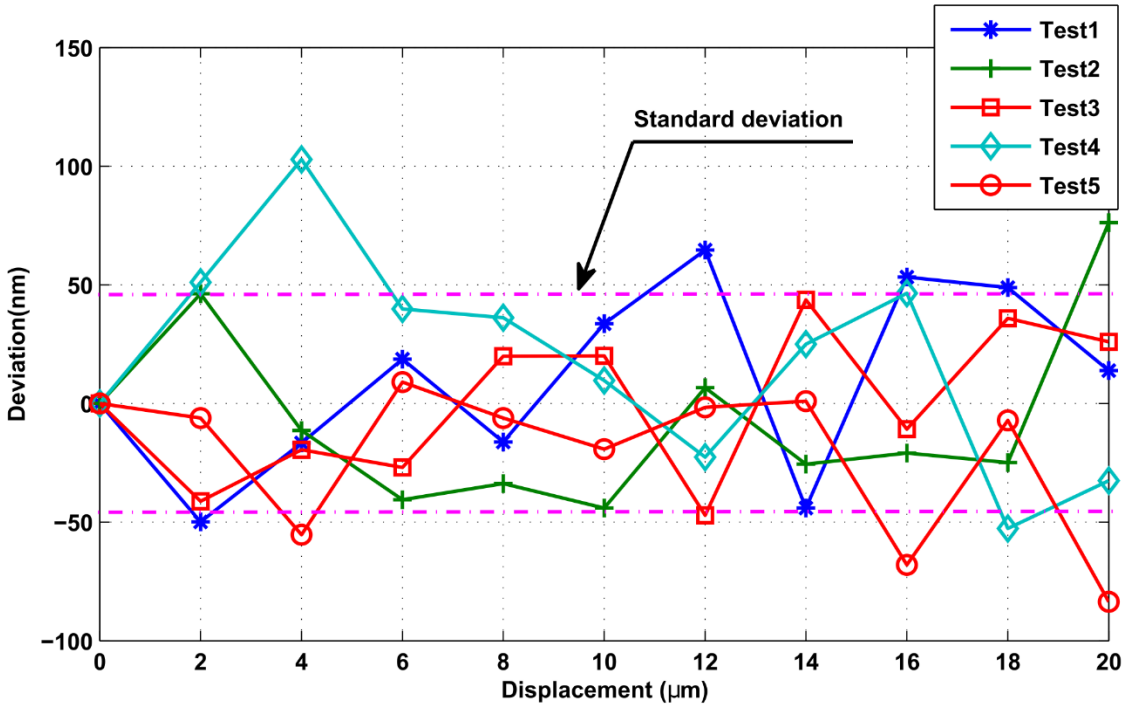

Figure 29 Repeatability test for the sensor head

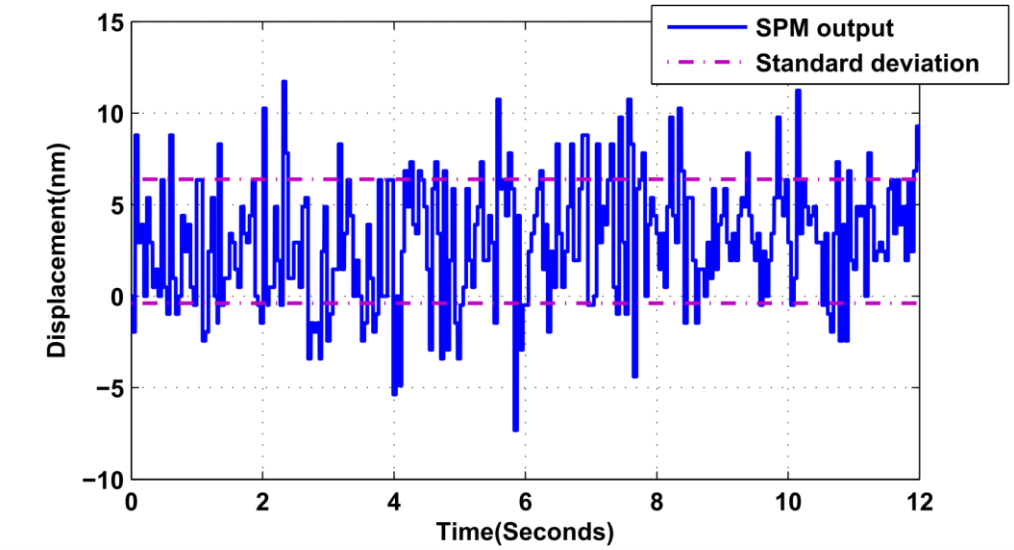

Figure 30 Time domain recording of the sensor head output sampled at 1 KHz

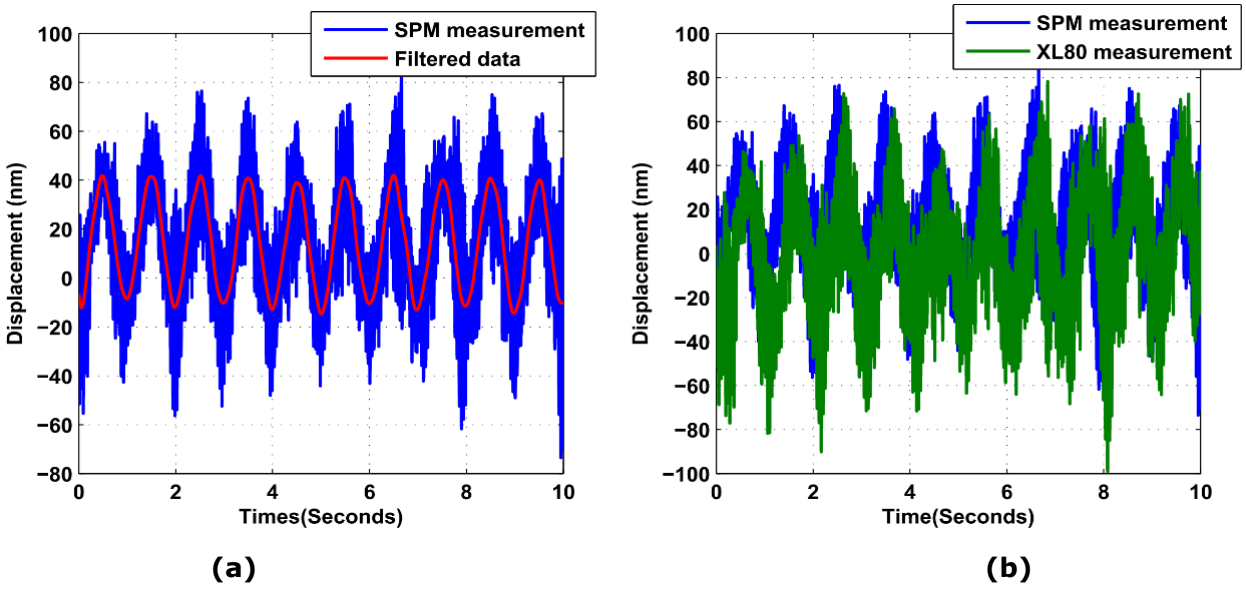

Figure 31 SPM sensor head resolution test result

Figure 31a illustrates the SPM head output with low pass filter at 10Hz.

Figure 31b shows the measured voltage equivalent displacement of the SPM head and the output of the XL-80 laser interferometer. As it can be observed, the SPM output is sinusoidal in nature and is comparable with the reference measurement from the laser. A short time delay can be noticed between the two signals, this is due to the mismatch between trigger

inputs of the two data logging applications. Due to the very small magnitude of the sinusoid, the SPM head result includes the SPM noise and mechanical noise in the setup; both SPM head and XL-80 measurement are affected by noise in the setup equally and hence can be ignored. The SD of noise in SPM head is 17 nm and that of XL-80 is 13 nm. Thus, system resolution is comparable to that of laser interferometer.

4.3.5 Immunity against variation in power supply and ambient light

Stability of the SPM head output depends on the stability of the input power supply. Any variation in the power supply will affect the intensity of the light beam emitted by the LED. This in turn will have an effect on the incident light on a receiver. Since displacement is a function of the intensity of an incident light on the receiver, there is a possibility of a false displacement reading with respect to input voltage.

Thus, a stabilised DC power supply was used to energize the circuit. However, in the field it is possible that output of the DC power supply is susceptible to variation in mains-line power. In order to reduce the effect of power supply variation, as mentioned in section 2, a four-sensor configuration was used to design the SPM sensor and equation 1 was used to calculate the final output.

To investigate the sensitivity of a sensor to power supply variation, the output of the DC supply voltage was changed within $\pm$ 10 mV and the output of all four sensors S1, S2, S3 and S4 was measured as V1, V2, V3 and V4. Figure 32 shows the a) differential voltage (DV1) output between sensor S1 and S2, b) differential voltage (DV2) output between sensor S3 and S4 as well as c) average of the two differential outputs (DV1 and DV2). It can be clearly seen that from Figure 32 that the use of the differential voltage schema reduces the influence of power supply variation and the final average output voltage of an SPM head is within $\pm$ 2 mV, which equates to ±12 nm.

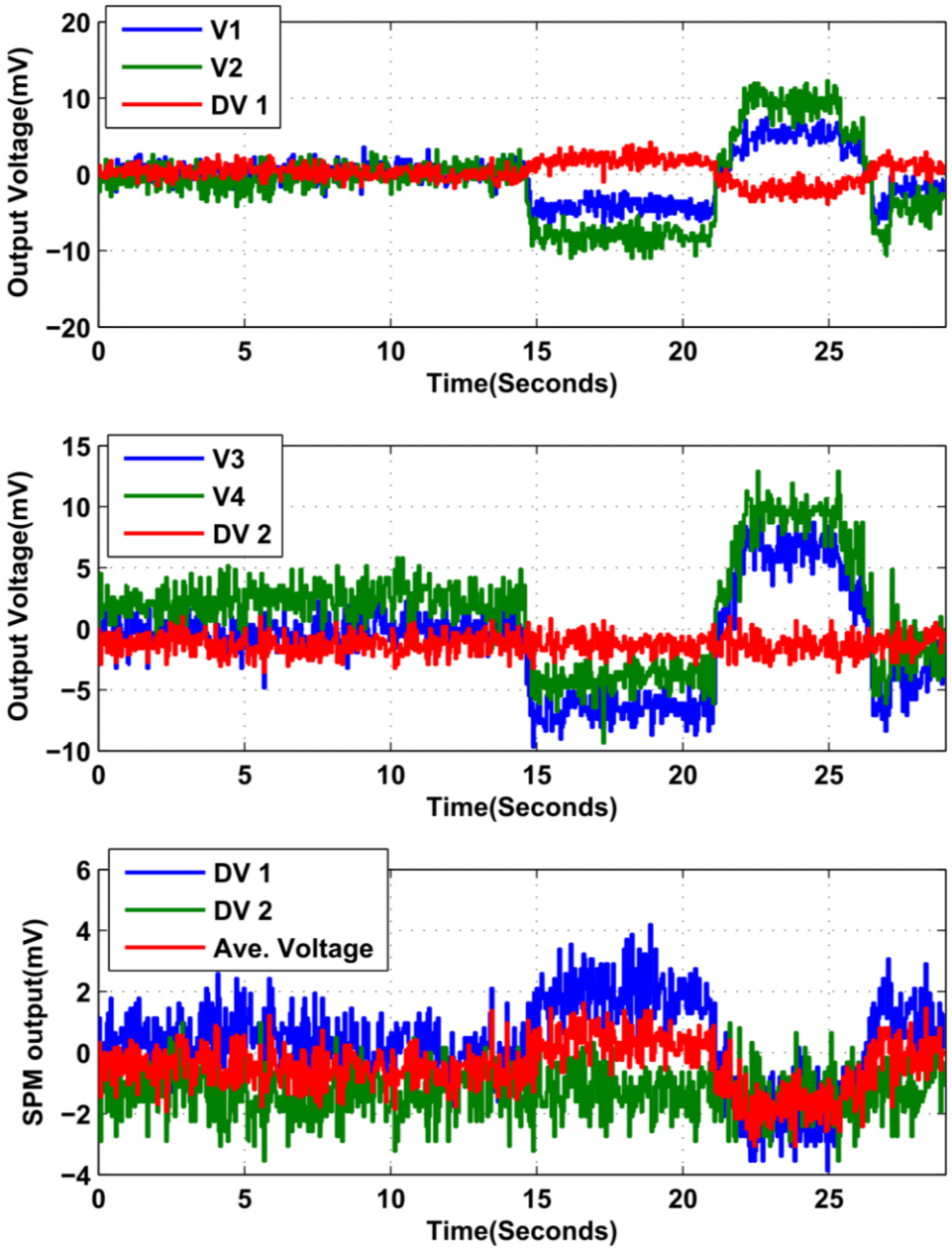

Figure 32 SPM sensor head insensitivity to the variation in power supply voltage; a) Differential voltage (DV1) between sensor S1 and S2, b) differential voltage (DV2) between sensor S3 and S4, c) final SPM output (average Voltage)

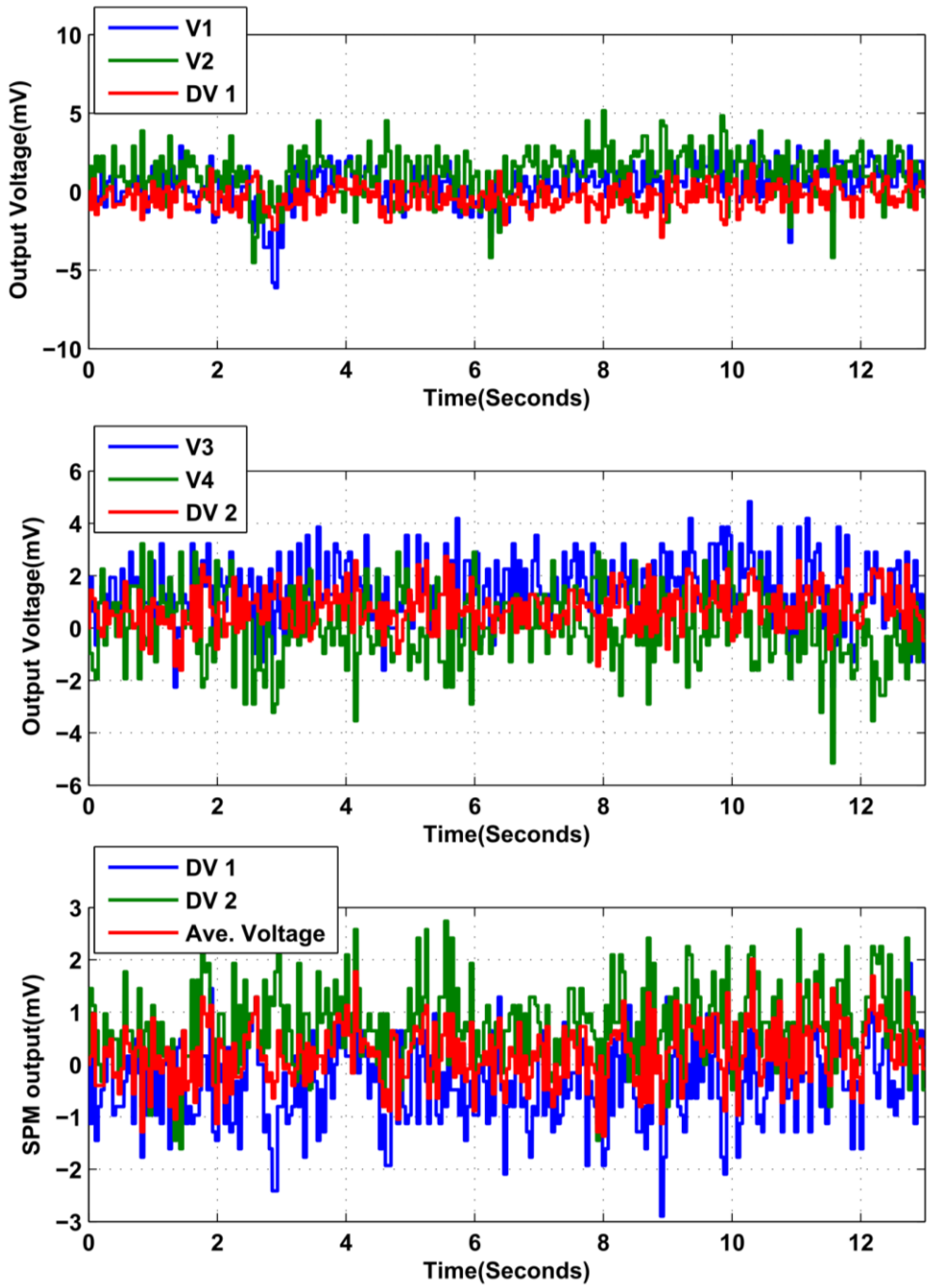

Figure 33 SPM sensor head insensitivity to the variation in ambient light; a) Differential voltage (DV1) between sensor S1 and S2, b) differential voltage (DV2) between sensor S3 and S4, c) final SPM output (Ave. Voltage)

Change in ambient light can also cause misreading of optical systems. In the prototype head, the receiver (phototransistor) has peak spectral sensitivity wavelength of 920 nm in the spectral range of approximately 850 to 975 nm with 90% relative sensitivity. The emitter has peak emission wavelength of 940nm, which is near to the peak spectral

sensitivity wavelength of the receiver. The small size of the emitter and receiver aperture window (width of 150 μm) with gap of 1 mm between emitter and receiver along with meticulous sensor head design can minimize the influence of ambient light.

The four sensor configuration helps to reduce the effect of ambient light; to examine this, strobe light effect using white LED source was generated. The intensity of the light was kept at 250 and 360 Lux to simulate the factory conditions. The results of the test at 250 Lux is shown in Figure 33. Differential voltages DV1 (Figure 33a) and DV2 (Figure 33b) decreases the effect variations in individual sensor outputs (V1, V2, V3 and V4) due changes in the incident light. The SPM output, which is an average of DV1 and DV2, keeps the final output within $\pm$ 1 mV (±6 nm). The results at 360 Lux were identical. Further improvements in the results can be achieved by keeping the sensor inside an enclosure to protect from ambient light variations.

4.3.6 Sensor Drift

Long term stability of the sensor is important, to ensure the validity of the measurement results. Drift in the displacement sensor output can take place even though there is no change in the environmental or measurement conditions, due to signal conditioning electronics for example and is normally measured against elapsed time.

This experiment was conducted in a temperature-controlled environment, in which the temperature variation was maintained at less than 1^{o}C. The experimental setup is shown in Figure 25. The temperature was measured using a digital temperature sensor DS18B20 and the test duration was 9 hours. This test was run by keeping the mechanical shutter nominally stationary for the entire duration. The Renishaw XL-80 laser interferometer was used to validate the test results.

Figure 34 shows the result of the conducted experiment. The measured environmental temperature variations were within 0.5 ^{o}C. The SPM head output during this period changes by 0.22 μm and the XL-80 reading changes by 0.3 μm. The deviation in the differential displacement between SPM head and XL-80 reading is within $\pm$ 0.2 μm; some of the detected variations are likely due to the quantization of the XL-80 long term logging application. Thus, in a relatively stable temperature, the differential drift between the XL-80 and SPM head is less than the uncertainty of the setup.

To investigate the effect of setup temperature variation on the prototype SPM sensor head, the temperature of the environment was increased using a heating coil (2000W) for two and half hours (Heating process) and then allowed to cool down. The heating coil temperature was gradually increased to avoid any thermal shock to the CMM structure. The results are shown in Figure 35.

For the purpose of analysis, the differential displacement between the XL-80 and SPM head on the experiment (shown by the green line in Figure 35) can be considered to isolate the effect of thermal distortion of a CMM structure. The XL-80 optics were carefully setup (Figure 35) to minimize the effect of dead path error and Abbe error, which were reduced to 75 mm and 25 mm respectively. During the first 50 minutes of the heating cycle, initial drift of 0.8 μm can be observed in the differential displacement (shown by green line in Figure 35); thereafter displacement variation is within 0.4 μm for rest of the heating cycle. The displacement is a maximum of 2 μm during the cooling cycle for a drop in temperature of 2 ^{o}C. It can be observed that parameters are related but there is no direct correlation of the sensor output deviation to the temperature. It is assumed that the variation is likely due to the residual offsets of the setup and CMM movement. The results confirm that the sensor is very robust to ambient temperature variation.

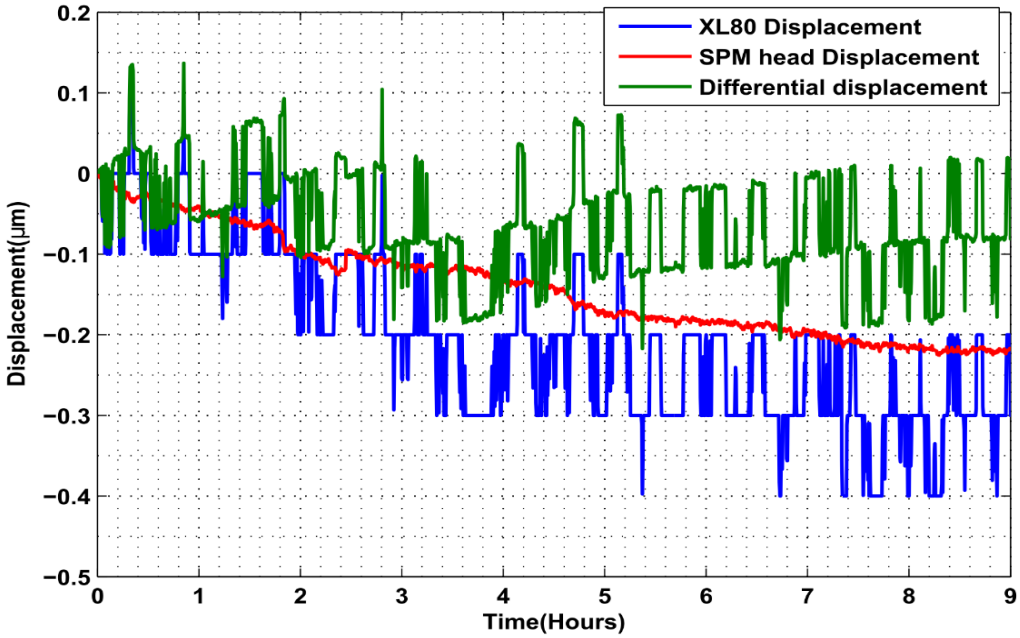

Figure 34 Measurement results for SPM head stability test

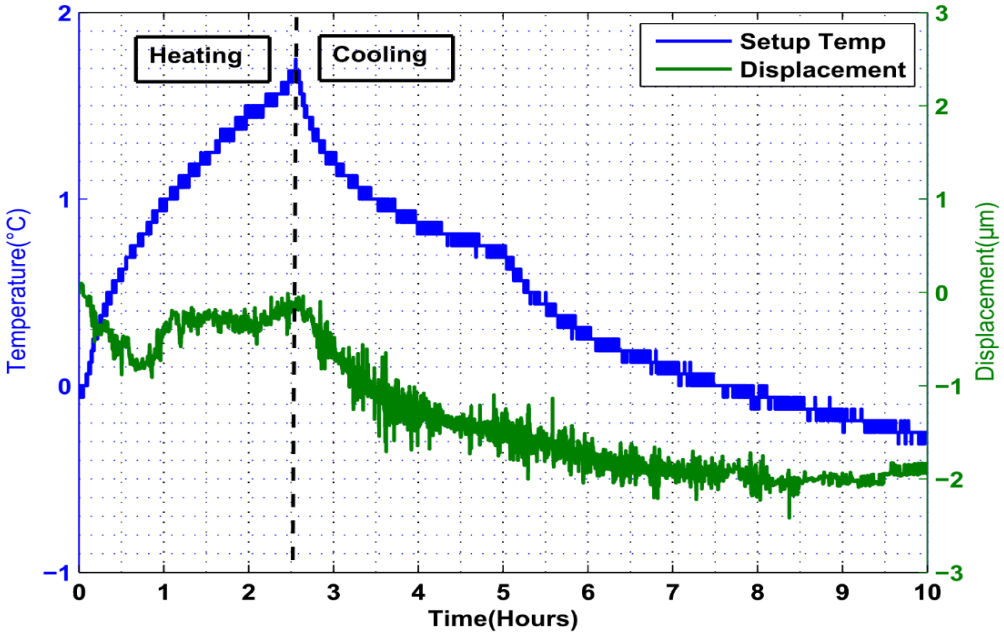

Figure 35 Temperature drift of the SPM head

4.5 Sensor cost

In this study, we have used commercially available and inexpensive (0.5 GBP each) infrared transmissive sensors, also known as slotted photo-microsensors or photo-interrupters. The remainder of the device consists of basic electrical components (resistors, capacitors and connectors) and mechanical housing. The cost in 2015 was calculated as £26. The output of the sensor is compatible with any standard data acquisition hardware and software. However, an industrial quality data acquisition system (typically >= 16bit, high SNR) would be recommended; even a good quality, 24-channel system would only add approximately £600.

The cost of the sensor can be compared to that for a comparable capacitive or inductive sensor, which are in the region of £1000 per sensor. A data acquisition system would also be required. High-quality laser triangulation devices can be acquired for a similar price to the capacitive sensors, while even low-cost laser triangulation devices cost several hundreds of pounds.

Typical applications for these sensors would include mechanical structural deformations monitoring, piezo-actuator control, and vibration monitoring system. For the machine tool fusion problem being addressed in this thesis, both elongation and distortion should be

monitored, therefore for a single element (such as the column) at least four sensors are required, although better results can be achieved with higher spatial density. For this example, the comparative cost of a system using the proposed sensor would be approximately £700 plus fixturing. The same system using capacitive probes would be approximately £4600 plus fixturing. These savings will increase as the number of elements being monitored rises.

4.6 Sensor applications

The intended application for this sensor is to reduce the largest uncertainty component during on-machine probing, namely the thermal error, using sensor data fusion. The novel displacement sensor can be used with suitable reference rod fixed to the structure for direct measurement of thermos-elastic deformation within the structure of the machine tool. This displacement data can be utilised with temperature sensor data using sensor fusion technique to compensate for thermal error.

The inert rod is used to measure the small distortion relative between the two anchoring points of (i) the rod and (ii) the sensor head. The range of the sensor therefore only needs to be sufficiently large to measure this displacement, rather than the distance between the two points. The measurement range of the sensor is 20 micrometres in the linear range and 60 micrometres full-scale, which can be used if calibrated. By applying the sensors on a structural member in stages, to detect localised distortion, the magnitude of the localised elongation will be within the range of the sensor. If a larger range were required, for example if measuring the overall elongation of a machine ram, then a design modification to the sensor would be required.

The measurement range for alternative sensors is similarly a compromise with resolution or accuracy. Inductive, capacitive and LVDT devices could all be found with ranges limited to a few micrometres or up to several millimetres. The choice of sensor therefore becomes an engineering design problem.

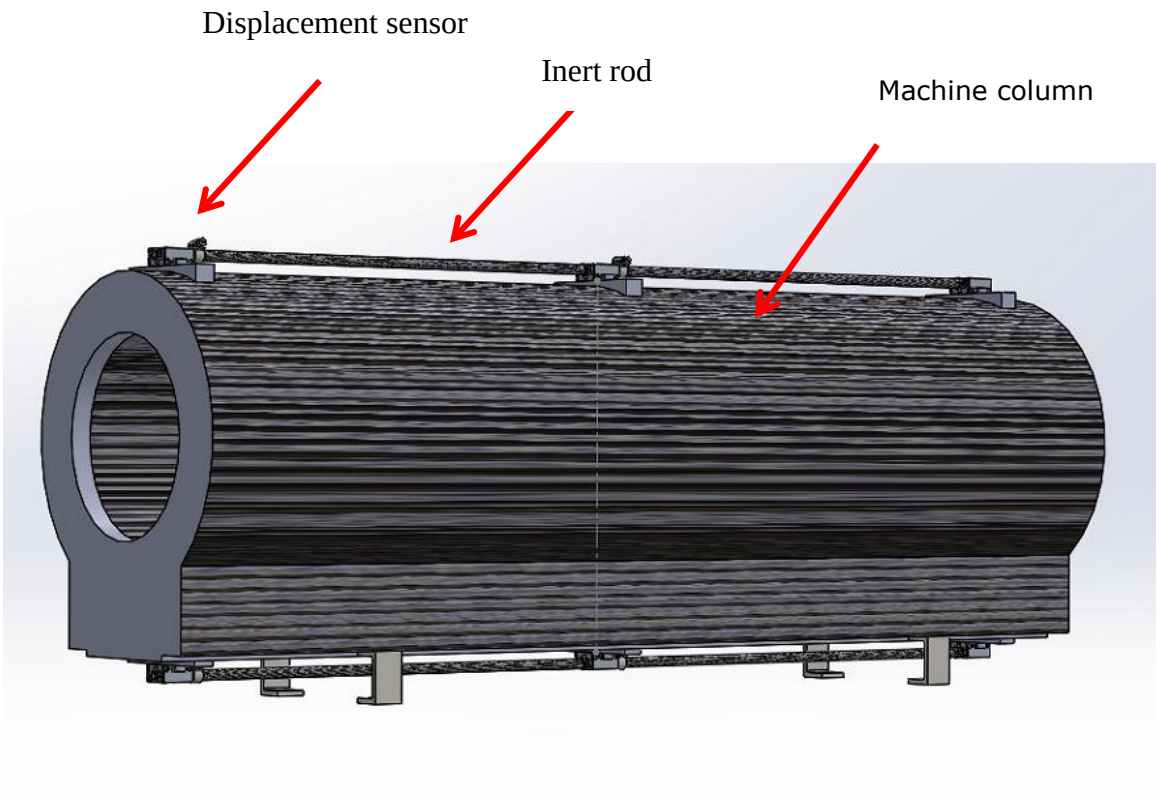

Figure 36. Displacement sensors with rods installed on a column for distortion measurement.

4.7 Summary

In this chapter, the design of a new nanometre-scale resolution displacement sensor based on an opto-electro-mechanical sensing head has been described and the capabilities of a prototype system have been fully characterised. The proposed system is capable of self-compensation against the perturbations due to power supply and ambient light variations. Although the design of the shutter is in contact with the object to be monitored, overall sensor design is minimally invasive. The cost of the prototype sensor head is 26 GBP, less than 10% of their uncalibrated capacitive and inductive counterparts without electronics. The output of the sensor is compatible with any standard data acquisition hardware and software. It is a low cost, compact sized sensor with small footprint that can be designed with a relatively small number of components without any complex signal processing circuits.

Static and dynamic experiments were carried out to investigate the performance characteristics of the prototype sensor head. The static linear range and resolution (6σ)

were evaluated to be 20 μm and 21 nm respectively, with a sensitivity of 0.1648 V/μm. The linearity error is within ±1 % of full-scale range. The repeatability of the sensor is 90 nm and the observed noise in the sensor signal is 21nm without the use of any filter.

The practical limitation of the current implementation is the mechanical shutter design with tight tolerances on its physical dimensions. The potential applications include, but are not limited to, mechanical structural deformation monitoring, piezo-actuator control, vibration monitoring systems, etc.

Chapter 5 - Development of modular machine tool structural monitoring system

This chapter is published in a conference proceeding by Potdar et. al. [116]

Although designed to be structurally stiff, machine tool deformation takes place due to the various sources of errors such as shifting mass, component weight, temperature etc. In order to facilitate research activities and acquire further scientific insight on the deformation process, a computer-based on-line monitoring system has been developed. A variety of sensors can be used to capture data for numerous parameters like temperature, displacement, strain etc.

This chapter presents the design and implementation of a LabVIEW based multi-sensor data acquisition program. It was designed in a three-layer modular structure. In addition to data acquisition, the program is also capable of data processing, logging and implementing various error reduction techniques using online communication between LabVIEW and the MATLAB run-time engine for computation purpose. These calculated compensation values are then transferred to the machine controller via Ethernet. This chapter also describes an example of application of such a system for a 5-axis CNC machine tool.

The motivation for this work came from a practical application for a modular machine tool structural monitoring and compensation system requiring the development of a multi-sensor data capture system. This DAQ system can capture data from several sensors like digital temperature sensor, laser position sensor and Fibre Bragg Grating (FBG) sensor for measuring temperature, displacement and strain respectively. Data can be logged in a format that can be used off-line by third party applications such as MATLAB or Microsoft Excel. Apart from these tasks, this application is programmed to implement compensation techniques during the process using parametric models and artificial intelligence techniques such as Artificial Neural Network (ANN) and Adaptive Neuro Fuzzy Inference System (ANFIS). Obtained compensation values are then transferred to the machine controller using Ethernet.

The Objectives of this chapter are to design a simple, reliable and flexible DAQ system, to implement this program to integrate different sensors and test the application on a real machine application.

5.1 System Overview

In this chapter a computer based on-line monitoring system has been developed. A block diagram of this system is as shown in Figure 37. The system hardware consists of a number of sensors and a computer. The system communicates with a CNC machine tool Siemens 840D interface. The Sensors used are:

The digital temperature sensors used are 1-wire protocol. Unlike traditional analogue temperature sensors, e.g. thermocouples, RTD etc., these sensors have an advantage of communicating serially on a 1-wire bus system when using multiple sensors, which significantly reduces the cabling, and interface effort. In addition, they do not require any special signal conditioning hardware thus reducing the complexity and cost of the system.

They have a programmable resolution of 12 bit ($0.0625^{O}C$) with response time of 750ms and a temperature range of $-55^{O}C$ to $+125^{O}C$. To communicate with a computer, it additionally requires an adapter either USB or serial port.

The laser position sensors used are Riftek RF603. They are used for measuring displacement of a test bar (attached at the bottom of a moving spindle) caused by thermal distortion of the machine.

They work on the principle of laser triangulation and have a base distance of 10mm with measurement range of 2 mm. Resolution of this sensor is 0.01% of its measurement range. The resolution and measurement range of this sensor is suitable for the application. This sensor uses a serial port interface to communicate with the computer, which in some cases requires a RS232-USB converter. They are capable of producing analogue output if required. Alternate sensors were explored for the operation, e.g. eddy current sensors (base distance 0.5 mm). The base distance was not suitable for the operation for the safety reasons.

The Fibre Bragg Grating (FBG) sensors are used for strain measurement purpose[118]. FBG sensors have inherent advantages of fibre optic sensors; they are relatively immune to various perturbations like stray electromagnetic variations, capacitive effects etc., compared to their non-optical counterparts, e.g. resistive strain gauges. FBGs have wavelength-encoded information thus providing immunity against power supply fluctuations as well as insusceptibility to noise caused by variations in ambient light levels. Additionally, drift in

measured strain value of FBG sensors is relatively small, allowing a direct comparison between instant and reference strain levels, even after long time periods and repeated system shutdowns. Apart from this, FBG's offer high resolution and accuracy.

FBG's are supplied by SMARTEC (based in Switzerland). They use Fabry-Perot Tuneable filter technology. Multiple FBG sensors are used in the wavelength range of 1510 to 1570 nm. The resolution is 0.2 με and accuracy is 2 με. FBG sensors have their own reading unit by Micron Optics, which can read at 2 Hz and has 4 optical channels expandable up to 16 channels. The reading unit communicates with the computer using the Ethernet protocol.

FBG sensors and temperature sensors can be used for structural monitoring of the machine tool for off-line and on-line research purposes. Strain values obtained from FBG and temperature values from temperature sensors can be captured and recorded over the desired time period. Logged data can be used for further off-line analysis purpose.

The software installed on the Data Computer (DC) performs all the major tasks like data acquisition, logging and processing. To make advanced on-line analysis and computation more efficient, the software includes a live interface with the MATLAB run time engine. This program computes the compensation values, which are transferred to another LabVIEW program on the Communication Computer (CC). This communication is realized through the Ethernet protocol.

The Program on the CC uses a Dynamic Data Exchange (DDE) link to communicate with the machine controller via Ethernet. Finally, compensation values are applied to the machining process by updating values in the part program. This rudimentary method of compensation is suitable for research purpose, but would be replaced by more robust methods in a commercial implementation.

5.2 Software Design

This section discusses the different criteria that were kept in the mind while designing the software. It also talks about the software architecture.

5.2.1 Design Criteria

The software was designed to provide a simple machine tool structural monitoring system for researchers using LabVIEW based multi sensor data acquisition program. Several aspects that were considered are mentioned as follows:
Usability: All the functions of the program can be performed under the required conditions reliably. Flexibility: It should be flexible enough to modify various parameters and configurations for different sensors. Reusability: Modules designed in this program should be able to be used by other programs without any modification or with trivial changes. Extensibility: Additional features can be easily incorporated without any substantial alterations to the program structure. Cost-efficiency: Cost involved in the development and maintenance of the program should not be high.

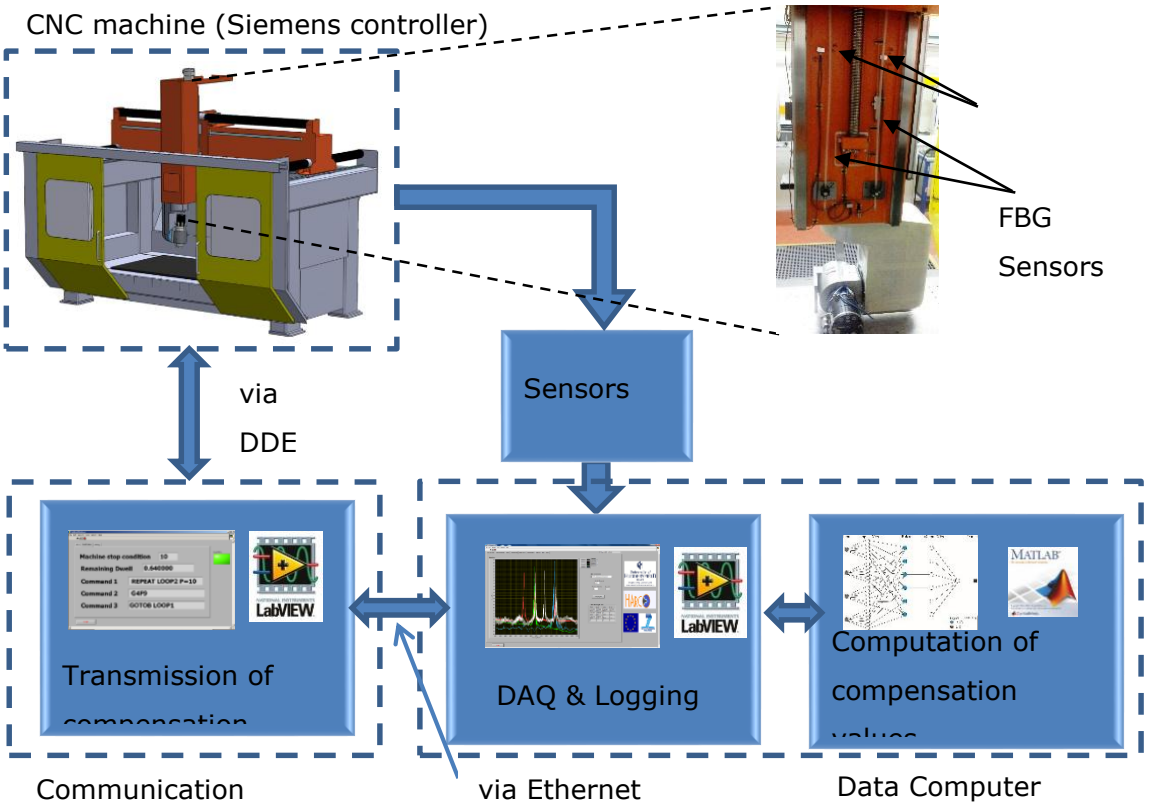

Figure 37. System Overview

Numerous factors need to be considered while selecting the programming language, such as programming skills of the developer, availability of the drivers for various sensors, time

required for the development of the program, parallel programming capability, ease of debugging etc., [119, 120] Considering the above mentioned factors and due to the several other advantages of LabVIEW over other text based languages, it was selected for developing a data acquisition program [121, 122].

5.2.2 Software structure

For any software, well designed architecture is crucial for its success. This program was designed in a modular fashion to offer independent as well as interconnected control of various signals and the three-tier structure was implemented for the development.

The top layer consists of graphical user interface developed using a LabVIEW user interface control. The low level tier is designed for the communication by means of hardware drivers and LabVIEW I/O commands to send and receive data from sensors and hardware devices. The middle tier connects top and bottom layer and provides platform for the development. It performs many tasks and is made up of some of the core modules: FBG Module, Temperature sensor module, laser position sensor module, Controller communication, LabVIEW and MATLAB online communication, data logging and error handling module. Each of these key modules are discussed in detail in later sections. All the principle modules are programmed in independent loops to improve the reusability of the program. The three-tier structure is as shown in the Figure 38.

A modular structure in the software allows integration of new types of sensors or additional sensors without making considerable modifications to the system architecture to easily achieve the desired extensibility. Apart from sensors, extensibility permits the addition of new features in the software as per the requirement in the later stages of research.

5.2.3 Data acquisition process.

A typical data acquisition process is as illustrated in
Figure 39. The system is first initialised to establish a communication between computer and different sensors. In the second step, depending on the type of the sensor, the program either reads the raw data or sends configuration command. For example, in case of laser position sensor, it reads the raw data; for temperature sensor, a convert command is sent for temperature conversion and for FBG sensors, channels are configured. Subsequent steps in the flowchart are based on the parameters set by the user. Data acquisition process is

started from capturing the data form the sensors. Sampling rate of each type of sensor can be controlled individually. Raw data is processed to obtain engineering values before displaying it and saving it to a file if required. After data is read from all the configured sensors, program completes the acquisition operation.

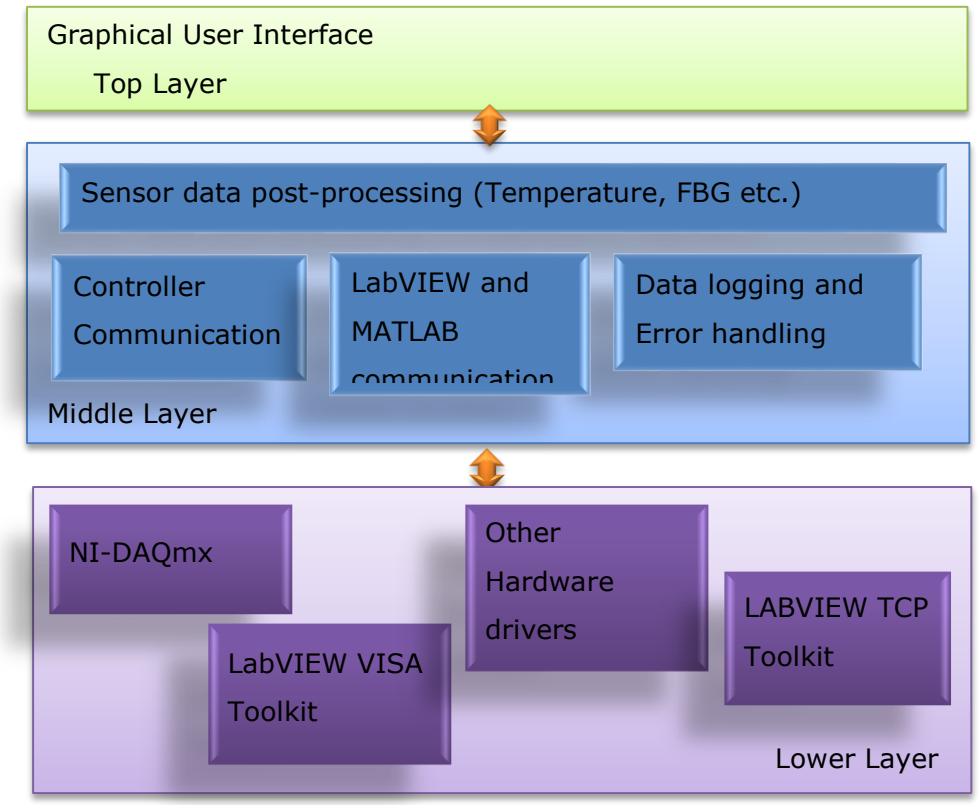

Figure 38. Three tier structure of the program

5.3 Implementation of Main Modules

5.3.1 Sensor data acquisition Module

Different modules are created for different sensors to maintain the modularity of the structure. Software Development kit (SDK) for programming these sensors is provided by

their manufacturers. These SDK's contain sample LabVIEW sub-VIs (Virtual Instrument) and drivers necessary to perform fundamental operations.

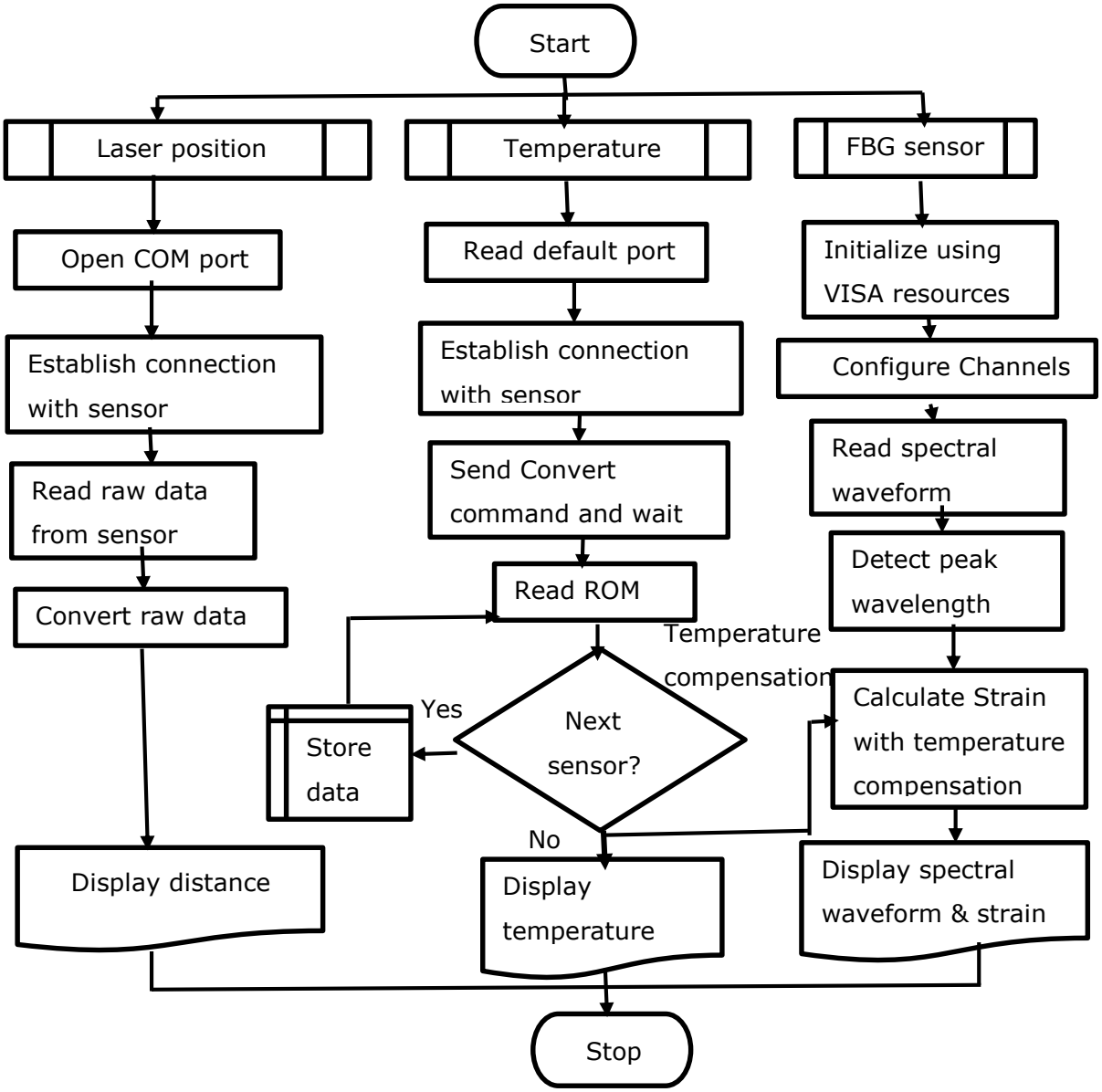

Figure 39. Flowchart for data acquisition

5.3.2 LabVIEW and MATLAB interface module

This LabVIEW DAQ program is designed to implement various machine tool error compensation algorithms based on ANFIS, ANN and physical models. Modelling, training and

analysis of these compensation techniques was carried out in MATLAB. Due to this, many complex inherent functions of the MATLAB were utilized during the design phase. It was observed that direct conversion of MATLAB code into the LabVIEW was time consuming and prone to error during translation which potentially could generate different output for the same input. Thus, an interface between LabVIEW and MATLAB was used to simplify the adoption of off-line optimised model with reduced uncertainties that would be involved in the code conversion.

This interface was achieved using LabVIEW's MATLAB Script module. It uses Microsoft ActiveX technology for communication. Thus, .m file generated by MATLAB can be directly imported into the LabVIEW eliminating the need for code conversion. Some of the off-line models such as ANFIS generate files in ".fis" format. Such a files can be called in the LabVIEW code without any recompilation.
Data captured from various sensors by LabVIEW is passed in the MATLAB Script code containing compensation model, which in turn generates the corresponding output. This output is returned backed to LabVIEW, which is passed to the machine controller.

5.3.3 Controller communication module

The purpose of this module is to establish a bi-directional communication between the machine tool controller and the CC. This communication link is established in two steps. In the first step, calculated compensation value is transferred from the DC to CC using Ethernet. Standard TCP (Transmission Control Protocol) toolkit is used for this purpose. In the second step, the DDE link using Ethernet is used to communicate with the controller. These compensation values are then used to modify the parameters in the controller, which are subsequently used by the CNC code to modify the values of Machine Co-ordinate System (MCS) during the machining process. MCS values can be transferred from the controller back to the LabVIEW program for analysis.

5.3.4 Data Logging Module

Data captured from all the sensors as well as MCS values with absolute time can be logged using this module. This is achieved with the help of LabVIEW file I/O functions. Data is saved in ".CSV" (comma-separated values) format. This format was chosen because it can

be easily imported in other applications for further analysis purpose. Data logging time is programmable.

5.4 Demonstration of the software

5.4.1 Program overview

In this section, a brief introduction to the developed LabVIEW program is provided. Screenshots of the front panel of the software are illustrated in Figure 45. For each individual module such as for different sensors, compensation, communication and data logging separate tab is created. This way modularity of the structure is maintained in the front panel as well.

The front user interface contains 7 key segments: FBG spectrum, strain, temperature, laser sensor, compensation, communication and data log. Various configuration settings and sampling time for each type of sensor is programmable. Data for each sensor can be plotted live. Different compensation models can be configured as per the required parameters and their output can be plotted and observed in continuous manner.

5.4.2 Examples of the software application

In this section, three brief examples of the software application are mentioned. In the first two examples, tests were performed on a 5-axis Geiss machine tool. Third example discusses about the performance evaluation test of the laser tracker (LT).

The first was performed for the period of 14 days and machine was not in operation during this period. The purpose of this test was to monitor the thermal response of the crossbeam structure of the machine tool with change in environmental temperature. FBG sensors were mounted on the crossbeam structure (refer Figure 37) with digital temperature sensor to observe the thermal response. Data for all the sensors was logged every minute. All the measured data was used for the post analysis purpose. Test result is shown in Figure 40.

The primary motive of the second test was to observe the deformation taking place in the ram of the machine along the Z-axis direction due to the heating of the C-axis motor during prolonged operation and to compensate it during the running process itself.

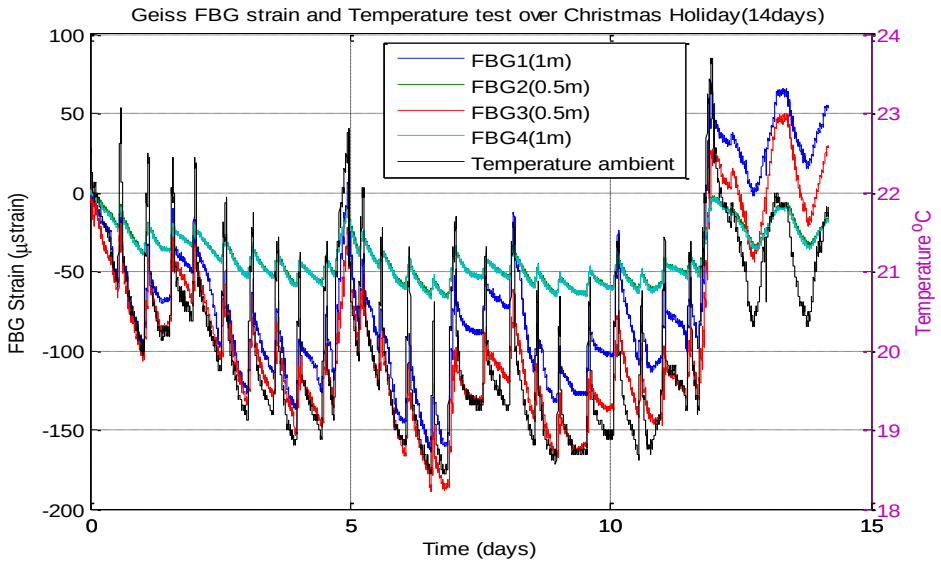

Figure 40. Test results for environmental thermal response of crossbeam

FBG sensors were mounted on each side of the ram structure (refer Figure 37). The design and implementation of ANFIS model for thermal error reduction is carried out by Ali Abdulshahed as part of his PhD thesis [123]. The Output of the FBG sensors was used by the ANFIS compensation model. Calculated compensation values were used to modify the CNC code to maintain the position of the ram. Laser position sensors were used for the validation purpose. Data for all the sensors was logged at every 1 second. On-line screenshots of the output of the compensation model and laser sensor are shown in Figure 45 and test results are shown in Figure 46. Residual error in the range of 10 μm was observed during the test.

ANFIS Design

The structure of ANFIS used in this study is shown in Figure 41. It is a five-layer network. The ANFIS model was developed using MATLAB. The ANFIS constructs a fuzzy inference system (FIS) whose membership function parameters are tuned using the hybrid optimisation method. The hybrid optimisation method is a combination of the least-square method and the backpropagation algorithm. The Sugeno fuzzy reasoning with Gaussian membership functions (MFs) for each inputs were used. The Sugeno fuzzy system was utilised in this study because of its computational efficiency, versatile procedures and ability better ability for handling non-linear relations of input and output [124]. The Gaussian type

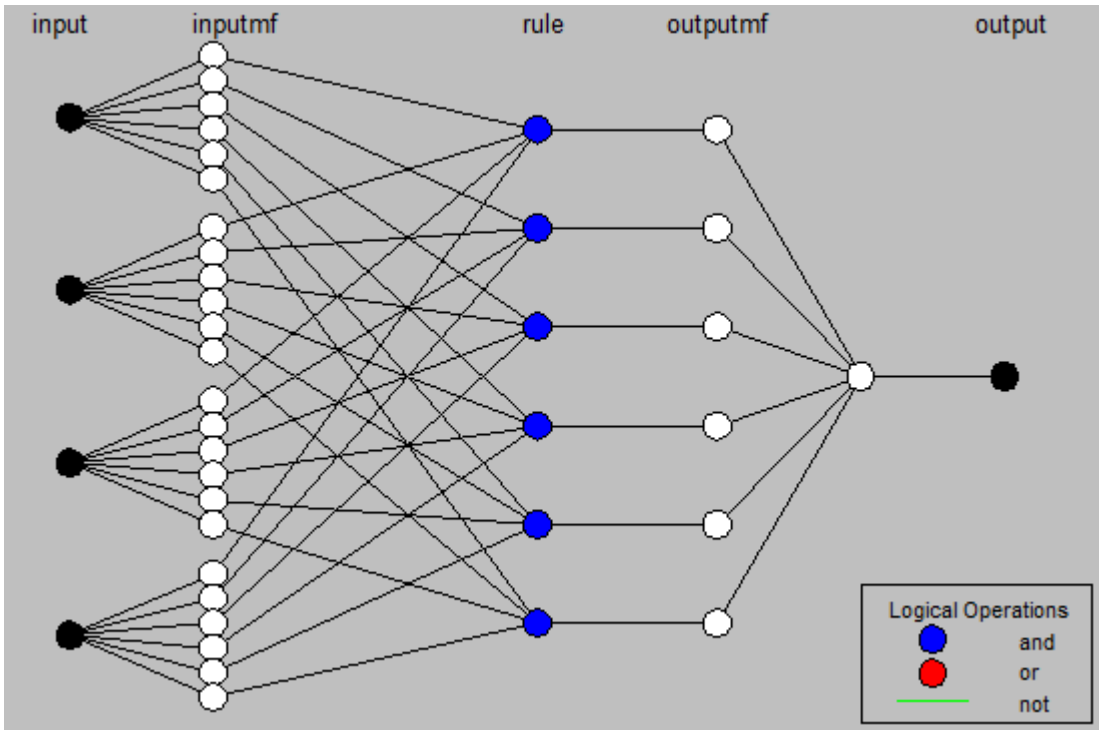

Figure 41. ANFIS structure for thermal error modelling

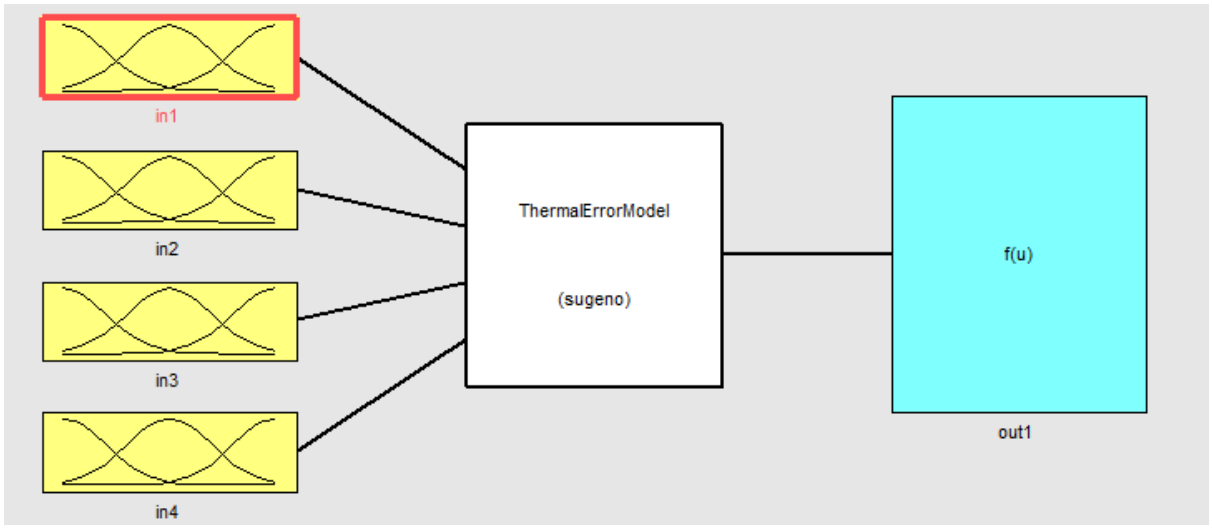

Figure 42. Fuzzy block scheme for thermal error model.

MF was incorporated because it provides a smoother model behaviour [125]. A linear defuzzifier was used in the output part of each rule; and total output is the weighted average of each rule output. The network consists of four inputs (FBG data), one output (thermal error) and six membership functions for each input. The fuzzy block scheme is presented in Figure 42. The Figure 43 shows the membership functions (MFs) used for input

variable and Figure 44 illustrates the MF used for output variable. Six fuzzy rules are derived from six MFs.

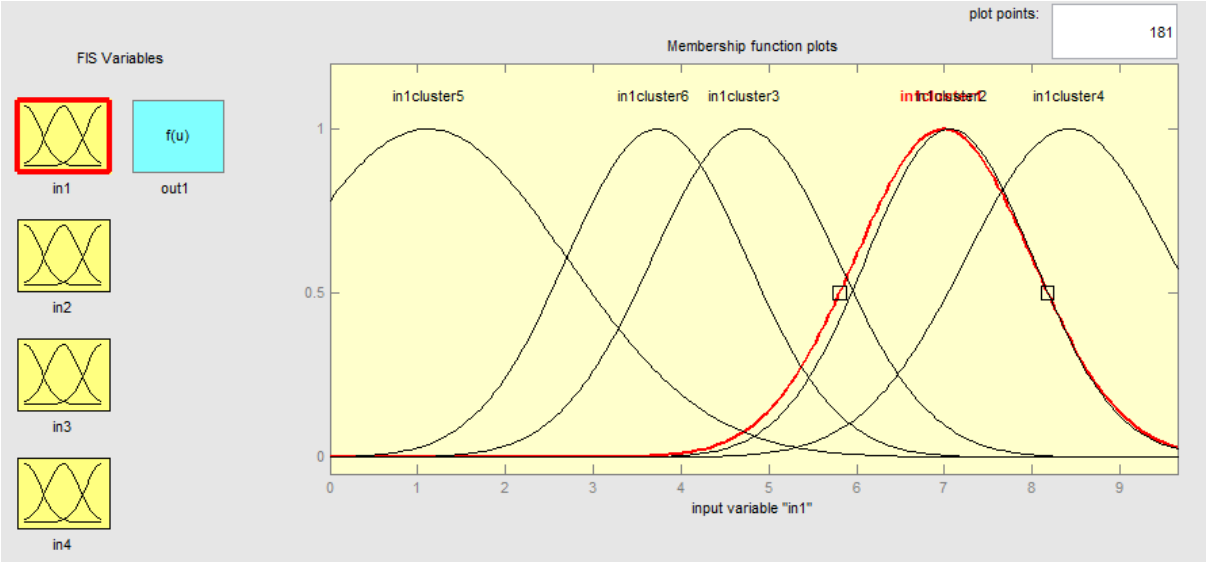

Figure 43. Membership function block for input variable

Figure 44. Membership function block for output variable

Figure 45. Compensation model output during the operation

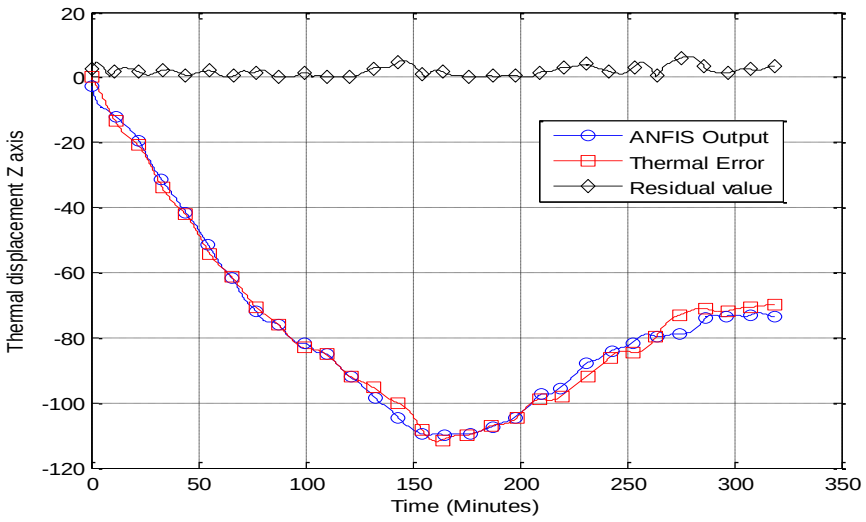

Figure 46. Test Results for thermal displacement of Z-axis

Figure 47. Test results for thermal response of laser tracker

In the third example, only temperature measurement module of the software was used for performance evolution of the laser tracker. This test was carried out for the period of 14 hours, data was logged at every 25 sec. Data acquisition for temperature and LT was carried out using different softwares. Figure 47 illustrates test results showing effect of temperature variation on reparability of LT

5.5 Summary

Using the LabVIEW environment a machine tool structural monitoring application was developed; offering the prospect of using computer based data processing to expedite the development path. This program was created in the modular structure to provide user-friendly software and to allow desired flexibility and extensibility. Various modules prepared in this program can be easily used for other applications with minimal or no alterations.

This chapter also describes an example of application of such a system for data monitoring, logging, control model calculation and communication for compensation values for a 5-axis CNC machine tool. The extensibility of the design is of paramount importance to efficient development.

Chapter 6 - Application of multi sensor data fusion

This chapter is published in a conference proceeding by Potdar et. al [126].

Due to the various heat sources on a machine tool, there exists a complex temperature distribution across its structure. This causes an inherent thermal hysteresis, which is undesirable as it affects the systematic tool –to-workpiece positioning capability. To monitor this, two physical quantities (temperature and strain) are measured at multiple locations. This chapter is concerned with the use of Principal Component Analysis (PCA) and Artificial Neural Networks (ANN) to fuse this potentially large amount of data from multiple sources. PCA reduces the dimensionality of the data and thus reduces training time for the ANN, which is being used for thermal modelling. This chapter shows the effect of different levels of data compression and the application of rate of change of sensor values to reduce the effect of system hysteresis. This methodology has been successfully applied to the ram of a 5-axis gantry machine with 90 % correlation to the measured displacement.

6.1 Introduction

In the current work, data is acquired from two sources: temperature sensors for temperature measurement and Fibre Bragg Grating (FBG) sensors for strain measurement. Neural Network (NN) can map the nonlinear relationship by training with back-propagation algorithm [127]. As the relationship between thermal deformation of the machine and temperature measurement is nonlinear [100], it is reasonable to use Artificial Neural Network (ANN) to build the thermal deformation estimation model. However ANN sometimes loses its generalization capability due to the over fitting which reduces the robustness of its estimation ability. To make sensor fusion useful, it is essential to pre-process data and to consider temporal development of data in an appropriate way [128]. In this case, Principal Component Analysis (PCA) is used for dimensionality reduction of the data and to improve the ANN's estimation performance while reducing the training time.

This chapter also demonstrates different levels of data compression i.e. comparison of ANN performance is made with various kinds of inputs. Inputs being: i) all available sensors, ii) principal components of all sensors, iii) sensors having good correlation with the measured output and iv) principal components of these correlated sensors. This methodology is then applied to the ram of a 5-axis gantry machine.

6.2 System Architecture

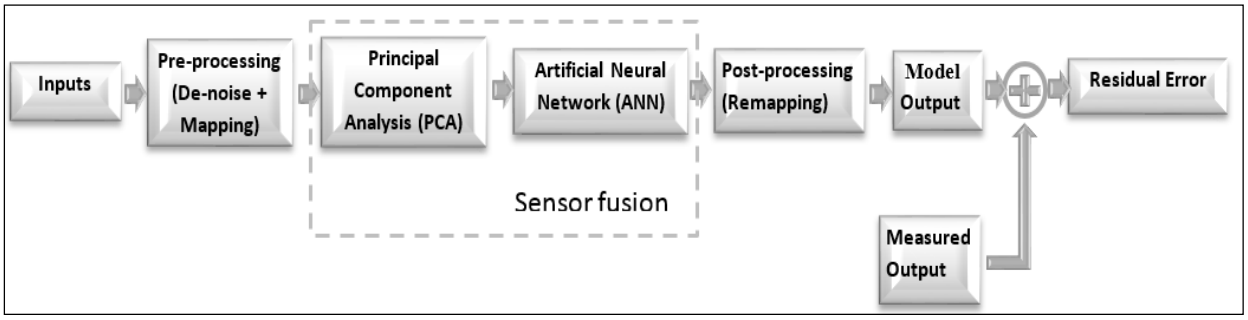

Figure 48. System architecture of the PCA-ANN based prediction model.

A block diagram of the system architecture is shown in Figure 48. Eight FBG and six temperature sensors were used as a system input. A Laser position sensor was used to measure the displacement in the ram of a machine. Technical specifications of all the sensors used can be found in [116]. Data obtained from measurements was pre-processed using a moving average filter with window size of five to remove any undesired noise signal before normalising it. This processed input data was used for PCA, which was further on used to train the ANN model, and after the completion of training, used as input layer to test the model with a completely new and independent set of inputs. The ANN's predicted output was compared with the measured thermal displacement response in terms of percentage correlation (% R) and Root Mean Square Error (RMSE) between them to check the performance of the thermal model.

PCA is a statistical technique and is used to transform a set of inter-dependent variables into significant and independent ones called Principal Components (PCs). This transformation is performed in such a way that the first PC has the largest possible variance and each succeeding PC in turn has the highest variance possible while being orthogonal to the preceding one. The detailed mathematical background of PCA is given by Jolliffe [129]. Experimentally obtained measurement data was represented by a 720 × 14 sensor data matrix. The fourteen columns correspond to the eight FBG and six temperature sensors and the 720 rows are data samples for each sensor. This data matrix is the input data set for PCA. Figure 49 illustrates the percentage of total variance by fourteen principal components, corresponding to fourteen sensors, obtained by PCA of three tests. First PC represents the maximum information which explains more than 90 % of total variance and the combined PC1, PC2 and PC3 holds more than 99 % of the information while remaining PCs account for less than 1 % of the total data. Hence, to ensure the dimension reduction

and integrity of the original data, first three PCs were selected. Thus, the new data set is of the dimension 720 × 3. This is the new input set for the ANN model.

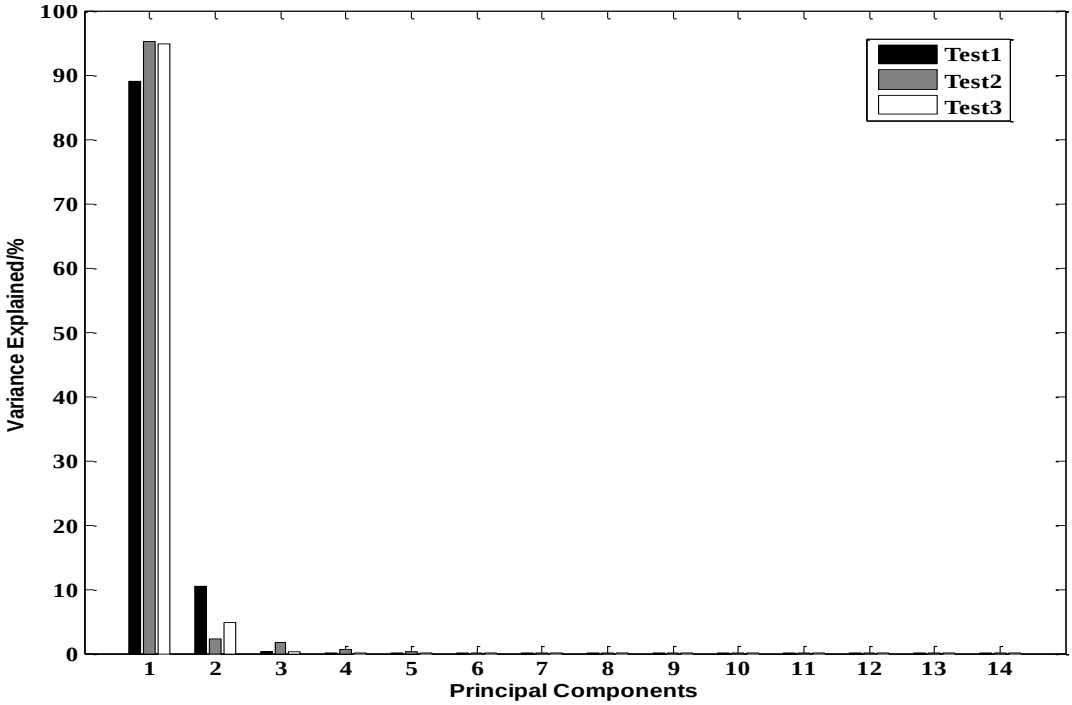

Figure 49. Percentage of total variance illustrated by all the principal components for three tests

ANN design

For thermal modelling using sensor fusion, a three layer feed forward ANN based on multilayer perceptron was selected. To reduce the training time of the ANN and to check its performance with reduced data set obtained using PCA, four models were created. Model 1 was trained with all available input sensors i.e. fourteen sensors (FBGs and temperature sensors) and model 2 was trained with three PCs extracted from fourteen sensors.

Model 3 consisted of only those sensors which had the highest correlation among all sensors with measured displacement. From Table 7 we can comment that the first three FBG sensors have highest correlation with the measured data as well as temperature sensor one, three and four. Hence, we selected three FBGs and three temperature sensors for this model. PCA was performed on these correlated sensors and three PCs extracted from them were used to train model 4.

FBG Sensor	% correlation with measured displacement	Temperature sensor	% correlation with measured displacement
1	98.04	1	96.5
2	91.86	2	79.32
3	99.31	3	81.05
4	69.28	4	81.14
5	81.62	5	64.16
6	86.68	6	44.69
7	82.81		
8	77.77		

Table 7. Table presenting % correlation of all the sensors with the measured thermal displacement

The size of the input layer was either fourteen, three or six depending on the model. The hidden layer was made up of ten neurons and one neuron in the output layer. The method of supervised learning using back propagation strategy with Levenberg-Marquardt algorithm was used. Table 8 illustrates in detail the ANN architecture and training parameters used in the investigation. The ANN structure used in this study is presented in Figure 50 and the training statistics are shown in Figure 51.

For learning purposes, each data matrix was divided into three sets: a training set consisting of 70 % of data; a validation set using 15 %; and a testing set of 15 %. The training data set was used to train the ANN by adjusting its weights, the validation set was used to minimize over-fitting and the test set was used to evaluate the performance of the ANN after completion of the training phase. Once the learning of the ANN was completed, an independent data set was presented to the ANN model and the performance of all the four models was checked.

MATLAB was used for all the PCA and ANN training, testing and analysis of the data.

Parameters	Type/Value
Number of neurons in Input layer	3/6/14 (model dependent)
Number of hidden layers	1
Number of neurons in hidden layer	10
Number of neurons in output layer	1
Training algorithm	Levenberg-Marquardt
Training Function	trainlm
Transfer function	Sigmoid for hidden layer and linear for output layer
Performance criteria	Mean Square error (MSE)

Table 8. Details of developed ANN network

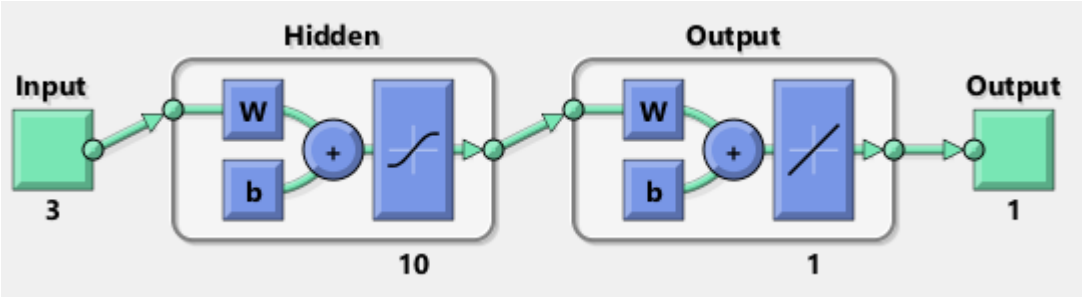

Figure 50. ANN structure for thermal error modelling using sensor fusion

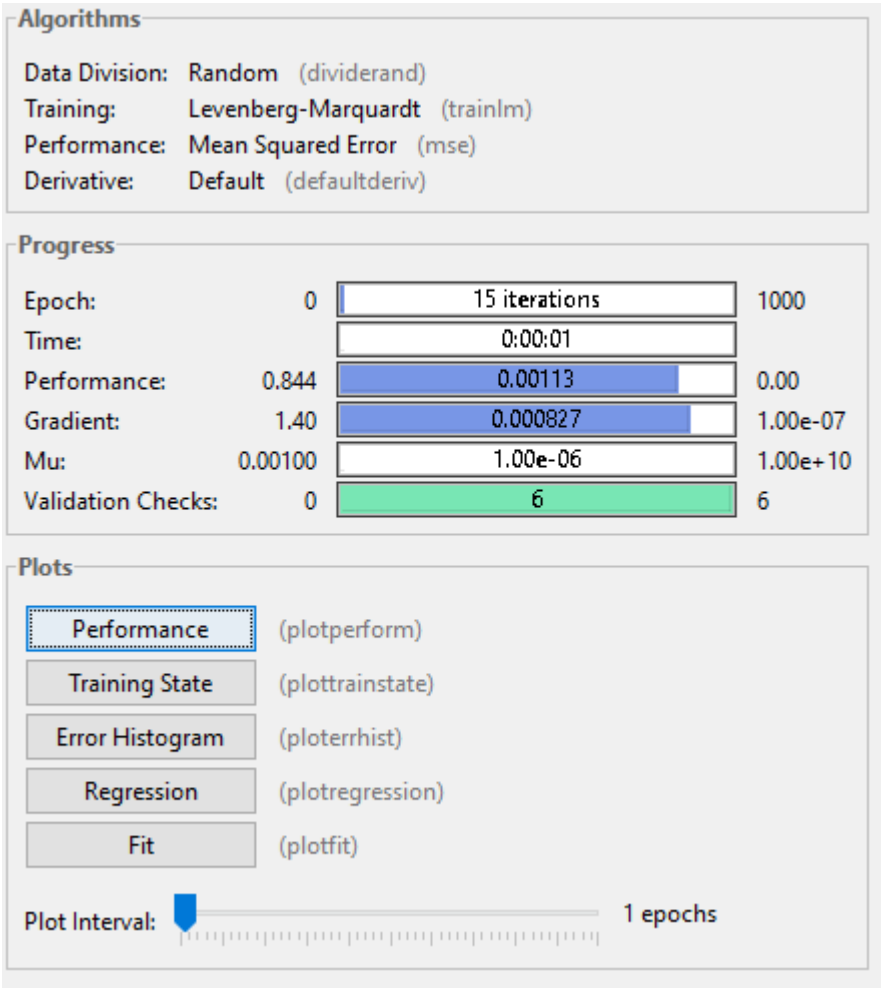

Figure 51. ANN training statistics

6.3 Experimental Setup

The experimental setup is described in Figure 52**.** Tests were performed on a 5-axis gantry machine, the aim of which was to monitor thermal displacement in the Z direction due to C-axis motor heating while in operation. Temperature sensors (T1, T2, T3 etc.) were mounted on front and rear faces of the ram. Location of temperature sensors was decided after examining the heat distribution measured using a thermal imaging camera. Additionally, FBG sensors were also mounted on the ram structure. Displacement in the Z direction is measured by laser triangulation sensors. For data acquisition and logging, applications using LabVIEW were developed. This is reported in Potdar et al [116].

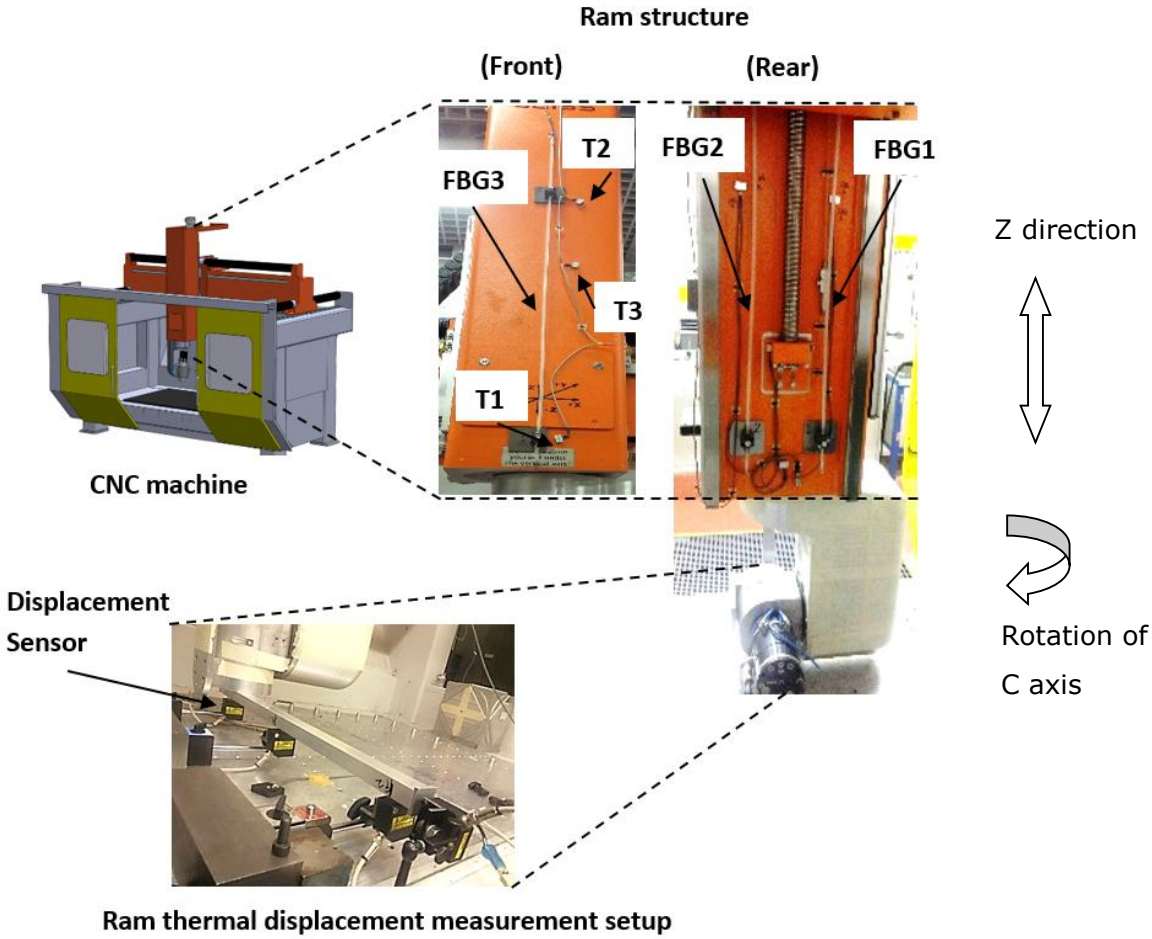

Figure 52. CNC machine and ram structure with sensors location.

Tests consisted of a heating and cooling cycle lasting for approximately three hours each. During the heating period, the C-axis motor was rotated at 60 revolutions per minute to simulate 5-axis machining and held stationary during the cooling phase. To facilitate the laser measurement during the heating phase the C axis was stopped intermittently. Sampling rate for FBGs and temperature sensor was 30 seconds. Results of the experiment are discussed in the next section.

The data represented in both Figure 53 and Figure 54 belongs to test number 3, which was completely independent to the training phase of the ANN. Figure 53 demonstrates the variation of temperature change taking place during the test duration of six hours. Data from only three temperatures sensors with highest correlation is selected for the demonstration purposes based on table 1. As expected, an increase in temperature can be observed due to the heat induced by the C-axis motor located inside the bottom of the ram. Surprisingly the thermal time constant was high, evident from the gradient after three

hours. During the cooling cycle, increase in temperature slows but no typical exponential cooling occurred. Figure 53 shows the thermal displacement in the negative Z direction indicating expansion that reached a maximum of 120 µm after three hours. A further analysis revealed that the thermal displacement decreased when the motor was non-operational.

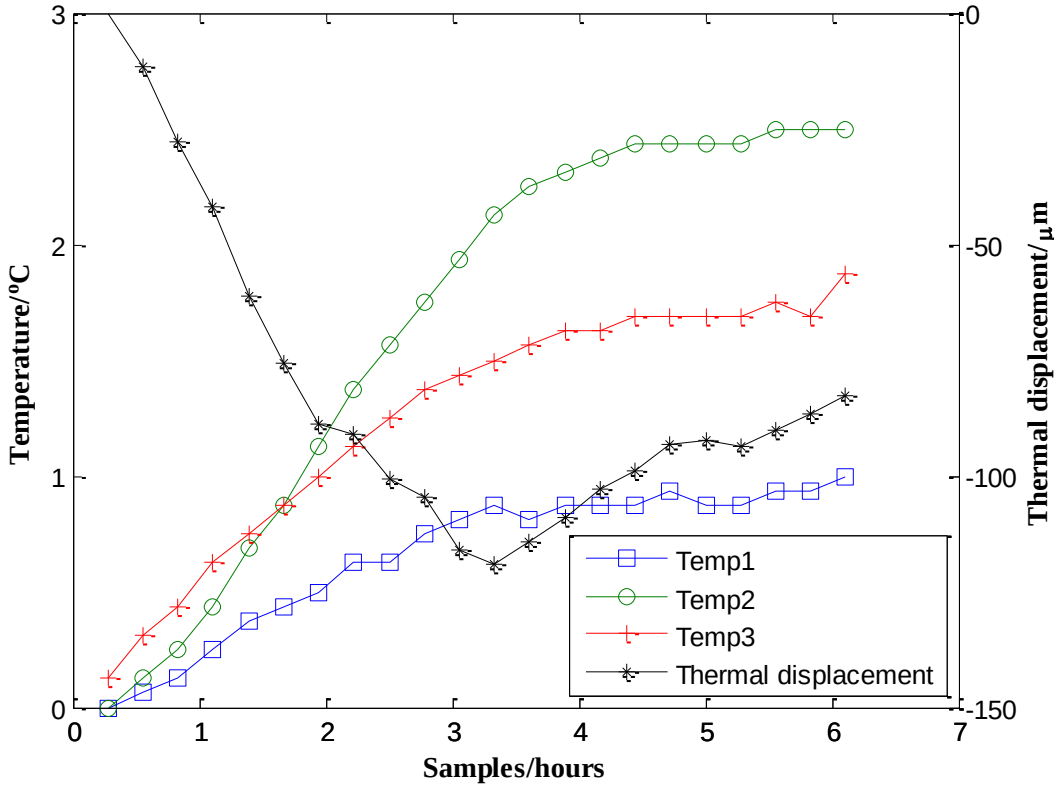

Figure 53. Temperature variation and corresponding thermal response in Z direction of the ram.

Similarly, Figure 54 shows the expected response of the FBG sensors. During the heating increased strain due to expansion can be observed and steady reduction during the cooling stage. The FBG's provide the overall strain over the length of ram structure, but not localised distortion.

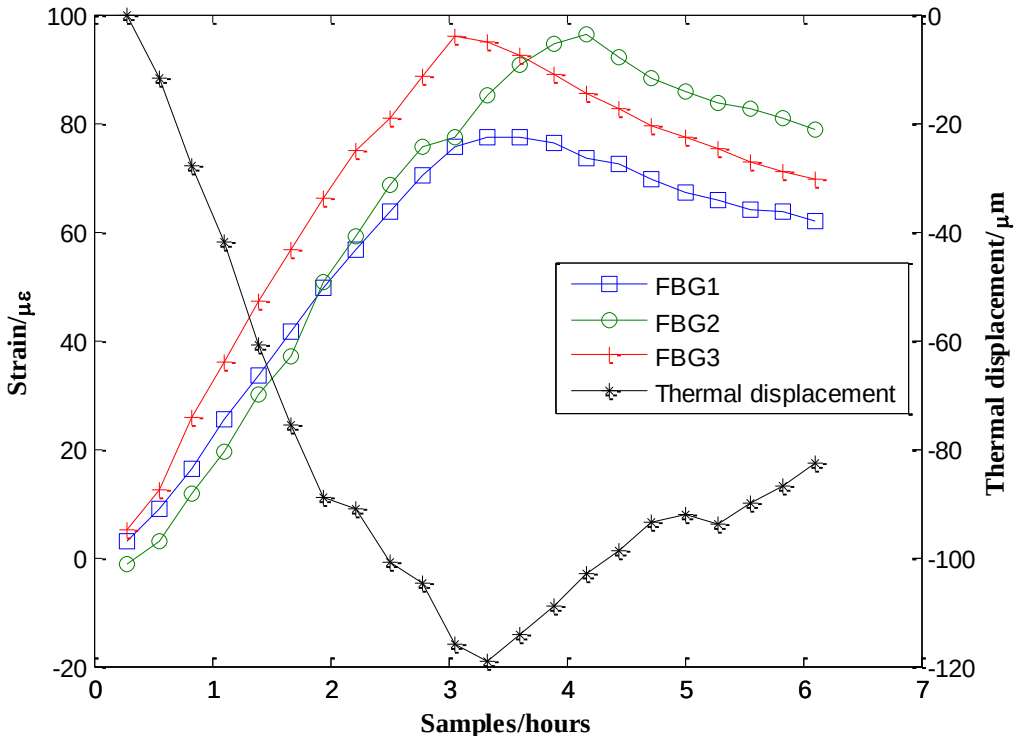

Figure 54. Variation in strain and corresponding thermal response in Z direction of the ram

6.4 Result

Estimated thermal displacements obtained from the four models were compared with the actual measured displacement. Table 9 compares percentage correlation between measured output and predicted output by four models. Although model 4 training is marginally worse than the other 3 models, it is appreciably better than them for both the validation trials. It can be clearly seen that the model 4 output has better than 90 % correlation to the measured displacement compared to the other models.

The RMSE for all the four models is presented in Table 10. Again, excluding the training (test one), model four shows lowest RMSE, 8 μm for test two and 12 μm for test three.

From Table 11, it can be seen that training time for the ANN is reduced from 59 seconds for model 1 to 1.28 seconds for model 4. This is mainly due to the reduction in the dimension of the input dataset from 720×14 to 720×3, showing the validity of the technique. Applying this method to a full machine model would have greater benefits.

Test no.	Model 1 R/%	Model 2 R/%	Model 3 R/%	Model 4 R/%
1 (Training)	99.99	99.83	99.83	99.28
2	26.85	77.56	88.41	94.20
3	26.74	57.56	82.58	96.14

Table 9. Table showing percentage correlation (R) between ANN output and measured output

Test	Model 1 RMSE/µm	Model 2 RMSE/µm	Model 3 RMSE/µm	Model 4 RMSE/µm
1 (Training)	2	2	2	4
2	51	16	12	8
3	168	36	36	12

Table 10. Table showing root mean square error (RMSE) between ANN output and measured output

	Model 1	Model 2	Model 3	Model 4
Training Time/Second	59	0.53	1.87	1.28

Table 11. ANN training time required for all models.

Figure 55 (a, b, c and d) shows outputs of the four models with measured thermal displacement. Additionally it also shows the residual error, obtained by calculating the difference between predicted and measured output. Maximum residual error for model 1 is 220 µm, model 2 is 50 µm, model 3 is 40 µm and for model 4 is 26 µm. Thus model 4 shows improvement of 78 % (absolute error) over the original measured thermal displacement of 120 µm.

a.

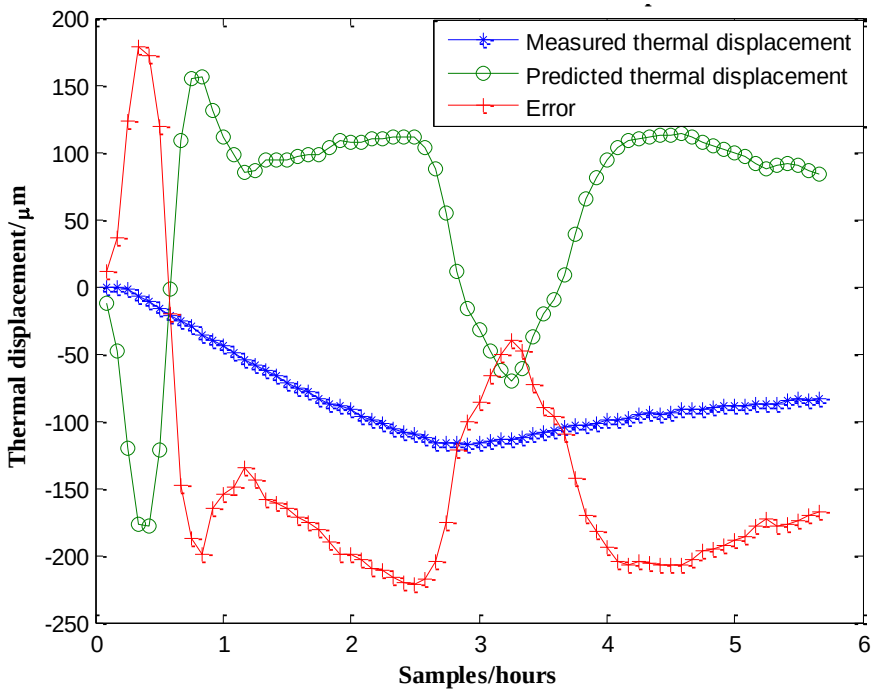
Measured thermal displacement
Predicted thermal displacement
Error
Thermal displacement/μm
Samples/hours
200
150
100
50
0
-50
-100
-150
-200
-250
0
1
2
3
4
5
6

b.

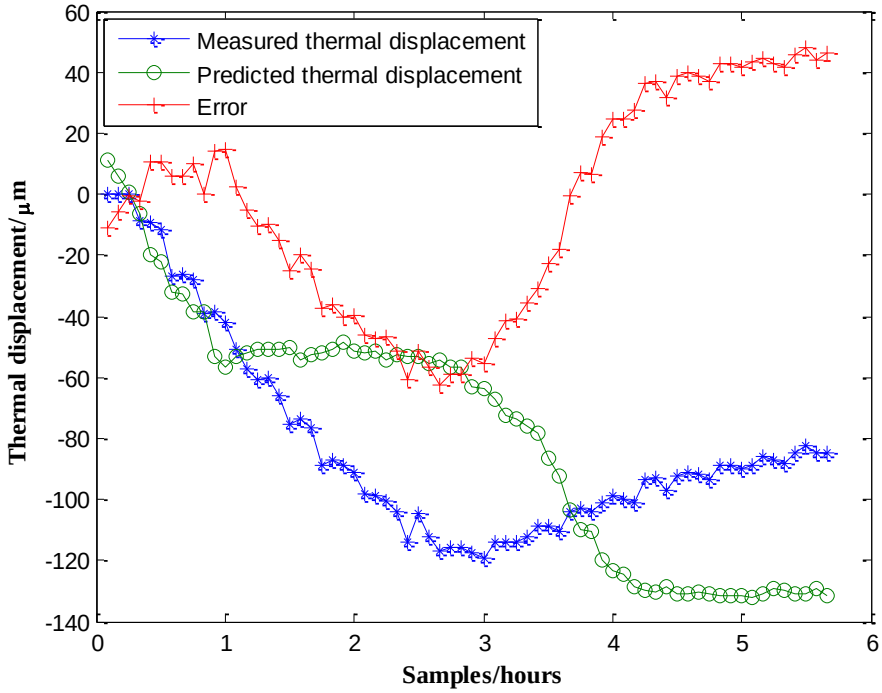
Measured thermal displacement
Predicted thermal displacement
Error
Thermal displacement/μm
Samples/hours
60
40
20
0
-20
-40
-60
-80
-100
-120
-140
0
1
2
3
4
5
6

c.

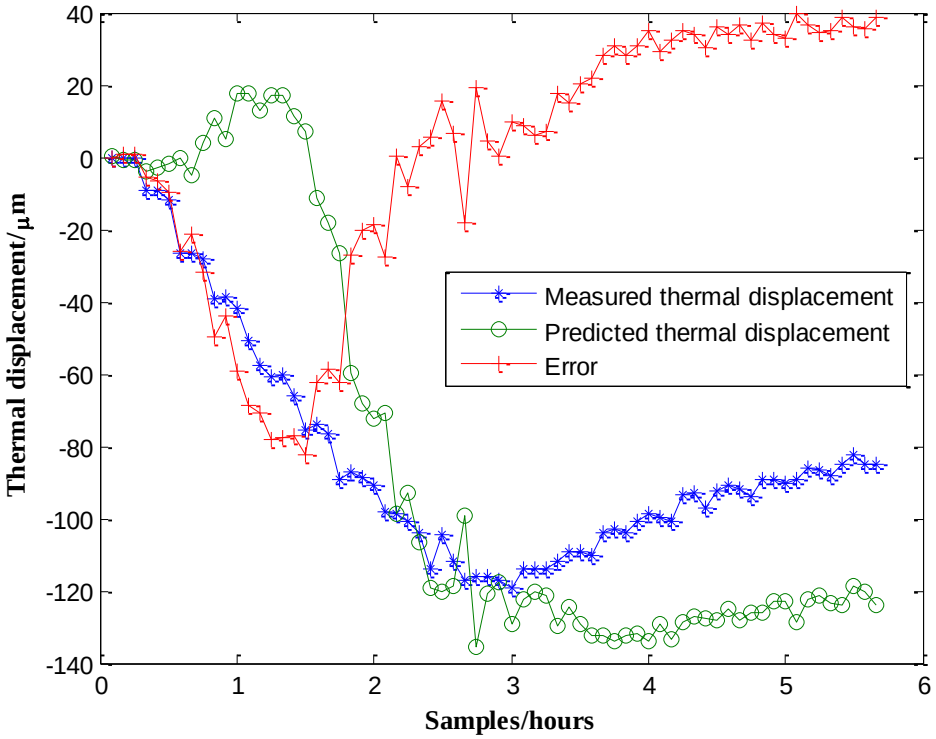

d.

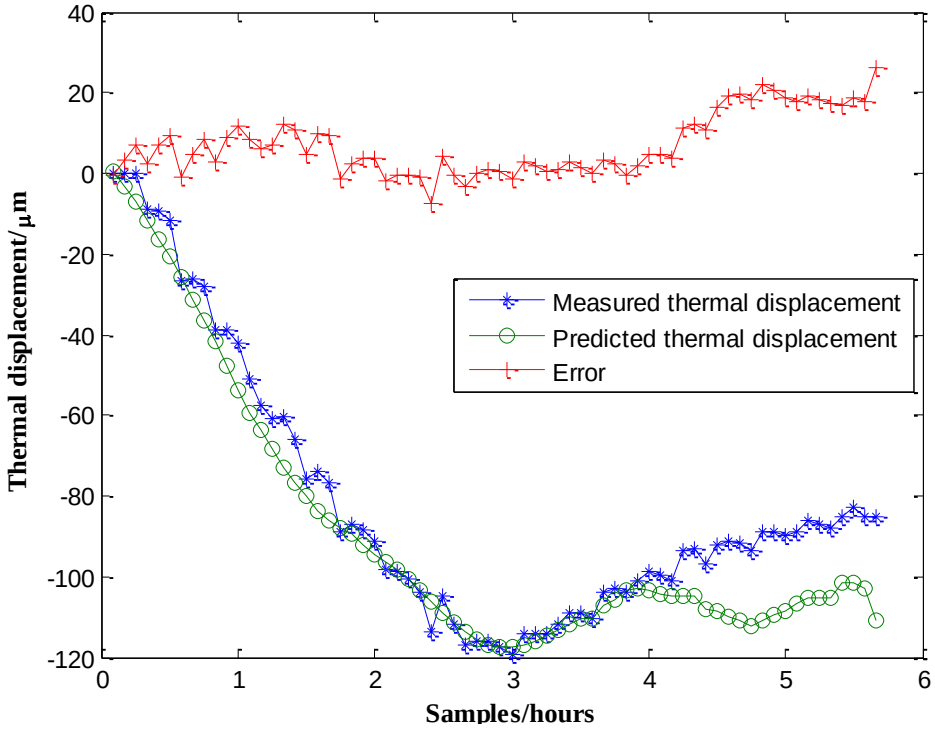

Figure 55. Comparing measured output and predicted output of test 3 for all models; a) model 1 b) model 2 c) model 3 d) model 4.

6.5 Summary

In this chapter, output scores of the PCA used to train a sensor fusion model developed using ANN for thermal error modelling. ANN model output with correlated sensors with extracted PCs showed better than 90 % correlation with the measured data compared to other models and least RMSE. Thus, it can be concluded that predication and generalization capability of the ANN was improved. The method of correlation analysis used for temperature and FBG sensors reduces the number of variables in modelling and thus can reduce the cost of the system.

PCA further reduces the dimensionality of the measured input data, thus reducing the computation time of the ANN. This can be especially useful in case of large amount data obtained for a long period of time or if close to real time calculations are needed for active compensation.

Chapter 7 – Conclusion and future work

This thesis has investigated the use of on-machining probing as a means of acquiring the data necessary for the calibration of thermal correction models affected by uncertainty. Therefore, method of improvement is required. It then goes on to design and develop a displacement sensor for data fusion to reduce the uncertainty. Software capable of multi-sensor data acquisition with the ability to apply fusion technique was designed and implemented using LabVIEW. A sensor fusion technique by means of artificial neural network (ANN) and principal component analysis (PCA) was developed.

Metrology is a science, which considers all the factors contributing to the uncertainty of the measurement. This includes machine tools errors as well as effects from the machining process, both of which should be minimised. Machine tool errors hinder the possibility of achieving tight accuracy requirements for high-value manufacturing processes. The volumetric accuracy of the machine tools primarily depends on the magnitude of quasi-static geometric errors; non-rigid body errors; and thermal errors. Thermal errors can contribute more than 50 % of the total machine errors. Due to the complex interaction of various factors, thermal errors are non-linear and transient in nature. Hence, it is relatively complicated to achieve an accurate error map for them.

The error correction can be achieved using pre-calibrated or active error compensation techniques. The pre-calibrated compensation techniques are effective only when both machining and measurement processes are repeatable in nature. The active error compensation is a potentially more desirable solution in an industrial application, since, an on-line semi-closed loop is used, the error is monitored during the actual process and the same is used for on-line error compensation. However, the downside to such a strategy is the additional cost requirement and physical constraint that such a system would require.

An attractive solution is to fuse on-line measurement to supplement a pre-calibration schema. Thus, there is a need for an on-line measurement system for error monitoring so the machining process can be altered during the same operation. On-machine probing is a readily available technology that can help achieve this. However, this is intermittent, so fusing with sensor providing continuous data yields greater returns.

The thesis then discusses the advantages and disadvantages of the coordinate measuring machines (CMMs) and on-machine probing (OMP). An on-machine probe is a relatively

inexpensive and easy to use accessory that can be directly and automatically mounted on the spindle of CNC milling machine or in the lathe turret. Thus, this kind of arrangement provides functionality similar to a CMM measurement. However, a machine tool does not have the stability of a CMM due to the factors described above.

Taking experimental data from a machine tool to assess the distortion that comes from thermal changes is the means by which thermal error models are calibrated, either to tune parameterised models or for self-learning techniques, such as Artificial Intelligence (AI).

The uncertainty of measurement plays a critical factor in the fidelity of models that are achieved by empirical means, so should be minimised.

Traditional methods of measuring the thermal distortion include laser interferometers, spindle analysers, etc. These are well-defined, independent metrology tools, whose uncertainties are therefore well understood. However, the availability of on-machining probing systems means that utilising them for capturing data is extremely attractive; the capital cost has already been borne and there is no additional requirement for specialist knowledge/training to set them up.

The main limiting factor in using the probe as a reliable, traceable part of the quality audit for a produced part is that the same axes that create the part also drive the measurement device. This means that some of the errors in machining will not be picked up by the measuring procedure; it is not an independent check. Probes measure parts while moving the erroneous machine tool axes, thus on-machine measurement data inevitably includes the probing errors as well as errors originated from the inaccuracies of a machine tool. This thesis has considered the influencing factors on the accuracy of on-machine probing systems when used to calibrate a thermal model.

Thus, the goals of the research were formulated as follows:

1.To investigate and evaluate the uncertainties of on-machine probing for machine tool thermal error model calibration.

2. To reduce the uncertainty using sensor data fusion.

3. To develop a novel displacement measurement sensor.

7.1 Contribution to knowledge

This section summarises the most important contributions of the research work.

7.1.1 Investigation of sources of uncertainties and sensor data fusion

This thesis investigates the uncertainty contributors at granular level for on-machine probing for a particular case of thermal error model calibration. **Thermal errors are often found to be the largest contributing factors for OMP**. In experiments on production machine, these were found to reach a magnitude of up to 220 µm. Hence, they need to be reduced significantly.

Machine tool geometric error, although less than thermal errors in magnitude, make a significant contribution towards the uncertainty of OMP, but can be considerably reduced owing to their repeatable nature using machine tool calibration and modern advanced compensation.

The probing system errors owing to factors such as pre-travel variation, time delay and time delay variation can have a specific known value. Thus, they can be compensated using probe calibration. However, it must be evaluated on a machine by-machine basis. The probe-tool changing and relocation repeatability for the tested machine was under 0.5 µm, making it an insignificant contributor. Similarly, probe repeatability was obtained by experimental analysis; it was less than 0.5 µm.

It was observed that there is a direct correlation between environmental temperature variation and thermal error displacement. Thus, if there are greater variations in environmental temperature, corresponding variations in displacement error can be expected. Nevertheless, environmental temperature changes takes place very slowly. Typical probing routine time is comparatively short. Hence, the influence of environmental temperature as an uncertainty contributor is insignificant unless there is a large variation. During on-machine probing, if probing speed is consistent then the influence of machine vibration can be neglected.

Factors such as surface contamination due to thin film of coolant and workpiece distortion owing to clamping do not contribute significantly to the uncertainty. The probing

repeatability of 0.3 µm without coolant and 0.5 µm with coolant was observed during the experimental analysis. If the lubrication, e.g. cutting oil, were used then this needs to be considered. The FEA simulation of workpiece distortion due to clamping, in the case of equal application of force on a simple workpiece was in the range of 0.004 µm to 0.6 µm. This deformation on a whole is insignificant. Consideration of deflection on thin walled workpieces is the subject of further work. The resultant workpiece thermal error due loss of heat to the surrounding while probing is taking place is 13 µm for a particular case study. This value is arrived at again using FEA.

To reduce the influence of the significant uncertainty source, the thermal error, sensor data fusion model using ANN and PCA was developed. The output of this model showed better than 90% correlation with the measured thermal displacement error. Fibre Bragg Grating (FBG) and temperature sensors were used to train the sensor fusion model.

The PCA helps in the dimensionality reduction on the measured data, thus reducing the computation time of the ANN. It condenses the input sensor data size from 720 x 14 to 720 x 3. The training time for ANN was reduced to 1.3 sec from 59 sec. This can be especially useful in case of large amounts of data obtained for a long period of time or if close to real-time calculations are needed for active compensation.

PCA further helps to improve generalization capability of the ANN. This is because when all the sensor input data is fed to the ANN during supervised learning process, ANN sometimes loses its generalization capability due to the over fitting which reduces the robustness of its estimation ability. Due to the dimensional reduction aspect of the PCA, not all of the input data is used to train the ANN model, thus, reducing the overfitting problem of ANN. The same is reflected by the overall improvement in the root mean square error (RMSE) between ANN output and measured output. The highest RMSE is 12 µm for the optimal model (model 4), an improvement from 168 µm for the initial model (model 1). In addition, correlation is better than 90 % between ANN output and measured output.

LabVIEW based modular structured software was built, capable of multi-sensor data acquisition (DAQ), sensor fusion using various techniques and able to communicate with the controller. Any commercial sensor in the market has either some application provided by the manufacturer or open source software for capturing and/or analysing data. There is no general DAQ software available for this purpose. Software provided by manufacturers has restricted usage for research application. They often lack the flexibility and extensibility

required for research. Thus, the software offering the prospect of using computer-based data processing to expedite the development path was developed. This program was created in the modular structure to provide user-friendly software and to allow desired flexibility and extensibility. Another advantage is the ability to deploy advanced MATLAB models within the data acquisition system.

7.1.2 Displacement *sensor*

The use of temperature-only thermal compensation models has been shown to leave residual error, due in part to the thermal hysteresis. While consideration of this aspect was not part of this work, it became clear that supplementing temperature data with direct distortion measurement would provide greater accuracy in the model.

In this thesis, the testing of a novel photo-microsensor based displacement sensor is presented. This sensor has a static linear range and resolution (6σ) of 20 μm and 21 nm respectively, with a sensitivity of 0.1648 V/μm. The linearity error is within ±1 % of full-scale range. The repeatability of the sensor is 90 nm and the observed noise in the sensor signal is 21nm without the use of any filter.

The proposed system is capable of self-compensation against the perturbations due to power supply and ambient light variations. Although the design of the shutter is in contact with the object to be monitored, overall sensor design is minimally invasive. The cost of the prototype sensor head is 27 GBP, less than 10% of their uncalibrated capacitive and inductive counterparts without electronics. The output of the sensor is compatible with any standard data acquisition hardware and software. It is a low cost, compact sized sensor with small footprint that can be designed with a relatively small number of components without any complex signal processing circuits.

This sensor can be used to reduce the error in the thermal model, and is therefore well placed to provide structural distortion data to be fused with the on-machine probing results to further reduce uncertainty of measurement.

7.2 Summary

This thesis investigates the sources of uncertainty for on-machine probing at a granular level with experiments and simulation.

Uncompensated geometric errors contribute considerably towards the on-machine probing (OMP) uncertainty, albeit, less than thermal errors in magnitude. However, they are repeatable in nature, thus, can be reduced significantly by calibration of the machine.

Thermal errors are the largest contributing factors for OMP with magnitudes of up to 220 µm being measured in this work. Hence, they need to be reduced significantly.

To reduce the thermal error, a PCA and ANN based senor fusion model was developed. The output of this model shows better than 90 % correlation with the measured data. Fibre Bragg Grating (FBG) and temperature sensors were used to train the sensor fusion model.

LabVIEW-based modular structured software was built, capable of data acquisition, sensor fusion using various techniques and able to communicate with the machine tool controller.

Finally, a novel photo-microsensors based displacement sensor is presented. This sensor has the potential to provide the information similar to the FBGs, but at a fraction of a cost. Thus, they can be utilised for the training of the sensor fusion model. The proposed sensor has a static range of 20 µm, resolution of 21 nm and repeatability of 90 nm.

7.3 Future work

The work in this thesis has provided the first step in evaluating and reducing the measurement uncertainty of on machine probing (OMP) for efficiently calibrating thermal error models.

This work can be extended to combine all the uncertainty contributors in OMP according to the established standards and then using Monte Carlo simulation to estimate their effects. This would have the benefit of providing an all-encompassing solution, which can then be generally applied throughout precision manufacturing.

In addition, the work can be further extended to include the use of on-machine tool-setters as a means of acquiring data. By their nature, these generally only provide information for a single-point on the machine and are therefore less useful than the spindle-mounted probes. However, they are often available, unlike probing spheres, so can provide useful feedback over time without being invasive to the normal manufacturing operation.

In this thesis, rudimentary finite element analysis has been carried out on an example with simple geometry to analyse the influence of clamping force and thermal load on a workpiece distortion. This work should be further extended for complex geometries with consideration of localised heat sources. It should also focus on the special case of "thin walled" parts, where the effects of clamping can be particularly significant.

More extensive analysis of the effect of variation in ambient conditions, such as temperature and vibration, can then be carried out by combining the additional FEA work with the statistical Monte Carlo approach.

The thesis has produced a prototype data fusion system, which has been trialled on part of a machine tool structure. This should be developed, using the new displacement sensor, to produce a complete system on a full machine tool, incorporating all the significant structural components.

References List

1. Dotson, C., *Fundamentals of dimensional metrology*. 2016.
2. Zhao, Y., et al., *Dimensional metrology interoperability and standardization in manufacturing systems.* Computer Standards & Interfaces, 2011. **33**(6): p. 541-555.
3. IMTI, *A Roadmap For Metrology Interoperability Integrated Manufacturing Technology Initiative.* (IMTI, Inc.), 2006.
4. Muelaner, J.E., B. Cai, and P.G. Maropoulos, *Large-volume metrology instrument selection and measurability analysis.* Proceedings of the Institution of Mechanical Engineers, Part B: Journal of Engineering Manufacture, 2010. **224**(6): p. 853-868.
5. Estler, W.T., et al., *Large-Scale Metrology – An Update.* CIRP Annals - Manufacturing Technology, 2002. **51**(2): p. 587-609.
6. Howarth, P., F. Redgrave, and M. Dansk Fundamental. *Metrology - in short*. 2008.
7. Gestel, N.V., et al., *Influence of feature form deviations on CMM measurement uncertainties.* International Journal of Precision Technology, 2011. **2**(2-3): p. 192-210.
8. Longstaff, A.P., et al., *The Role of Measurement and Modelling of Machine Tools in Improving Product Quality.* International Journal of Metrology and Quality Engineering, 2014. **4**(03): p. 177-184.
9. Lee, K.-I. and S.-H. Yang, *Accuracy evaluation of machine tools by modeling spherical deviation based on double ball-bar measurements.* International Journal of Machine Tools and Manufacture, 2013. **75**: p. 46-54.
10. Ramesh, R., M.A. Mannan, and A.N. Poo, *Error compensation in machine tools — a review: Part I: geometric, cutting-force induced and fixture-dependent errors.* International Journal of Machine Tools and Manufacture, 2000. **40**(9): p. 1235-1256.
11. *ISO 10360-1:2000 Geometrical Product Specifications (GPS) -- Acceptance and reverification tests for coordinate measuring machines (CMM) -- Part 1: Vocabulary*. 2000, International Standards Organization.
12. Tan, B., et al., *A thermal error model for large machine tools that considers environmental thermal hysteresis effects.* International Journal of Machine Tools and Manufacture, 2014. **82–83**(0): p. 11-20.
13. Schwenke, H., et al., *Geometric error measurement and compensation of machines—An update.* CIRP Annals - Manufacturing Technology, 2008. **57**(2): p. 660-675.
14. Postlethwaite, S. and D. Ford, *Geometric error analysis software for CNC machine tools.* LAMDAMAP 97, 1997: p. 305-316.
15. Longstaff, A.P., S. Fletcher, and D.G. Ford, *Practical experience of thermal testing with reference to ISO 230 Part 3*. 2003, WIT Press.

16. Bryan, J., *International Status of Thermal Error Research (1990).* CIRP Annals - Manufacturing Technology, 1990. **39**(2): p. 645-656.
17. Weck, M., et al., *Reduction and compensation of thermal errors in machine tools.* CIRP Annals - Manufacturing Technology, 1995. **44**(2): p. 589-598.
18. Mayr, J., et al., *Thermal issues in machine tools.* CIRP Annals - Manufacturing Technology, 2012. **61**(2): p. 771-791.
19. Li, Y., et al., *A review on spindle thermal error compensation in machine tools.* International Journal of Machine Tools and Manufacture, 2015. **95**: p. 20-38.
20. Mian, N.S., *Efficient machine tool thermal error modelling strategy for accurate offline assessment, PhD Thesis*. 2010.
21. Fletcher, S., *Computer aided system for intelligent implementation of machine tool error reduction methodologies, PhD Thesis*. 2001, University of Huddersfield.
22. Wang, J. and J. Guo, *Research on volumetric error compensation for NC machine tool based on laser tracker measurement.* Science China Technological Sciences, 2012. **55**(11): p. 3000-3009.
23. Ni, J., *CNC machine accuracy enhancement through real-time error compensation.* TRANSACTIONS-AMERICAN SOCIETY OF MECHANICAL ENGINEERS JOURNAL OF MANUFACTURING SCIENCE AND ENGINEERING, 1997. **119**: p. 717-725.
24. Zhan-Qiang, L., P.K. Venuvinod, and V.A. Ostafiev, *On-machine measurement of workpieces with the cutting tool.* Integrated Manufacturing Systems, 1998. **9**(3): p. 168-172.
25. Grosvenor, R.I., C. Kharpoutly, and K.F. Martin, *In-process measurement problems in machine tool applications.* International Journal of Production Research, 1991. **29**(2): p. 357-374.
26. Choi, J.P., B.K. Min, and S.J. Lee, *Reduction of machining errors of a three-axis machine tool by on-machine measurement and error compensation system.* Journal of Materials Processing Technology, 2004. **155–156**(0): p. 2056-2064.
27. Liu, H.B., et al., *Integration strategy of on-machine measurement (OMM) and numerical control (NC) machining for the large thin-walled parts with surface correlative constraint.* The International Journal of Advanced Manufacturing Technology, 2015. **80**(9): p. 1721-1731.
28. Kwon, Y., T.-L. Tseng, and Y. Ertekin, *Characterization of closed-loop measurement accuracy in precision CNC milling.* Robotics and Computer-Integrated Manufacturing, 2006. **22**(4): p. 288-296.
29. Zeleny, J. and M. Janda, *Automatic on-machine measurement of complex parts.* Modern Machinery Science Journal, 2009. **3**: p. 92-95.

30. Weckenmann, A., et al., *Probing Systems in Dimensional Metrology.* CIRP Annals - Manufacturing Technology, 2004. **53**(2): p. 657-684.
31. Cauchick-Miguel, P.A. and T.G. King, *Factors which influence CMM touch trigger probe performance.* International Journal of Machine Tools and Manufacture, 1998. **38**(4): p. 363-374.
32. Semotiuk, L., J. Józwik, and K. Ivan, *MEASUREMENT UNCERTAINTY ANALYSIS OF DIFFERENT CNC MACHINE TOOLS MEASUREMENT SYSTEMS.* Advances in Science and Technology Research Journal, 2013. **7**(19): p. 41-47.
33. Guiassa, R., et al., *Calibration of the cutting process and compensation of the compliance error by using on-machine probing.* The International Journal of Advanced Manufacturing Technology, 2014. **78**(5): p. 1043-1051.
34. *ISO 230-10:2011 Test code for machine tools -- Part 10: Determination of the measuring performance of probing systems of numerically controlled machine tools*. 2011, International Standards Organization.
35. Jankowski, M., A. Woźniak, and M. Byszewski, *Machine tool probes testing using a moving inner hemispherical master artefact.* Precision Engineering, 2014. **38**(2): p. 421-427.
36. Jankowski, M. and A. Wozniak, *Mechanical model of errors of probes for numerical controlled machine tools.* Measurement, 2016. **77**: p. 317-326.
37. *TE411 Innovations in touch-trigger probe sensor technology*, in *Renishaw technical paper*. 2010.
38. Pereira, P.H. and R.J. Hocken, *Characterization and compensation of dynamic errors of a scanning coordinate measuring machine.* Precision Engineering, 2007. **31**(1): p. 22-32.
39. HexagonMetrology. *m&h Temperature Probe Systems*. 2016 [cited 2016 3 March]; Available from: http://www.hexagonmetrology.es/en/mh-Temperature-Probe-Systems_2327.htm#.Vv0HGvnyuUk.
40. Heidenhain. *Touch probes for machine tools*. 2015 [cited 2016 3 March]; Available from: http://www.heidenhain.com/en_US/products-and-applications/touch-probes/.
41. BIPM, *Evaluation of Measurement Data Guide to the Expression of Uncertainty in Measurement.* 2008.
42. Forbes, A.B., *Measurement uncertainty and optimized conformance assessment.* Measurement, 2006. **39**(9): p. 808-814.
43. ISO/IEC, *ISO 14253-1:1998. Geometrical Product Specifications (GPS) – Inspection by measurement of workpieces and measuring equipment – Part 1: Decision rules for proving conformance or non-conformance with specifications*. 2008.

44. ISO/IEC, *ISO/IEC Guide 98-3:2008/Suppl 1:2008. Propagation of distributions using a Monte Carlo method.* 2008.
45. Saunders, P., et al. *The application of uncertainty evaluating software for the utilisation of machine tool systems for final inspection*. in *Laser Metrology and Machine Performance X - 10th International Conference and Exhibition on Laser Metrology, Machine Tool, CMM and Robotic Performance, LAMDAMAP 2013*. 2013.
46. Wilhelm, R.G., R. Hocken, and H. Schwenke, *Task Specific Uncertainty in Coordinate Measurement.* CIRP Annals - Manufacturing Technology, 2001. **50**(2): p. 553-563.
47. Weckenmann, A., M. Knauer, and H. Kunzmann, *The Influence of Measurement Strategy on the Uncertainty of CMM-Measurements.* CIRP Annals - Manufacturing Technology, 1998. **47**(1): p. 451-454.
48. Kruth, J.-P., et al., *Uncertainty determination for CMMs by Monte Carlo simulation integrating feature form deviations.* CIRP Annals - Manufacturing Technology, 2009. **58**(1): p. 463-466.
49. Salsbury, J.G., *A Simplified Methodology for the Uncertainty Analysis of CMM Measurements*, in *Conference on Precision Metrology /Applying Imaging and Sensoring*. 1995, Society of Manufacturing Engineers: Indianapolis.
50. Denkena, B., C. Schmidt, and M. Krüger, *Experimental investigation and modeling of thermal and mechanical influences on shape deviations in machining structural parts.* International Journal of Machine Tools and Manufacture, 2010. **50**(11): p. 1015-1021.
51. Raghu, A. and S.N. Melkote, *Analysis of the effects of fixture clamping sequence on part location errors.* International Journal of Machine Tools and Manufacture, 2004. **44**(4): p. 373-382.
52. Baldwin, J.M., et al., *Application of simulation software to coordinate measurement uncertainty evaluations.* Measure, 2007. **2**(4): p. 40-52.
53. Shao, X.-D., et al., *SIMULATION OF WORKPIECE DEFORMATION CAUSED BY RELEASING THE CLAMPING FORCE.* Transactions of the Canadian Society for Mechanical Engineering, 2013. **37**(3): p. 703-712.
54. De Meter, E.C., et al., *A model to predict minimum required clamp pre-loads in light of fixture–workpiece compliance.* International Journal of Machine Tools and Manufacture, 2001. **41**(7): p. 1031-1054.
55. Rai, J.K. and P. Xirouchakis, *Finite element method based machining simulation environment for analyzing part errors induced during milling of thin-walled components.* International Journal of Machine Tools and Manufacture, 2008. **48**(6): p. 629-643.

56. Majumdar, P., R. Jayaramachandran, and S. Ganesan, *Finite element analysis of temperature rise in metal cutting processes.* Applied Thermal Engineering, 2005. **25**(14–15): p. 2152-2168.
57. Dogu, Y., E. Aslan, and N. Camuscu, *A numerical model to determine temperature distribution in orthogonal metal cutting.* Journal of Materials Processing Technology, 2006. **171**(1): p. 1-9.
58. Fleischer, J., R. Pabst, and S. Kelemen, *Heat Flow Simulation for Dry Machining of Power Train Castings.* CIRP Annals - Manufacturing Technology, 2007. **56**(1): p. 117-122.
59. Peng, Y., et al., *A Cr-N thin film displacement sensor for precision positioning of a micro-stage.* Sensors and Actuators A: Physical, 2014. **211**: p. 89-97.
60. Maekawa, A., et al., *Experimental validation of non-contacting measurement method using LED-optical displacement sensors for vibration stress of small-bore piping.* Measurement, 2015. **71**: p. 1-10.
61. Berkovic, G. and E. Shafir, *Optical methods for distance and displacement measurements.* Advances in Optics and Photonics, 2012. **4**(4): p. 441-471.
62. Bell, D.J., et al., *MEMS actuators and sensors: observations on their performance and selection for purpose.* Journal of Micromechanics and Microengineering, 2005. **15**(7): p. S153.
63. Haitjema, H., P.H.J. Schellekens, and S.F.C.L. Wetzels, *Calibration of displacement sensors up to 300 µm with nanometre accuracy and direct traceability to a primary standard of length.* Metrologia, 2000. **37**(1): p. 25.
64. Nouira, H., et al., *Investigation of the influence of the main error sources on the capacitive displacement measurements with cylindrical artefacts.* Precision Engineering, 2013. **37**(3): p. 721-737.
65. Nabavi, M.R. and S.N. Nihtianov, *Design Strategies for Eddy-Current Displacement Sensor Systems: Review and Recommendations.* Sensors Journal, IEEE, 2012. **12**(12): p. 3346-3355.
66. Lee, C. and S.-K. Lee, *Multi-degree-of-freedom motion error measurement in an ultraprecision machine using laser encoder — Review.* Journal of Mechanical Science and Technology, 2013. **27**(1): p. 141-152.
67. Lee, J.-Y., et al., *Optical heterodyne grating interferometry for displacement measurement with subnanometric resolution.* Sensors and Actuators A: Physical, 2007. **137**(1): p. 185-191.
68. ChaBum, L., K. Gyu Ha, and L. Sun-Kyu, *Design and construction of a single unit multi-function optical encoder for a six-degree-of-freedom motion error measurement*

in an ultraprecision linear stage. Measurement Science and Technology, 2011. **22**(10): p. 105901.

69. Zhang, Z., et al., *A new laser displacement sensor based on triangulation for gauge real-time measurement.* Optics & Laser Technology, 2008. **40**(2): p. 252-255.
70. Boltryk, P.J., M. Hill, and J.W. McBride, *Comparing laser and polychromatic confocal optical displacement sensors for the 3D measurement of cylindrical artefacts containing microscopic grooved structures.* Wear, 2009. **266**(5–6): p. 498-501.
71. Fleming, A.J., *A review of nanometer resolution position sensors: Operation and performance.* Sensors and Actuators A: Physical, 2013. **190**(0): p. 106-126.
72. Perret, L., et al., *Fiber optics sensor for sub-nanometric displacement and wide bandwidth systems.* Sensors and Actuators A: Physical, 2011. **165**(2): p. 189-193.
73. Bera, S.C. and S. Chakraborty, *Study of magneto-optic element as a displacement sensor.* Measurement, 2011. **44**(9): p. 1747-1752.
74. Kim, M., et al., *A new capacitive displacement sensor with high accuracy and long-range.* Sensors and Actuators A: Physical, 2006. **130–131**(0): p. 135-141.
75. Wang, H., et al., *Ultrastable eddy current displacement sensor working in harsh temperature environments with comprehensive self-temperature compensation.* Sensors and Actuators A: Physical, 2014. **211**: p. 98-104.
76. Wang, H. and Z. Feng, *Ultrastable and highly sensitive eddy current displacement sensor using self-temperature compensation.* Sensors and Actuators A: Physical, 2013. **203**: p. 362-368.
77. Missoffe, A., et al., *New simple optical sensor: From nanometer resolution to centimeter displacement range.* Sensors and Actuators A: Physical, 2012. **176**(0): p. 46-52.
78. Mueller, T. and E. Reithmeier, *Image segmentation for laser triangulation based on Chan–Vese model.* Measurement, 2015. **63**: p. 100-109.
79. Lee, C., S.-K. Lee, and J.A. Tarbutton, *Positioning control effectiveness of optical knife edge displacement sensor-embedded monolithic precision stage.* Sensors and Actuators A: Physical, 2015. **233**: p. 390-396.
80. Shieh, J., et al., *The selection of sensors.* Progress in Materials Science, 2001. **46**(3–4): p. 461-504.
81. Lin, F., S.T. Smith, and G. Hussain, *Optical fiber displacement sensor and its application to tuning fork response measurement.* Precision Engineering, 2012. **36**(4): p. 620-628.

82. Bosetti, P. and S. Bruschi, *Enhancing positioning accuracy of CNC machine tools by means of direct measurement of deformation.* The International Journal of Advanced Manufacturing Technology, 2012. **58**(5-8): p. 651-662.
83. Li, J., H. Neumann, and R. Ramalingam, *Design, fabrication, and testing of fiber Bragg grating sensors for cryogenic long-range displacement measurement.* Cryogenics, 2015. **68**: p. 36-43.
84. Majumder, M., et al., *Fibre Bragg gratings in structural health monitoring—Present status and applications.* Sensors and Actuators A: Physical, 2008. **147**(1): p. 150-164.
85. Delmas, J.R., *Optoelectronic displacement sensor, US4338722 A*. 1982, Microlec, S.A.
86. Kaufmann, M., et al., *Optoelectronic displacement sensor with correction filter, US4812635 A*. 1989, Bbc Brown Boveri Ag.
87. Shan, Y., J.E. Speich, and K.K. Leang, *Low-Cost IR Reflective Sensors for Submicrolevel Position Measurement and Control.* Mechatronics, IEEE/ASME Transactions on, 2008. **13**(6): p. 700-709.
88. Benet, G., et al., *Using infrared sensors for distance measurement in mobile robots.* Robotics and Autonomous Systems, 2002. **40**(4): p. 255-266.
89. Ramesh, R., M.A. Mannan, and A.N. Poo, *Error compensation in machine tools — a review: Part II: thermal errors.* International Journal of Machine Tools and Manufacture, 2000. **40**(9): p. 1257-1284.
90. Möhring, H.C., K.M. Litwinski, and O. Gümmer, *Process monitoring with sensory machine tool components.* CIRP Annals - Manufacturing Technology, 2010. **59**(1): p. 383-386.
91. Denkena, B., H.-C. Möhring, and K. Litwinski, *Design of dynamic multi sensor systems.* Production Engineering, 2008. **2**(3): p. 327-331.
92. Luo, R.C., Y. Chih-Chen, and S. Kuo Lan, *Multisensor fusion and integration: approaches, applications, and future research directions.* IEEE Sensors Journal, 2002. **2**(2): p. 107-119.
93. Banerjee, T.P. and S. Das, *Multi-sensor data fusion using support vector machine for motor fault detection.* Information Sciences, 2012: p. 96-107.
94. Fekih, A., H. Xu, and F.N. Chowdhury, *Neural networks based system identification techniques for model based fault detection of nonlinear systems.* International Journal of Innovative Computing, Information and Control, 2007. **3**(5): p. 1073-1085.
95. Ghosh, N., et al., *Estimation of tool wear during CNC milling using neural network-based sensor fusion.* Mechanical Systems and Signal Processing, 2007. **21**(1): p. 466-479.

96. Mahajan, A., K. Wang, and P.K. Ray, *Multisensor integration and fusion model that uses a fuzzy inference system.* Mechatronics, IEEE/ASME Transactions on, 2001. **6**(2): p. 188-196.
97. Aliustaoglu, C., H.M. Ertunc, and H. Ocak, *Tool wear condition monitoring using a sensor fusion model based on fuzzy inference system.* Mechanical Systems and Signal Processing, 2009. **23**(2): p. 539-546.
98. Huang, Y. and T. Hoshi, *Optimization of fixture design with consideration of thermal deformation in face milling.* J. Manuf. Sys., 2001. **19**(5): p. 332-40.
99. Yang, J., et al. *Applying neural network based on fuzzy cluster pre-processing to thermal error modeling for coordinate boring machine*. in *Procedia CIRP*. 2014.
100. Chang, C.-W., et al., *Thermal deformation prediction in machine tools by using neural network*, in *Neural Information Processing*, I. King, et al., Editors. 2006, Springer Berlin Heidelberg. p. 850-859.
101. Naeem, S.M., et al., *Efficient thermal error prediction in a machine tool using finite element analysis.* Measurement Science and Technology, 2011. **22**(8): p. 085107.
102. Miao, E.-M., et al., *Robustness of thermal error compensation modeling models of CNC machine tools.* The International Journal of Advanced Manufacturing Technology, 2013. **69**(9): p. 2593-2603.
103. Lee, J.-H., J.-H. Lee, and S.-H. Yang, *Development of thermal error model with minimum number of variables using fuzzy logic strategy.* KSME International Journal, 2001. **15**(11): p. 1482-1489.
104. Abdulshahed, A.M., A.P. Longstaff, and S. Fletcher, *The application of ANFIS prediction models for thermal error compensation on CNC machine tools.* Applied Soft Computing, 2015. **27**: p. 158-168.
105. Creighton, E., et al., *Analysis of thermal errors in a high-speed micro-milling spindle.* International Journal of Machine Tools and Manufacture, 2010. **50**(4): p. 386-393.
106. Abellan-Nebot, J.V. and F. Romero Subirón, *A review of machining monitoring systems based on artificial intelligence process models.* The International Journal of Advanced Manufacturing Technology, 2010. **47**(1): p. 237-257.
107. Chen, J.S. and G. Chiou, *Quick testing and modeling of thermally-induced errors of CNC machine tools.* International Journal of Machine Tools and Manufacture, 1995. **35**(7): p. 1063-1074.
108. Yang, H. and J. Ni, *Dynamic neural network modeling for nonlinear, nonstationary machine tool thermally induced error.* International Journal of Machine Tools and Manufacture, 2005. **45**(4–5): p. 455-465.

109. Yang, S., J. Yuan, and J. Ni, *The improvement of thermal error modeling and compensation on machine tools by CMAC neural network.* International Journal of Machine Tools and Manufacture, 1996. **36**(4): p. 527-537.
110. Abdulshahed, A.M., et al., *Thermal error modelling of a gantry-type 5-axis machine tool using a Grey Neural Network Model.* Journal of Manufacturing Systems, 2016. **41**: p. 130-142.
111. Abdulshahed, A.M., et al., *Thermal error modelling of machine tools based on ANFIS with fuzzy c-means clustering using a thermal imaging camera.* Applied Mathematical Modelling, 2015. **39**(7): p. 1837-1852.
112. Mostafaei, M., H. Javadikia, and L. Naderloo, *Modeling the effects of ultrasound power and reactor dimension on the biodiesel production yield: Comparison of prediction abilities between response surface methodology (RSM) and adaptive neuro-fuzzy inference system (ANFIS).* Energy, 2016. **115, Part 1**: p. 626-636.
113. Coromant, S. *Workpiece material groups*. 2016 [cited 2016 2 February]; Available from: http://www.sandvik.coromant.com/en-gb/knowledge/materials/workpiece_materials/workpiece_material_groups/pages/workpiece-material-groups.aspx?Country=gb.
114. Vallejo, A., et al., *Multi Sensor Data Fusion for High Speed Machining*, in *MICAI 2007: Advances in Artificial Intelligence: 6th Mexican International Conference on Artificial Intelligence, Aguascalientes, Mexico, November 4-10, 2007. Proceedings*, A. Gelbukh and Á.F. Kuri Morales, Editors. 2007, Springer Berlin Heidelberg: Berlin, Heidelberg. p. 1162-1172.
115. Potdar, A.A., S. Fletcher, and A.P. Longstaff, *Performance characterisation of a new photo-microsensor based sensing head for displacement measurement.* Sensors and Actuators A: Physical, 2016. **238**: p. 60-70.
116. Potdar, A., et al., *Development of modular machine tool structural monitoring system.* Advanced Manufacturing Engineering and Technologies NEWTECH 2013 Stockholm, Sweden 27-30 October 2013, 2013: p. 263.
117. *ISO 5725 -1 Accuracy (Trueness and Precision) of Measurement Methods and Results*. 1994, International Standards Organization.
118. Panopoulou, A., et al., *Dynamic fiber Bragg gratings based health monitoring system of composite aerospace structures.* Acta Astronautica, 2011. **69**(7–8): p. 445-457.
119. Flandorfer, H., F. Gehringer, and E. Hayer, *Individual solutions for control and data acquisition with the PC.* Thermochimica Acta, 2002. **382**(1–2): p. 77-87.

120. Anjos, J.M.S., G.K. Coracini, and E. Villani, *A proposal and verification of a software architecture based on LabVIEW for a multifunctional robotic end-effector.* Advances in Engineering Software, 2013. **55**: p. 32-44.
121. Whitley, K.N., L.R. Novick, and D. Fisher, *Evidence in favor of visual representation for the dataflow paradigm: An experiment testing LabVIEW's comprehensibility.* International Journal of Human-Computer Studies, 2006. **64**(4): p. 281-303.
122. Wang, L., et al., *The Application of LabVIEW in Data Acquisition System of Solar Absorption Refrigerator.* Energy Procedia, 2012. **16**: p. 1496-1502.
123. Abdulshahed, A., *The Application of ANN and ANFIS Prediction Models for Thermal Error Compensation on CNC Machine Tools*, in *School of Computing and Engineering*. 2015, University of Huddersfield. p. 164.
124. Tatar, A., et al., *Predictive model based on ANFIS for estimation of thermal conductivity of carbon dioxide.* Journal of Molecular Liquids, 2016. **224, Part B**: p. 1266-1274.
125. Mishra, R.N. and K.B. Mohanty, *Real time implementation of an ANFIS-based induction motor drive via feedback linearization for performance enhancement.* Engineering Science and Technology, an International Journal, 2016. **19**(4): p. 1714-1730.
126. Potdar, A., et al. *Application of multi sensor data fusion based on Principal Component Analysis and Artificial Neural Network for machine tool thermal monitoring*. in *Laser Metrology and Machine Performance XI, LAMDAMAP* 2015. Huddersfield,UK.
127. Freeman, J.A. and D.M. Skapura, *Neural networks: algorithms, applications, and programming techniques*. 1991: Addison Wesley Longman Publishing Co., Inc. 401.
128. Sick, B., *On-line and indirect tool wear monitoring in turning with artificial neural networks: A review of more than a decade of research.* Mech. Sys. and Sig. Process., 2002. **16**(4): p. 487-546.
129. Jolliffe, I., *Principal component analysis*. 2005: Wiley Online Library.